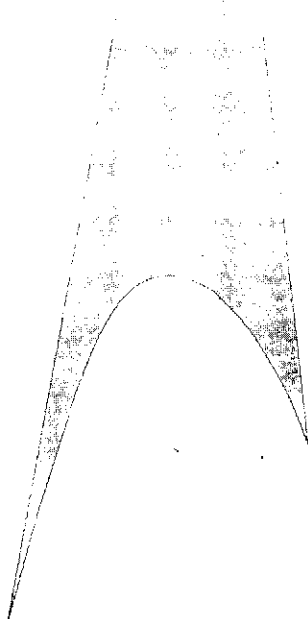


May 10, 1974



THE DEVELOPMENT OF A SOLAR-POWERED RESIDENTIAL HEATING AND COOLING SYSTEM

(NASA-TM-X-79089) THE DEVELOPMENT OF A
SOLAR-POWERED RESIDENTIAL HEATING AND
COOLING SYSTEM (NASA)

N74-26504

Unclas
G3/03 41406

REPRODUCED BY
NATIONAL TECHNICAL
INFORMATION SERVICE
U. S. DEPARTMENT OF COMMERCE
SPRINGFIELD, VA. 22161

NATIONAL AERONAUTICS AND SPACE ADMINISTRATION



1. REPORT NO. M-TU-74-3	2. GOVERNMENT ACCESSION NO.	3. RECIPIENT'S CATALOG NO.
4. TITLE AND SUBTITLE THE DEVELOPMENT OF A SOLAR-POWERED RESIDENTIAL HEATING AND COOLING SYSTEM		5. REPORT DATE May 10, 1974
7. AUTHOR(S)		6. PERFORMING ORGANIZATION CODE
9. PERFORMING ORGANIZATION NAME AND ADDRESS George C. Marshall Space Flight Center Marshall Space Flight Center, Alabama 35812		8. PERFORMING ORGANIZATION REPORT #
12. SPONSORING AGENCY NAME AND ADDRESS National Aeronautics and Space Administration Washington, D. C. 20546		10. WORK UNIT NO.
15. SUPPLEMENTARY NOTES		11. CONTRACT OR GRANT NO.
		13. TYPE OF REPORT & PERIOD COVERED Miscellaneous
		14. SPONSORING AGENCY CODE
16. ABSTRACT <p style="text-align: center;">This report describes the MSFC efforts to demonstrate the engineering feasibility of utilizing solar power for residential heating and cooling. These efforts have been concentrated on the analysis, design, and test of a full-scale demonstration system which is currently under construction at the National Aeronautics and Space Administration, Marshall Space Flight Center, Huntsville, Alabama.</p> <p style="text-align: center;">The basic solar heating and cooling system under development utilizes a flat plate solar energy collector, a large water tank for thermal energy storage, heat exchangers for space heating and water heating, and an absorption cycle air conditioner for space cooling.</p>		
17. KEY WORDS	18. DISTRIBUTION STATEMENT Unclassified-unlimited <i>James D. Ledbetter</i>	
19. SECURITY CLASSIF. (of this report) Unclassified	20. SECURITY CLASSIF. (of this page) Unclassified	

TABLE OF CONTENTS

	Page
SUMMARY	1
SECTION 1. INTRODUCTION	2
SECTION 2. DESCRIPTION OF THE SOLAR-POWERED RESIDENTIAL HEATING AND COOLING SYSTEM.....	3
SECTION 3. SOLAR ENERGY COLLECTOR STUDIES	8
3.1 Identification of Roll-Bond Material	8
3.2 Flow Passage Geometry Definition	8
3.3 Backside Insulation	9
3.4 Radiation Properties of Selective Coating	12
3.5 Wire/Tedlar Composite	12
3.6 Transmittance Test Using Pyrheliometer	20
3.7 Effect of Age and Exposure on Tedlar Transmittance	20
3.8 Comparison of Experimental Collector Performance with Analytical Predictions.....	20
3.9 Solar Flux and Incidence Angle Effects	26
3.10 Further Tilt Angle Studies	30
SECTION 4. ENERGY STORAGE SYSTEM STUDIES	32
4.1 Tank Selection	32
4.2 Tank Insulation Selection	32
4.3 Thermal Analysis of Tank	32
SECTION 5. PARAMETRIC TOTAL SYSTEM PERFORMANCE STUDIES	40
5.1 Modeling Techniques	40
5.2 Simulation Results	43
SECTION 6. AUTOMATIC CONTROL SYSTEM DESCRIPTION	54
6.1 Air Conditioning Mode	54

TABLE OF CONTENTS (Concluded)

	Page
6.2 Bypass Mode Flow	54
6.3 Air Conditioning Loop — Winter Operation . . .	56
SECTION 7. SOLAR COLLECTOR SEGMENT TEST RESULTS . . .	58
SECTION 8. CONCLUSIONS	69

LIST OF ILLUSTRATIONS

Figure	Title	Page
1.	System schematic	4
2.	MSFC collector design features	5
3.	Identification and location of thermocouples on thermal storage tank	7
4.	Roll-Bond panel design	10
5.	Predicted thermal performance of one Roll-Bond panel	11
6.	Heat transfer from collector to collector insulation for a step jump in Roll-Bond plate temperature	13
7.	Solar energy collection efficiency for a "typical clear summer day" (one tedlar cover).	14
8.	Solar energy collection efficiency for a "typical clear winter day" (one tedlar cover)	15
9.	Solar energy collection efficiency for a "typical clear summer day" (two tedlar covers)	16
10.	Solar energy collection efficiency for a "typical clear winter day" (two tedlar covers)	17
11.	Effect of number of covers on collection efficiency for "typical clear summer day"	18
12.	Effect of number of covers on collection efficiency for "typical clear winter day"	19
13.	Wire equilibrium temperature	21
14.	Effect of age and exposure on transmittance of 4-mil thick tedlar	23

LIST OF ILLUSTRATIONS (Continued)

Figure	Title	Page
15.	Analytical experimental comparison for solar collector test	24
16.	Analytical experimental comparison for 280°F solar collector test	25
17.	Energy flows for 165°F collector test	27
18.	Energy flows for 280°F collector test	28
19.	Effect of solar flux on collector performance	29
20.	Effect of incidence angle on collector performance	30
21.	Seasonal variation in ideal solar irradiation for various tilt angles (measured from horizontal)	31
22.	Auxiliary heat required for different collector areas and energy storage system capacities ($T_{\max} = 220^{\circ}\text{F}$)	33
23.	Auxiliary heat required for different collector area and energy storage system capacities ($T_{\max} = 250^{\circ}\text{F}$)	34
24.	Auxiliary heat required for different collector areas and energy storage system capacities ($T_{\max} = 280^{\circ}\text{F}$)	35
25.	Energy storage tank	37
26.	Heat loss through tank insulation	38
27.	Heat loss through tank support structure and supply lines . . .	39
28.	Basic components of the simulation program	41

LIST OF ILLUSTRATIONS (Concluded)

Figure	Title	Page
29.	Effect of cover design on system performance	45
30.	Effect of tilting collector twice a year on heating/cooling performance	46
31.	Effect of degraded properties on system performance	47
32.	Effect of collector covers on system performance for June and July operation only	48
33.	Effect of maximum tank operating pressure on system performance for June and July operation only	49
34.	Effect of tedlar transmittance on system performance for one-tedlar cover collector	50
35.	Effect of tedlar transmittance on system performance for two-tedlar cover collector	51
36.	Setup for demonstration test of solar-powered residential heating and cooling system	55
37.	Setup for evaluation of solar collector test bed	59
38.	Collector efficiency versus average collector temperatures . .	60
39.	Collector efficiency versus average collector temperatures . .	61
40.	Collector efficiency versus average collector temperatures . .	62
41.	Collector efficiency versus average collector temperatures . .	63
42.	Measured efficiency η for 2 ft by 21 ft solar collector	65
43.	Measured efficiency η for 2 ft by 21 ft solar collector	66
44.	Temperature distribution over 2 ft by 21 ft solar collector for test No. 20 (2/12/74) at approximately 12:00 noon and 1:30 p. m.	68

NOMENCLATURE

<u>Symbol</u>	<u>Description</u>
A	area
$A_{\text{collector}}$	solar collector area
Btu	British thermal unit
cfm	cubic feet per minute
cos	cosine function
\cos^{-1}	inverse cosine function
C_p	constant-pressure specific heat
D	diameter
deg	degree
$^{\circ}\text{F}$	degrees Fahrenheit
ft^2	square feet
gal/min, gpm	gallons per minute
hp	horsepower
hr	hour
H_2O	water
i. d.	inner diameter
I_o	incident solar flux (measured on plane of collector)
K	thermal conductivity
L	length
lbm, lb	pound mass
m_{water}	mass of water in the thermal energy storage tank
\dot{m}	mass flow rate
mph	miles per hour
o.d.	outer diameter
P	pressure

NOMENCLATURE (Concluded)

<u>Symbol</u>	<u>Description</u>
T_r	temperature of water returning from solar collector
T_t	temperature of water in thermal storage tank
UA	overall heat transfer coefficient
VM	Vuilleumier cycle
 <u>Greek Symbols</u>	
α_s	solar absorptance
Δ	difference
ϵ, ϵ_{ir}	infrared emittance
λ	wavelength
ϕ	tilt angle of collector
ρ	mass density
σ	ratio of auxiliary to total heat requirements (Q_{aux}/Q_{tot}) for June and July
$\frac{\partial \sigma}{\partial A}$	partial derivative of σ with respect to collector area (A)
$\frac{\partial \sigma}{\partial \alpha_s}$	partial derivative of σ with respect to solar absorptance (α_s) of collector plate
$\frac{\partial \sigma}{\partial \epsilon}$	partial derivative of σ with respect to emittance (ϵ) of collector plate
$\frac{\partial \sigma}{\partial \tau}$	partial derivative of σ with respect to solar transmittance (τ) of outermost collector cover
θ	incidence angle of solar radiation measured from collector normal
τ	solar transmittance of collector covers
τ_{eff}	effective solar transmittance
$\tau_{inner}, \tau_{in}, \tau_i$	solar transmittance of inner cover of collector
$\tau_{outer}, \tau_{out}, \tau_o$	solar transmittance of outer cover of collector

NOMENCLATURE (Continued)

<u>Symbol</u>	<u>Description</u>
psi	pounds per square inch
psia	pounds per square inch absolute
psig	pounds per square inch gage
Q	heat
\dot{Q}	heat transfer rate
\dot{Q}/A	heat transfer rate per unit area
Q_{aux} , $Q_{auxiliary}$	auxiliary heat requirement
Q_{tot} , Q_{total}	total energy required to provide heating and cooling
$^{\circ}R$	degrees Rankine
T	temperature
t	thickness or time
ton (of air conditioning)	12 000 Btu/hr
$T_{ambient}$, T_{amb}	ambient temperature
$T_{collector}$, T_{coll} , T_c	average plate temperature of solar collector
T_{max}	maximum allowable water temperature in thermal storage tank
T_{min} htg	minimum allowable water temperature for space heating
T_{min} cooling	minimum allowable water temperature for space cooling

THE DEVELOPMENT OF A SOLAR-POWERED RESIDENTIAL HEATING AND COOLING SYSTEM

SUMMARY

This report describes the MSFC efforts to demonstrate the engineering feasibility of utilizing solar power for residential heating and cooling. These efforts have been concentrated on the analysis, design, and test of a full-scale demonstration system which is currently under construction at the National Aeronautics and Space Administration, Marshall Space Flight Center, Huntsville, Alabama.

The basic solar heating and cooling system under development utilizes a flat plate solar energy collector, a large water tank for thermal energy storage, heat exchangers for space heating and water heating, and an absorption cycle air conditioner for space cooling. A complete description of the system is presented in Section 2.

Using previously developed computer tools, a wide range of solar energy collector studies has been conducted. The effects of collector design and operating conditions upon collector performance have been explored extensively, as described in Section 3.

Thermal analyses of the energy storage system have been conducted, as reported in Section 4.

Numerous parametric studies of the total system performance have been conducted using a sophisticated system simulation computer program. This program uses measured meteorological data and mathematical models of all system components to perform a transient energy transfer analysis through an entire year. Section 5 contains details and results of such simulations.

Practical methods of effecting automatic control of the overall solar heating and cooling system have been investigated, as described in Section 6. Pressure distribution studies also have been completed, as discussed in Section 7.

SECTION 1. INTRODUCTION

The current worldwide shortage of petroleum dramatically emphasizes the need for alternative energy sources. Among the possible alternative energy sources, the most pollution-free, non-depletable, boundless source of all is solar energy. One may reasonably expect that the sun will ultimately be harnessed to produce electricity, synthetic liquid and gaseous fuels, and high temperature thermal energy for industrial processes. However, the first major application of solar energy will be to heat and cool buildings since this application will require the fewest technological advances and the least expenditures of time and money.

Efforts are currently under way at Marshall Space Flight Center to demonstrate the engineering feasibility of using solar energy for this purpose. This report describes those efforts and presents the results of tests conducted thus far. The objectives of the work documented in this report include the following:

- To determine a solar energy collector design which would be efficient for both energy transfer and fluid flow.
- To generate the thermal design requirements for the energy storage system, which utilizes sensible heat storage in water.
- To properly size system components (including the collector and storage) and to determine a practical, efficient total system configuration by means of computer simulation of system performance.
- To evaluate the automatic control requirements of the full system.

SECTION 2. DESCRIPTION OF THE SOLAR-POWERED RESIDENTIAL HEATING AND COOLING SYSTEM

The test article is made up of several major subsystems as shown in Figure 1. These are the solar collector, hot water fired absorption air conditioner, heat storage tank, air conditioning system cooling tower, and three house trailers to simulate living quarters. The working fluid is deionized water pressurized to 30 psig to prevent boiling. The system operation is controlled automatically. This allows continuous unattended operation.

The heart of the test article is the solar collector. It consists of 31 segments; each segment is made up of an aluminum tray containing 7 heat exchangers. The heat exchangers are 1100 series aluminum, coated with an electroplated frequency selective coating that allows relatively high efficiency collection of solar energy at temperatures up to 260° F (Fig. 2). The heat exchangers are effectively insulated on the front face by a tedlar wire composite. The tedlar allows transmission of the solar energy, but greatly reduces convective heat losses from the heat exchanger. The tedlar cover also functions as a "greenhouse," trapping solar energy. The wire grid serves as structural support for the tedlar. The back of the heat exchanger is insulated by 6 in. of fiberglass household insulation. The heat exchangers are held in the aluminum trays by wooden strips which form channels on two sides of the exchangers. Teflon clips prevent the edges of the heat exchangers from touching the sides of the aluminum trays, and thus prevent thermal shorts. The fluid entrances and exits of the 31 segments are connected to manifolds that transport deionized water to and from the thermal storage tank. The collector system weight is 4600 lb, providing a roof loading equivalent to approximately 20 percent.

The trailer complex, which makes up the "dwelling" to be cooled and heated, is constructed of three surplus, office-type house trailers, two 10 ft by 58 ft and one 12 ft by 30 ft, secured together, with interconnecting doors and floor located air distribution ducting. The complex is positioned with its long dimension parallel to an east-west line in order that one face of the roof is facing due south so that the maximum solar energy input is possible. The nature of house trailer construction does not provide sufficient strength to support a roof structure of even minimum structural requirements; therefore, a free standing roof was constructed over the trailers to support the solar collector trays and associated plumbing. The roof is supported on fourteen 6-in.-diameter steel posts set in concrete, has a slope of 45 deg, and utilizes trussed rafter construction with rafters placed on 24-in. centers. The roof slope of 45 deg has been found to be the slope condition that provides a maximum

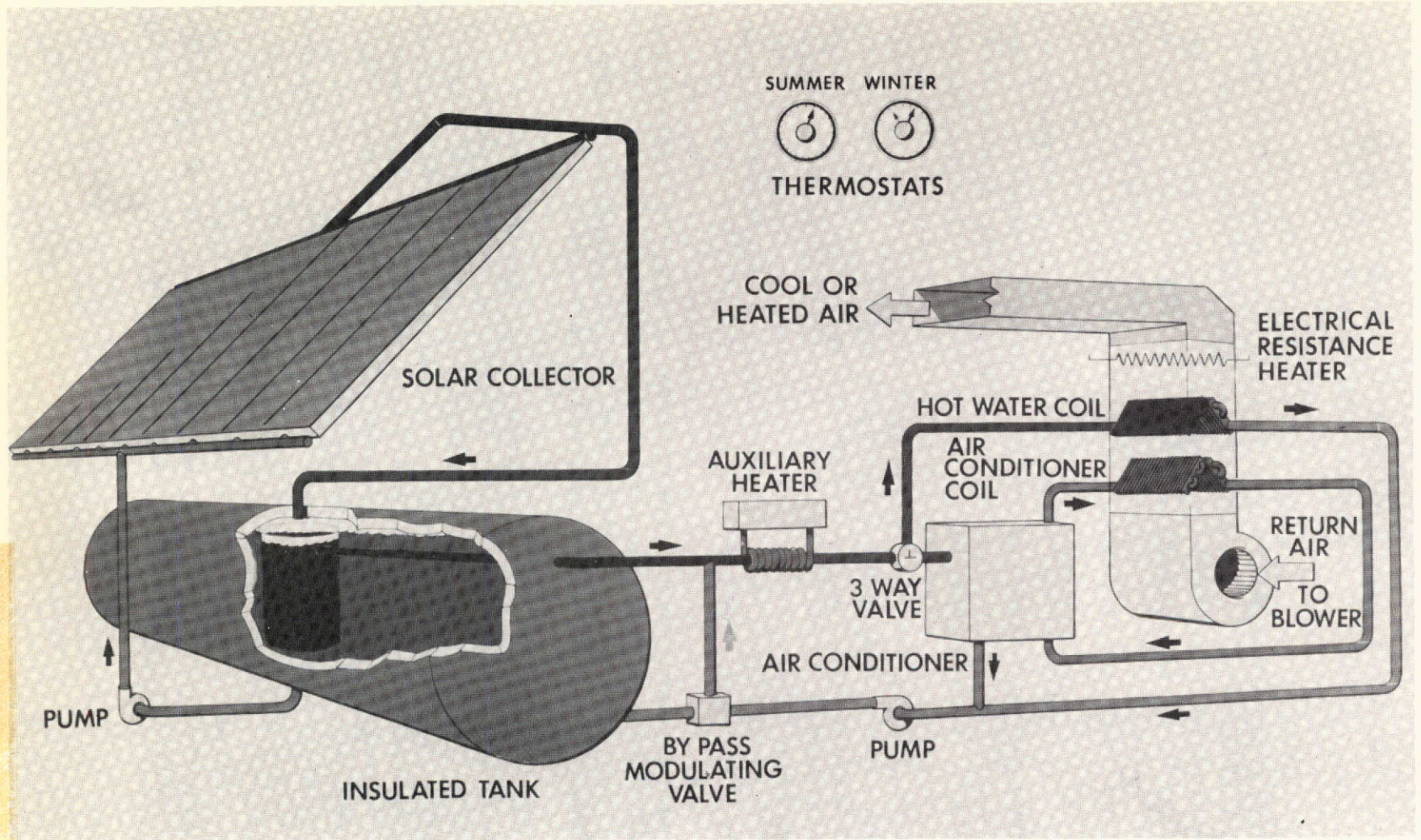


Figure 1. System schematic.

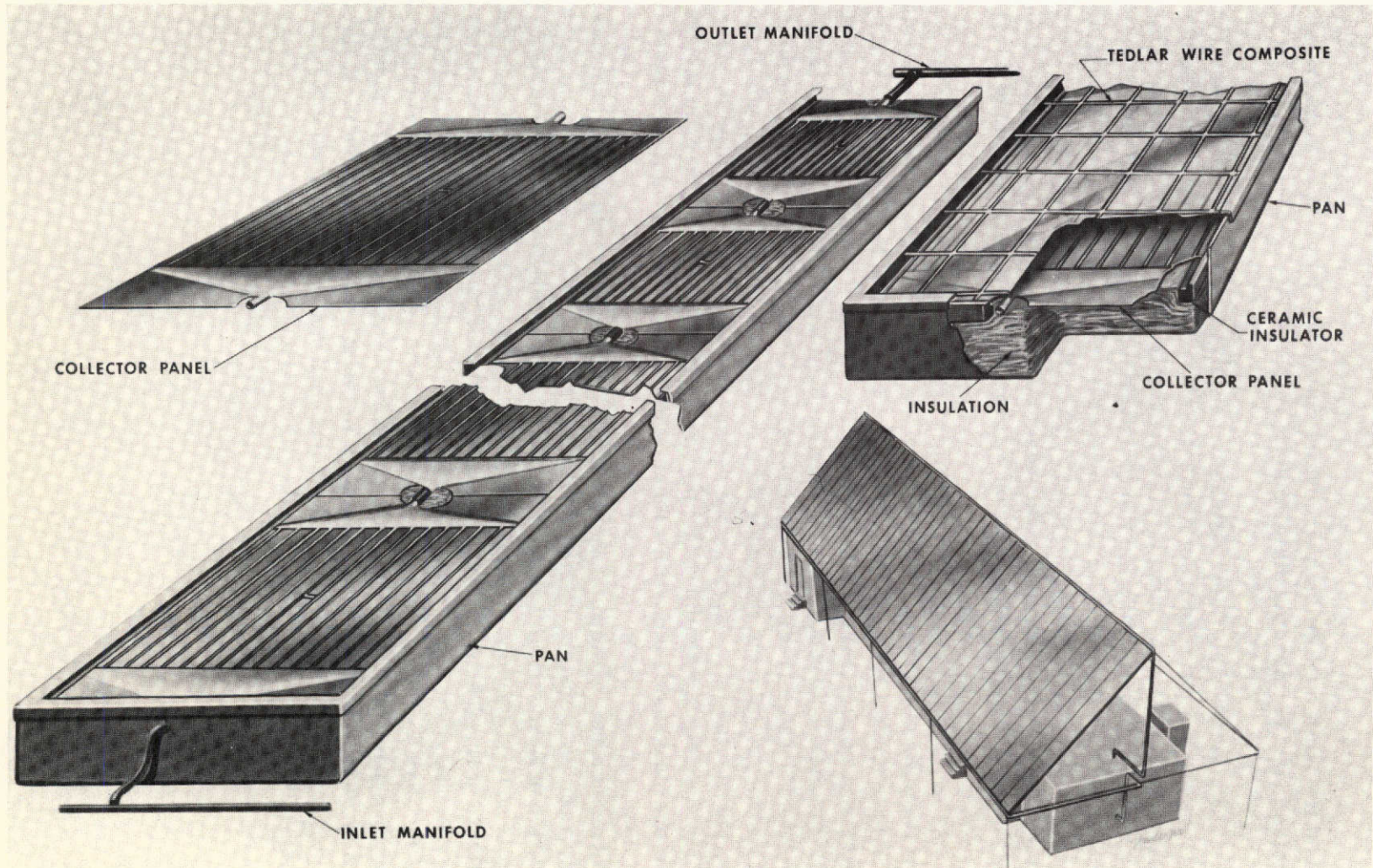
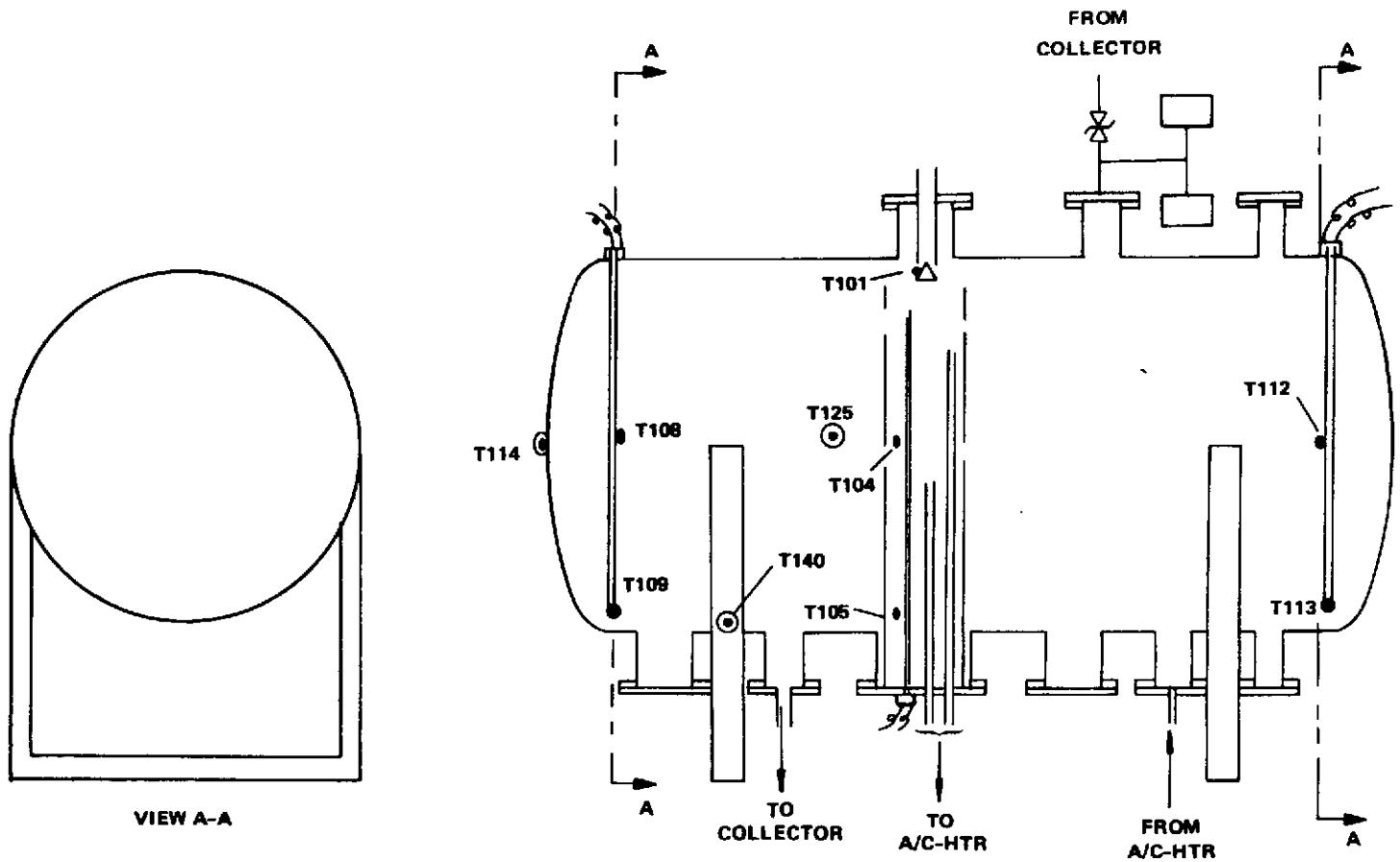


Figure 2. MSFC collector design features.

amount of solar input for all seasons of the year. The trailers have an area of 1500 ft² and the expected heat loss is equivalent to a conventionally constructed house of approximately 2500 ft².

The thermal storage subsystem is shown in Figure 3. The main components are a 4700-gal aluminum storage tank to contain 3600 gal of deionized water, pump valves and controls, a wooden house for weather protection, and household fiberglass insulation blown between the tank and interior of the house. The tank is from surplus and is significantly oversized from a cost optimization standpoint. The storage subsystem and the solar collector form the two major components of the heat collection and storage loop. The other fluid loop connects the absorption air conditioner and the thermal storage subsystem.

Cooling is provided to the trailer complex by a lithium bromide/water absorption air conditioner. The specific unit was commercially manufactured and sold through 1967 by ARKLA. This unit provides approximately 3 tons of cooling at a coefficient of performance of 0.67. The unit has been modified by removing the gas-fired burner and replacing it with a water heat exchanger. Hot (210° F) water from the thermal storage system is pumped through this heat exchanger to drive the absorption cycle air conditioner. An auxiliary electrical heater is installed in the water loop to insure hot water in the event the thermal storage system becomes inadequate. The lithium bromide/water cycle operates under a partial vacuum, approximately 100 mm Hg pressure in the generator and 8 mm Hg pressure in the evaporator. The refrigeration effect is obtained by water evaporating at the low pressure which provides an evaporator temperature of approximately 45° F. Heat rejection from the air conditioner is accomplished by a forced draft cooling tower. The cooling tower rejects heat by evaporating water into an air stream created by an electrically driven blower. The cooled water is circulated through the air conditioner adsorber and condenser to remove the heat of absorption and heat rejection by the fluid cycle. Heat required within the trailer during winter months is supplied by bypassing hot water from the storage tank around the air conditioner to an air/water heat exchanger located in the air distribution duct. If the water temperature in the storage tank becomes inadequate, supplementary heat can be added by electrical heaters in the air distribution duct.



NOTES:

1. ● INTERNAL THERMOCOUPLES; ◎ EXTERNAL THERMOCOUPLES.
2. (TIXX) - THERMOCOUPLES SYMMETRICALLY LOCATED ON OPPOSITE SIDE OR END.
3. VIEW A-A - EXTERNAL THERMOCOUPLES; NORTH END (NO PARENTHESIS).

Figure 3. Identification and location of thermocouples on thermal storage tank.

SECTION 3. SOLAR ENERGY COLLECTOR STUDIES

During the past months, numerous studies of flat-plate solar collectors were conducted. These studies and results are discussed in the following subsections.

3.1 IDENTIFICATION OF ROLL-BOND MATERIAL

Several large metal companies were contacted regarding the absorber plate of the flat-plate solar energy collector to determine the commercial availability of integral tube-in-sheet material. The major result of this survey was the identification of Olin Brass Roll-Bond material. This material is in the form of flat sheets with integral flow passages and appears ideal for solar collector applications. The material is available in aluminum alloys and copper alloys, and virtually any flow passage/manifold design can be fabricated with the silk screen/hot roll process used in manufacturing the Roll-Bond panels. Material cost is the major cost element, such that a cost of about 60 to 70 cents per square foot can be achieved for 0.060-in. thick aluminum Roll-Bond panels. Thinner sheets could be manufactured for less, although current tooling is set up for a minimum thickness of about 0.040 to 0.045 in., depending on material. Connectors can be attached during sheet manufacture, and sheets up to 36 by 110 in. are currently available. As a result of these desirable characteristics this material was selected for use in the MSFC demonstration system.

MSFC's plating facilities would allow application of the electroplating selective coating only on panels of small size. Therefore, a 2-ft wide by 3-ft long nominal panel size was adopted for the MSFC demonstration system. However, as noted above, larger panels could be used in mass-production applications.

3.2 FLOW PASSAGE GEOMETRY DEFINITION

After selecting the Roll-Bond material and the 2- by 3-ft size on the panels, the flow passage geometry had to be defined. There are three basic considerations involved in designing the flow passages and manifolding for the panels:

- Uniform flow distribution throughout the panel is required for good thermal and fluid flow performance.
- A small overall pressure drop through the panel is required to minimize pump power for fluid circulation.

- Passage spacing and sizing must be selected for high fin efficiency and high film coefficient to achieve good thermal performance.

Parametric fluid flow analyses and thermal analyses were conducted to define a design that would have favorable characteristics with respect to each of the three considerations cited above. For design purposes, a flow rate of 0.80 gpm was assumed to flow through the panel; this was calculated based upon locating seven small panels in series to yield about 42 ft² of collector. Under excellent operating conditions, 0.80 gpm flowing through 42 ft² of collector would allow about a 20° F rise in water temperature from inlet to outlet. This was taken to be a reasonable value for the maximum temperature rise.

The results of the parametric analyses indicated that the design shown in Figure 4 would be excellent from fluid distribution, pressure drop, and heat transfer viewpoints. This design utilizes 16 identical flow passages arranged in parallel. The passages are 0.375 in. wide and are spaced on 1.500-in. centers. The manifold is a simple triangular passage designed to feed each of the 16 passages with an equal flow of water. Although not shown in the figure, the manifold flow passage is twice the height of the 16 separate flow passages; i. e., the manifold outside height is 0.250 in. rather than the 0.125 in. used for the individual flow passages. This extra flow area minimizes pressure variations in the manifold.

The predicted thermal performance of the panel for typical operating conditions is shown in Figure 5. As shown in the figure, the temperature difference between plate and water is less than 1.5° F from inlet to outlet; this small temperature differential signifies excellent conductive and convective heat transfer. As also shown in Figure 5, the ΔP through the panel for the given conditions is only 0.04 psi, a totally acceptable value. A test panel was fabricated from plexiglass and a flow visualization test, using dye in water, was performed. The results verified a uniformly distributed flow through all the passages.

Since only a soft aluminum alloy was available as the material for the panels, some supports were included in the manifolds to reduce the unsupported spans in the manifold. These were required to maintain structural integrity under the pressurized conditions at which the collector will operate.

3.3 BACKSIDE INSULATION

The backside of the collector must be insulated to minimize heat losses. A transient thermal analysis of this backside insulation was conducted to

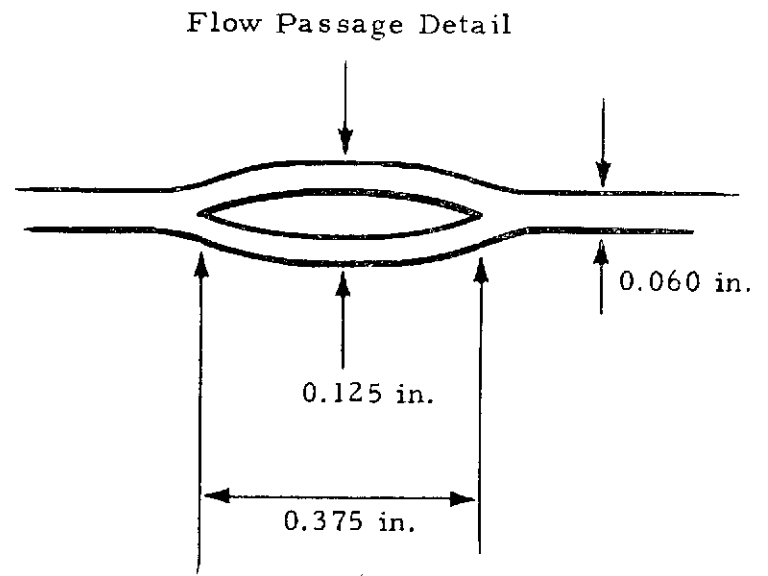
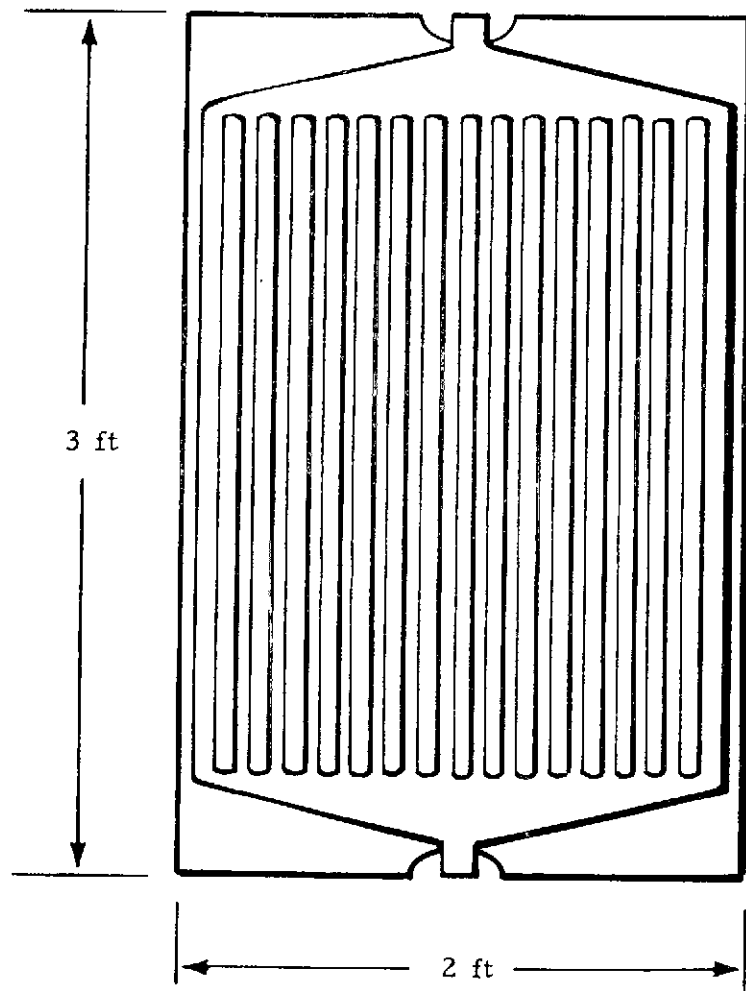
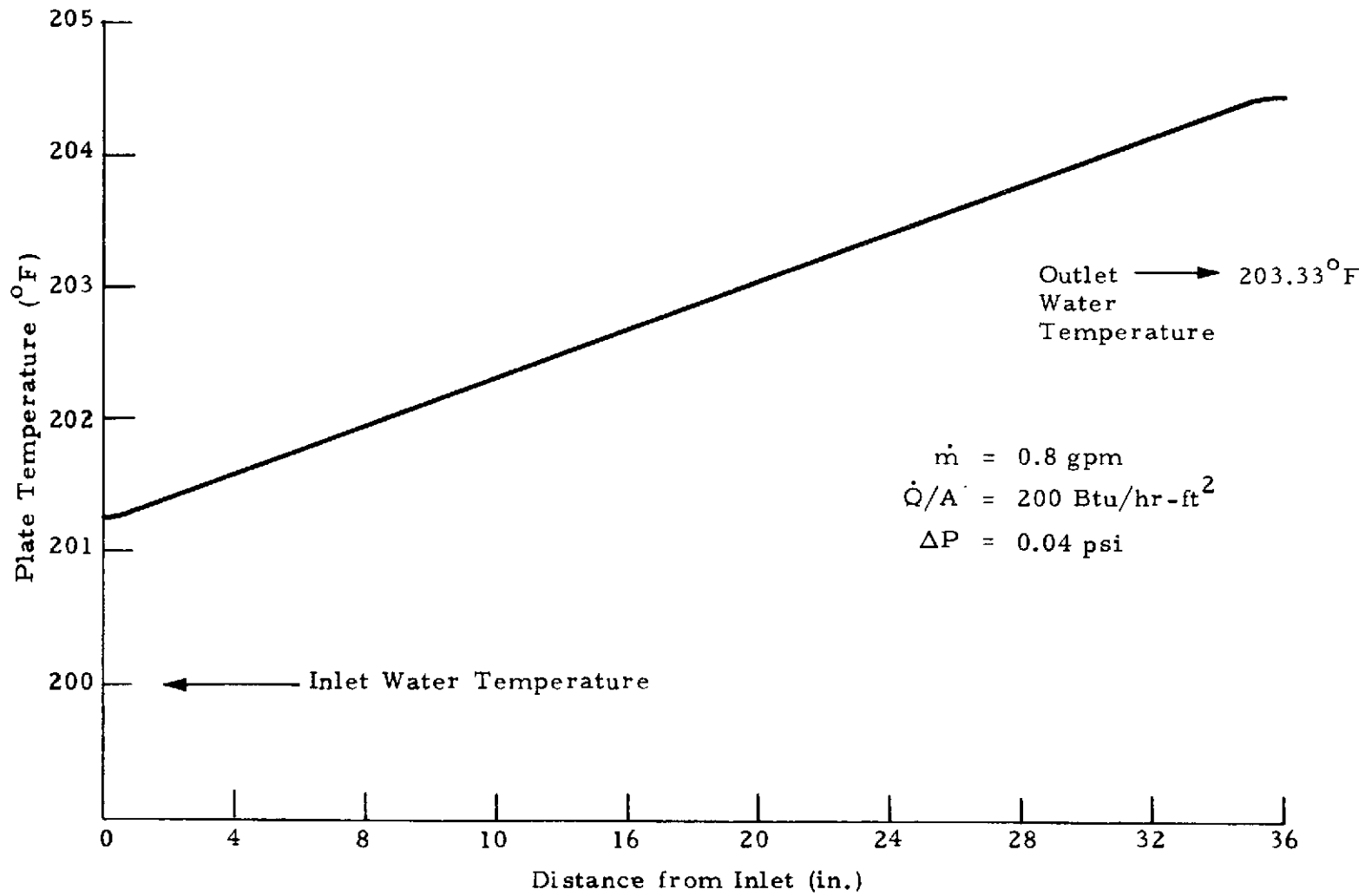


Figure 4. Roll-Bond panel design.



11

Figure 5. Predicted thermal performance of one Roll-Bond panel.

determine its heat transfer characteristics. Fiberglass insulation having a 6-in. thickness was assumed to be subject to a 200°F step jump in Roll-Bond plate temperature. The resultant heat transfer into the insulation is presented in Figure 6, for the given insulation properties. As shown in the figure, the steady-state heat flux of about 8 Btu/ft²-hr is reached in a few hours. This value was considered acceptable and 6 in. of fiberglass insulation were incorporated into the collector design. However, the fact that the heat loss from the plate is more than twice the steady-state value for about 1 hour should be remembered, especially in collector testing where data points are often obtained in quick succession at progressively higher temperatures.

3.4 RADIATION PROPERTIES OF SELECTIVE COATING

Parametric studies were conducted to determine the effect of selective coating properties on collector performance under typical operating conditions. Figures 7 through 10 present the results of these studies for typical clear summer and winter days for both single-glazed and double-glazed collector designs. The operating conditions are specified on the figures, and the solar absorptance and infrared emittance are parameterized. The great benefits of high solar absorptance and low infrared emittance are clearly demonstrated in these figures.

Figures 11 and 12 present comparisons of performance for the single- and double-glazed collectors. The large benefits offered by the double-glazing are apparent in these figures, especially for higher emittance values and lower solar absorptance values.

3.5 WIRE/TEDLAR COMPOSITE

The MSFC collector design will utilize tedlar bonded to a rectangular wire mesh for strength and rigidity. The wire mesh is a 2-in. by 4-in. welded steel mesh fencing material.

The wire mesh has one significant effect on the collector performance. It blocks about 7 percent of the solar radiation incident upon the tedlar, resulting in an effective perpendicular transmittance of 0.85 rather than the 0.92 quoted for plain tedlar.

During preliminary testing, the wire in the tedlar/wire composite transparent cover was observed to reach a much warmer temperature than the tedlar. To explain this effect and determine its magnitude and its dependence on wire surface properties, a thermal analysis was conducted. The results

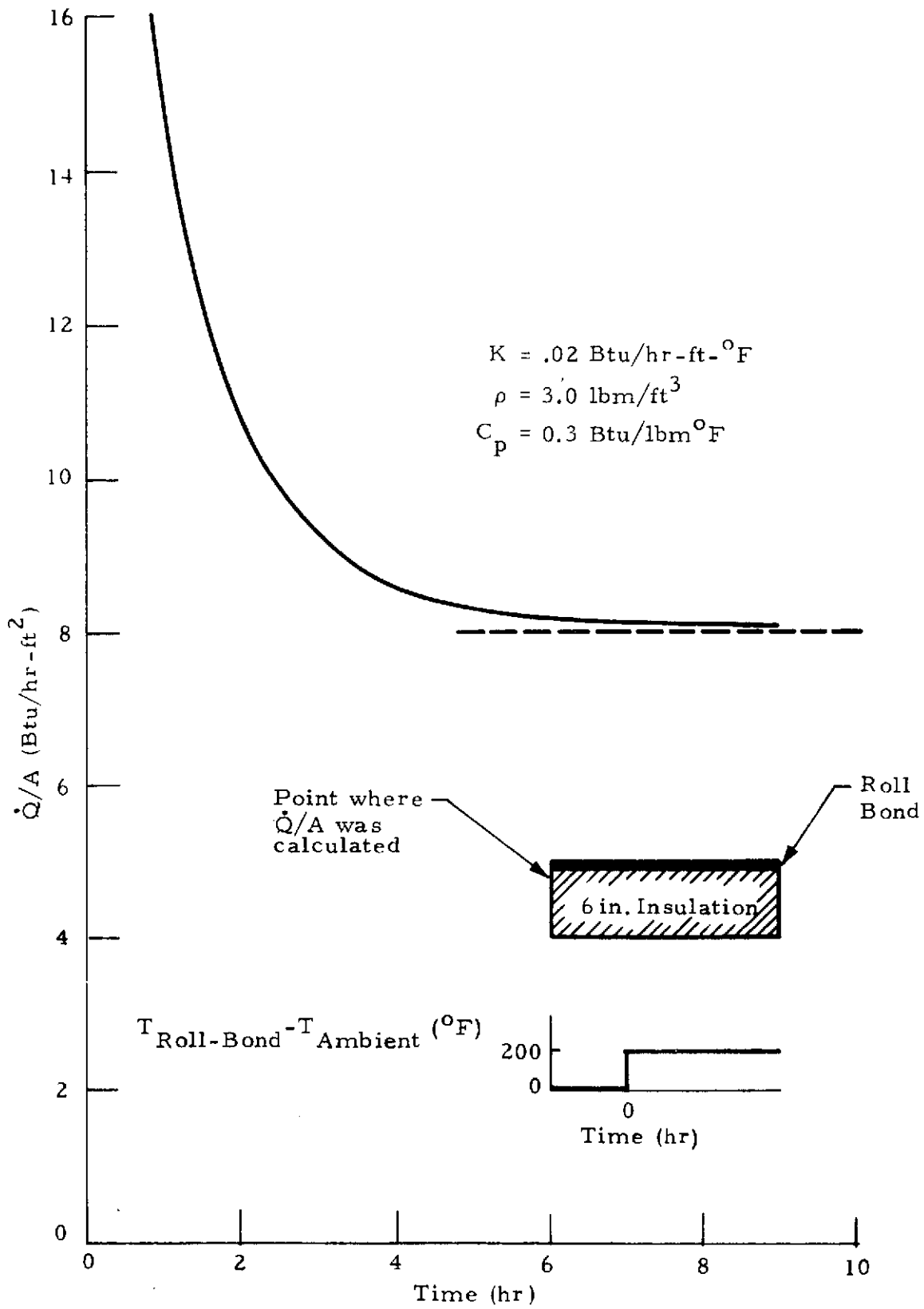


Figure 6. Heat transfer from collector to collector insulation for a step jump in Roll-Bond plate temperature.

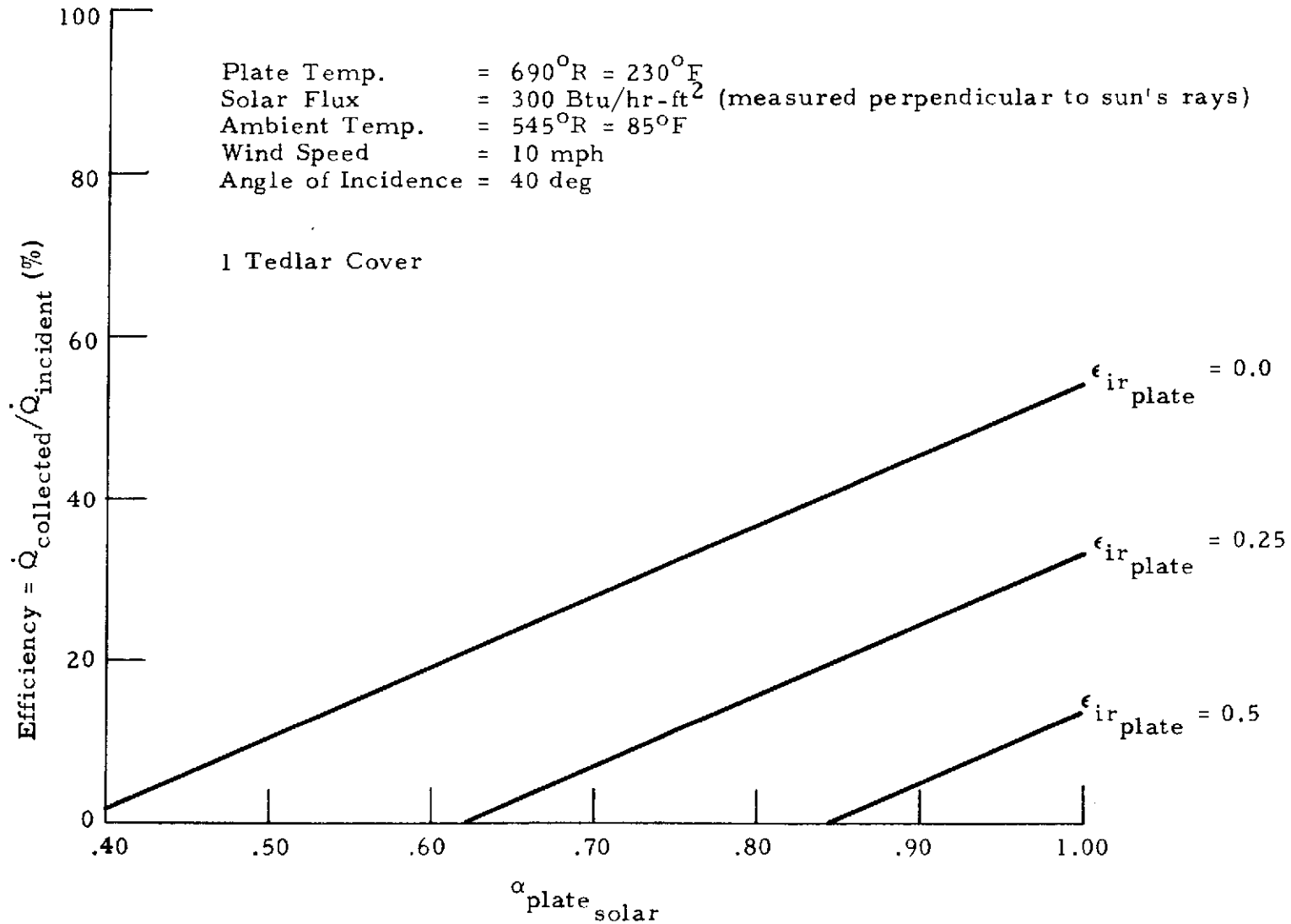


Figure 7. Solar energy collection efficiency for a "typical clear summer day" (one tedlar cover).

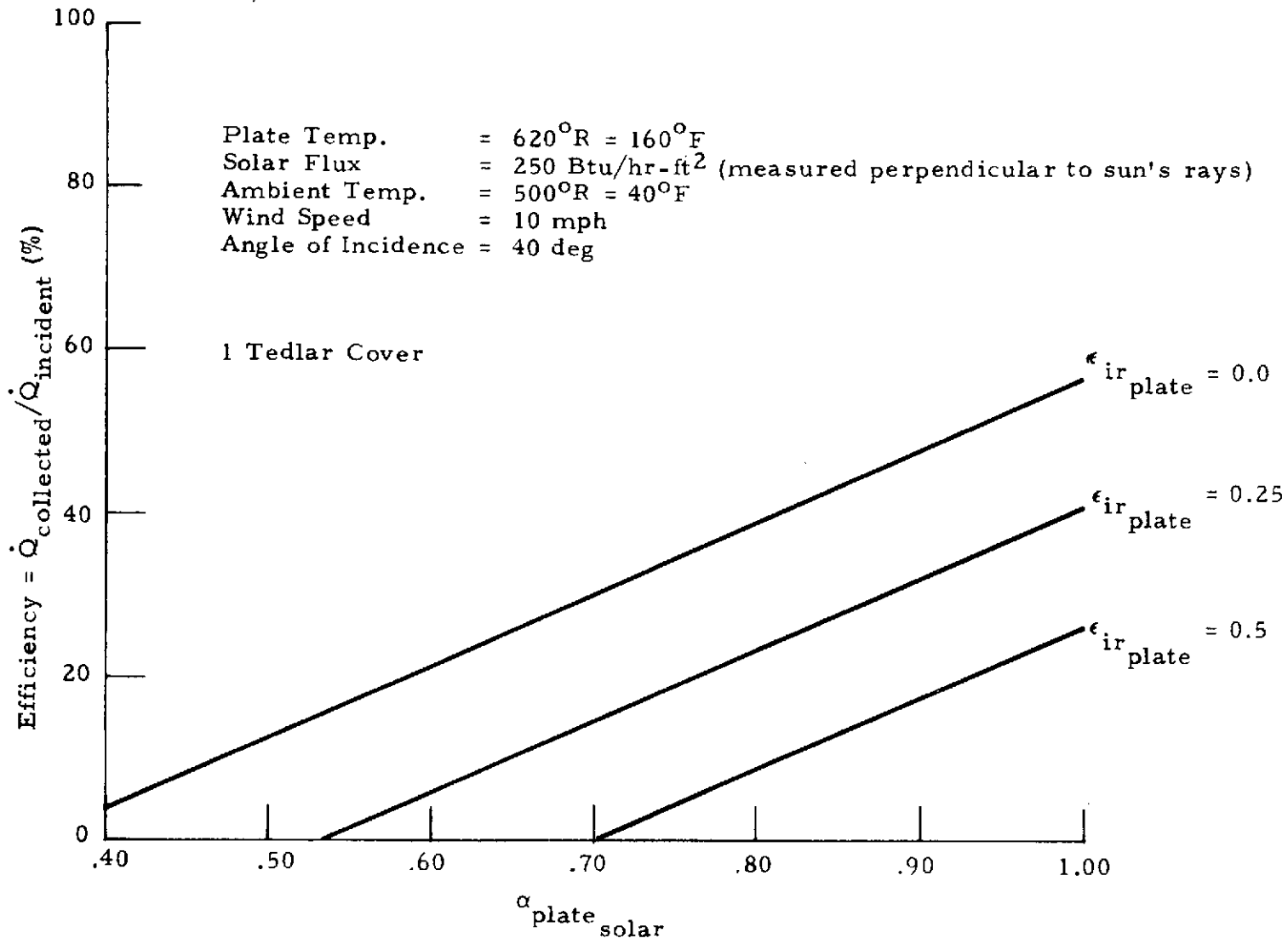


Figure 8. Solar energy collection efficiency for a "typical clear winter day" (one tedlar cover).

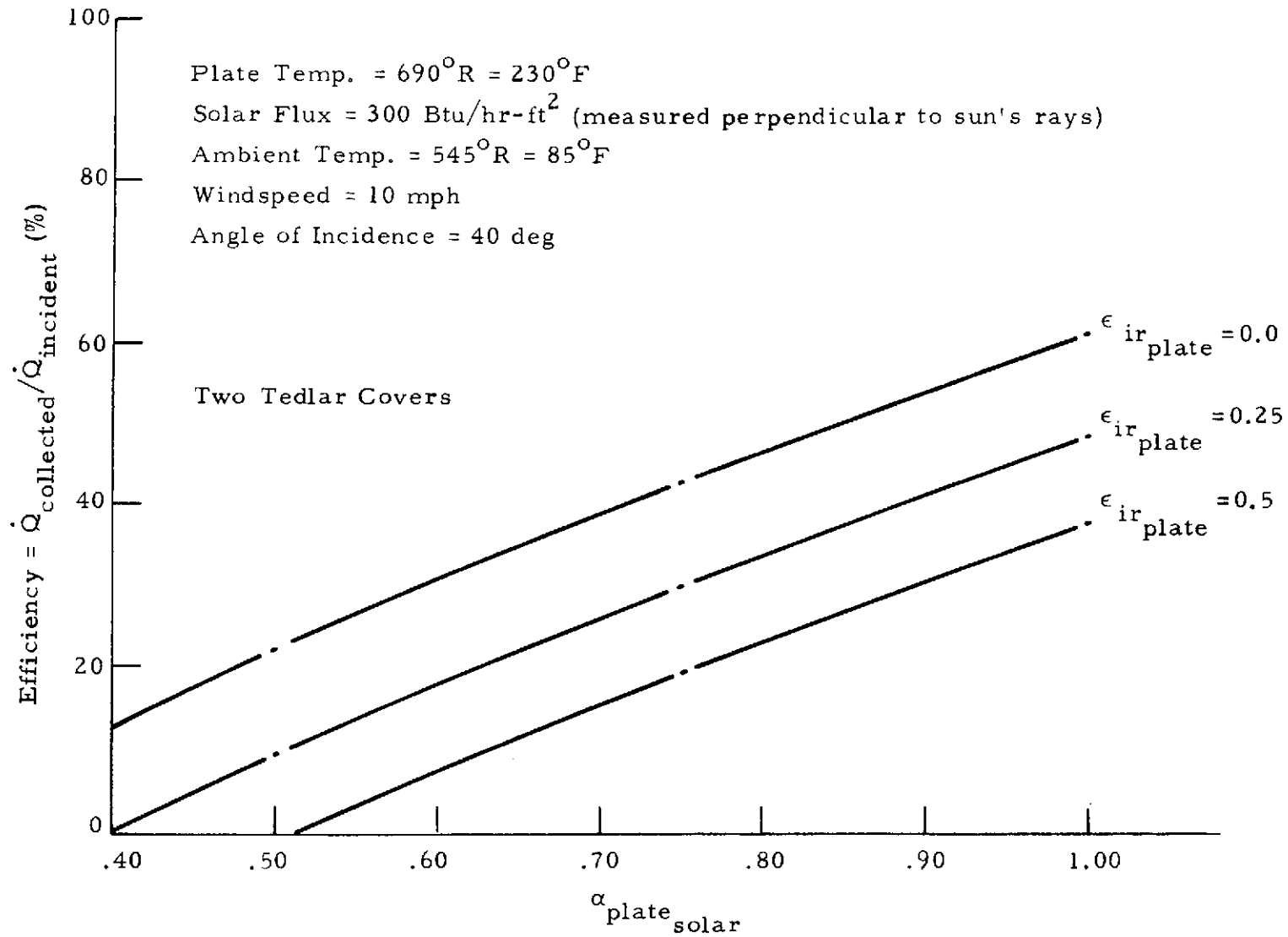


Figure 9. Solar energy collection efficiency for a "typical clear summer day"
 (two tedlar covers).

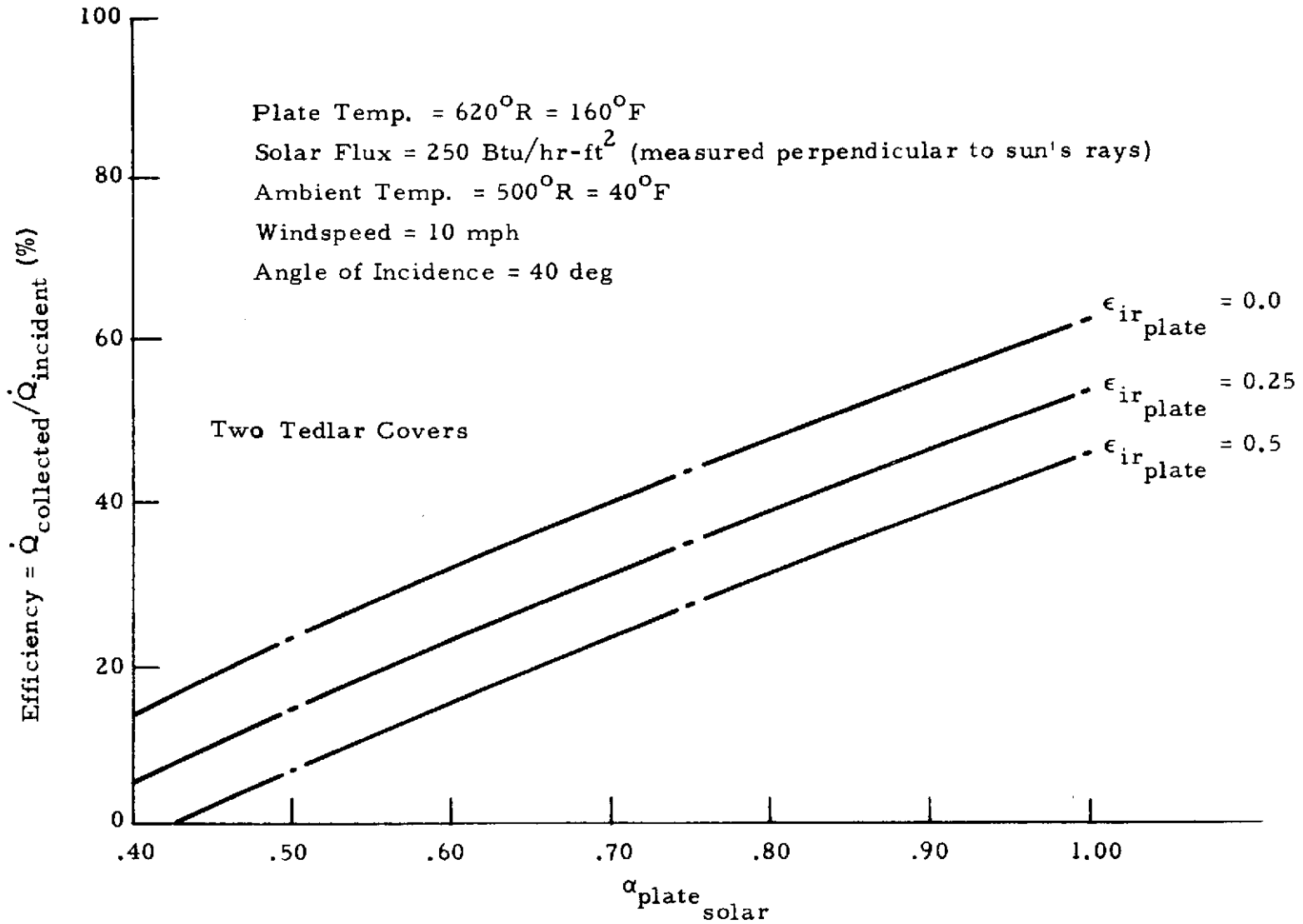


Figure 10. Solar energy collection efficiency for a "typical clear winter day" (two tedlar covers).

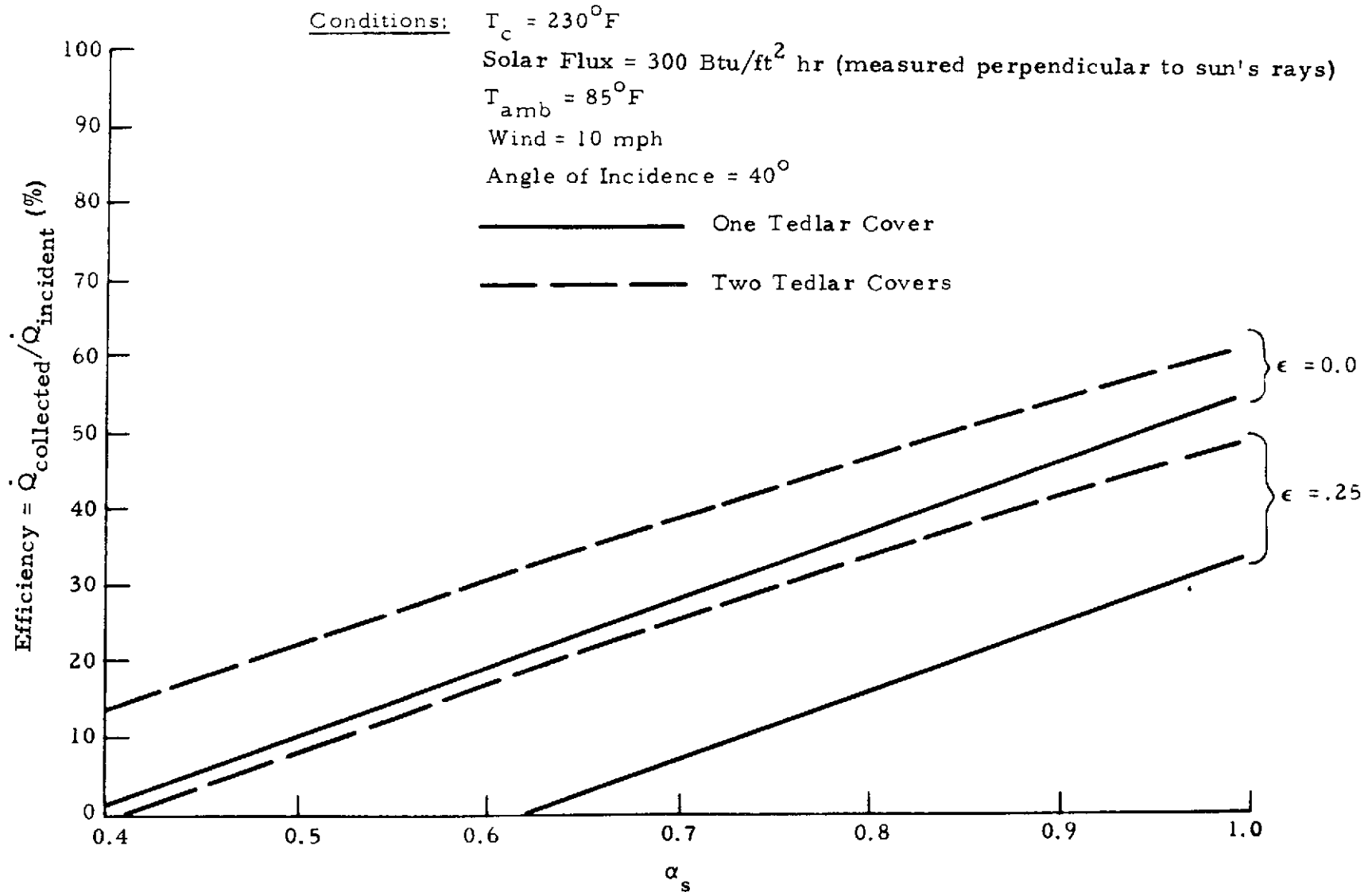


Figure 11. Effect of number of covers on collection efficiency for "typical clear summer day."

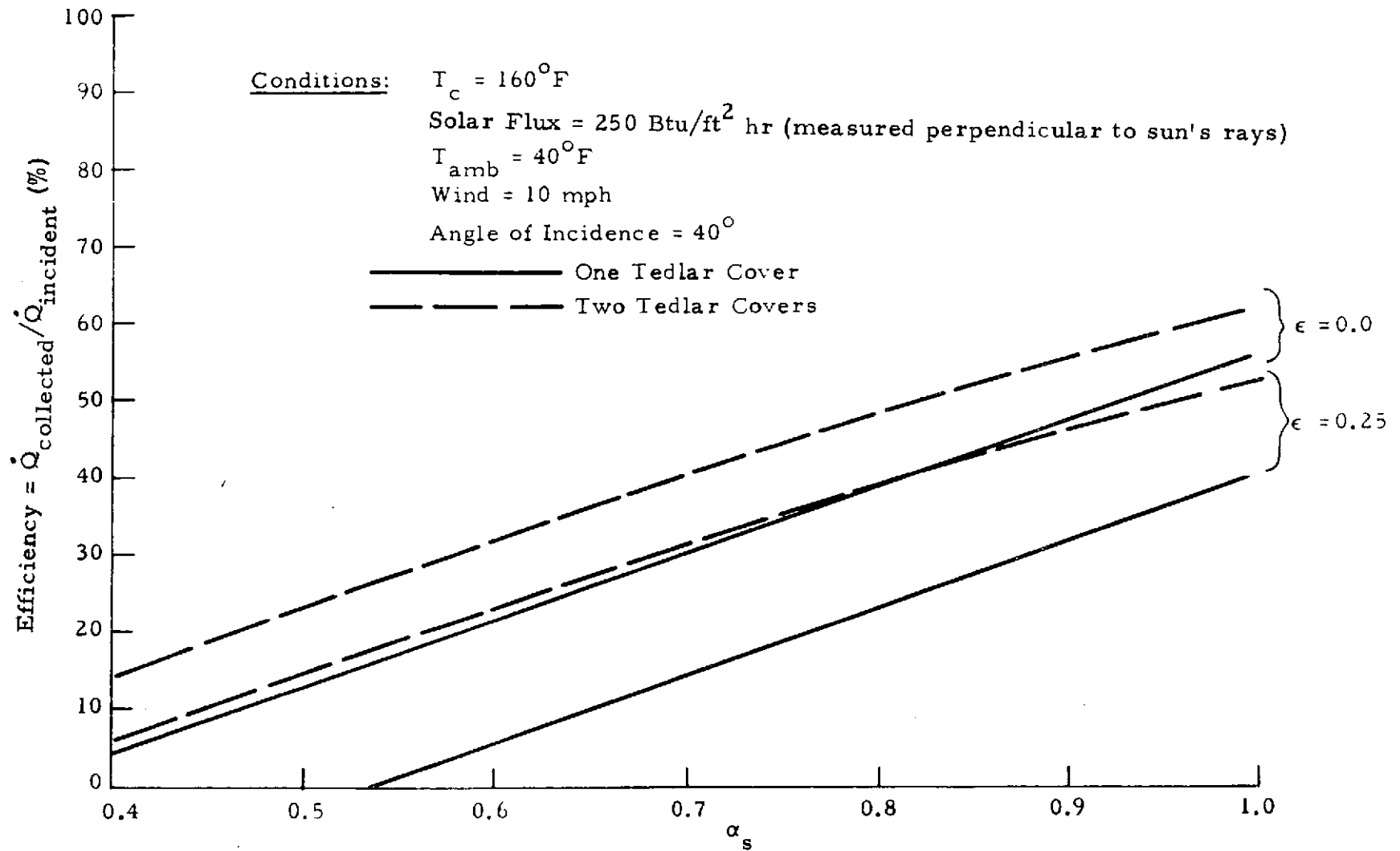


Figure 12. Effect of number of covers on collection efficiency for "typical clear winter day."

are shown in Figure 13. Note that the higher the emittance and the lower the absorptance are, the cooler the wire is. However, the temperature rise of the wire above the tedlar temperature will have no noticeable effect on collector efficiency, and the flexible nature of the adhesive between the wire and tedlar will prevent any thermal stress problems.

3.6 TRANSMITTANCE TEST USING PYRHELIOMETER

To obtain some approximate transmittance data for tedlar samples obtained from Du Pont, a test was conducted on a clear day. A pyrliometer was aimed approximately toward the sun and covered with different combinations of transparent covers. An approximate transmittance value was calculated by dividing the flux with the covers by the flux without covers. The results are presented in Table 1. Note that the tedlar is more transmissive than the glass for both one and two covers. These data are not considered highly accurate because of the test method and because the pyrliometer has not been calibrated for several years. However, these data do indicate that the tedlar is as transmissive as glass or more so, although it appears far less transparent to the naked eye.

3.7 EFFECT OF AGE AND EXPOSURE ON TEDLAR TRANSMITTANCE

Based upon some greenhouse data which has been collected, the effect of age and exposure on tedlar transmittance was evaluated. The spectral transmittance curves for a new piece of 4-mil thick tedlar and for a 5 year old piece exposed for that period in Florida are presented in Figure 14.

The area between the curves represents the degradation in transmittance, about 4 percent. Thus, the degradation with time should be about 1 percent per year. However, these transmittance curves both indicate an overall solar transmittance of about 70 percent, much lower than for the material to be used in the solar collector. Thus, the greenhouse data may be for tedlar containing an ultraviolet "screen" to block some of the shorter wavelength radiation. Hopefully, the degradation with age and exposure of the actual tedlar to be used will be as small as for the greenhouse tedlar.

3.8 COMPARISON OF EXPERIMENTAL COLLECTOR PERFORMANCE WITH ANALYTICAL PREDICTIONS

During the first quarter of 1974, testing of a solar collector module of approximately 40 ft², oriented southward with a 45-deg tilt off horizontal was initiated. The results of three quasi-steady-state tests are presented in

"Typical Clear
Summer Day"

Solar Flux = 300 Btu/hr ft² (measured perpendicular
to sun's rays)
T_{plate} = 230°F
T_{ambient} = 85°F
Wind = 10 mph
Angle of Incidence = 40°
One Tedlar Cover
T_{Tedlar} = 104°F

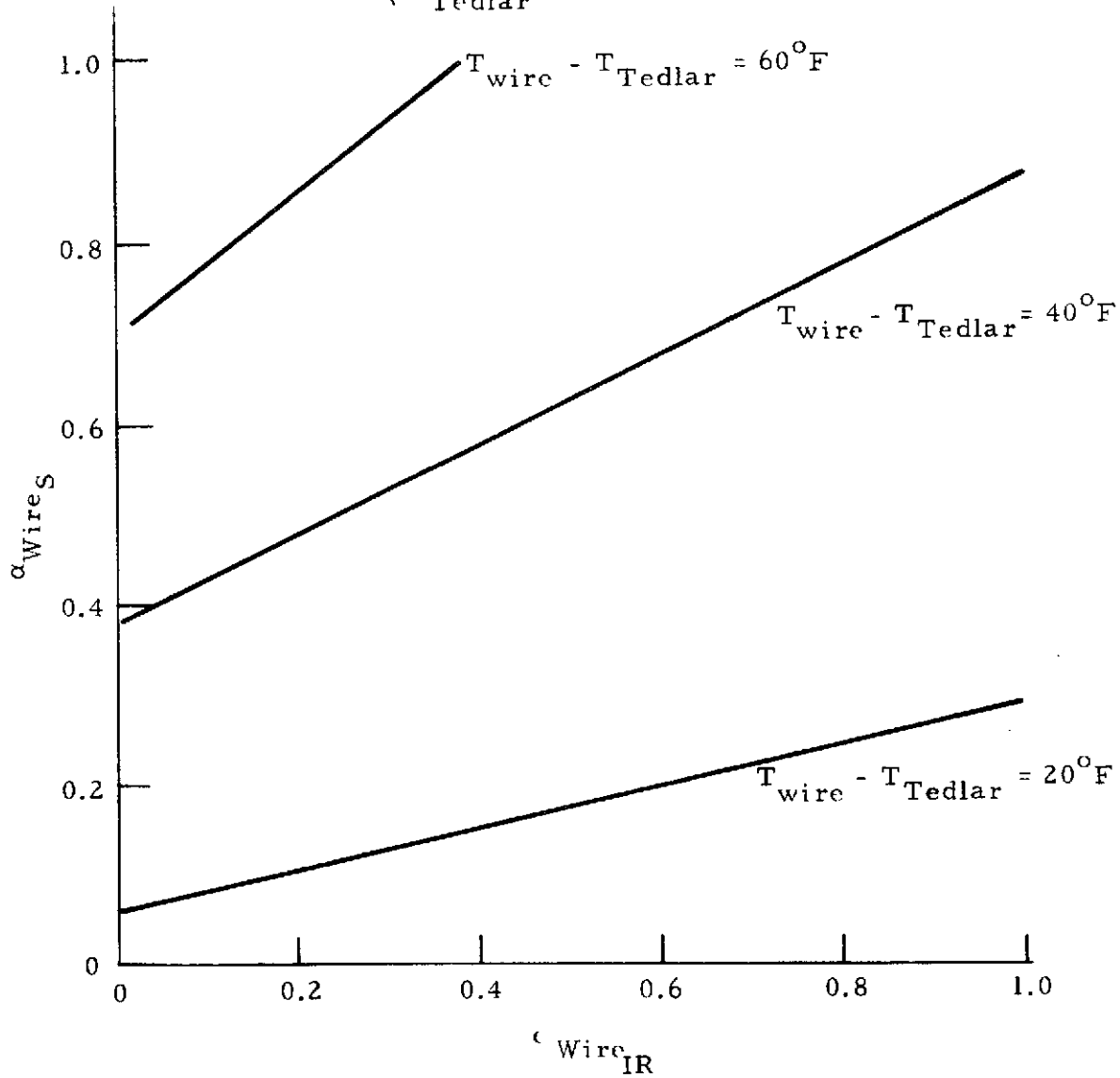


Figure 13. Wire equilibrium temperature.

TABLE 1. RESULTS OF TRANSMITTANCE TEST
 (~10 a.m., November 16, 1973)

Mean Solar Flux \approx 272 Btu/hr ft²

Test Number	Covers	Flux (Btu/hr ft ²)	$\tau_{\text{effective}}$
1	1 glass *	242	89%***
2	2 glass	210	77%
3	1 Tedlar **	244	90%
4	2 Tedlar	232	85%
5	1 glass + 1 Tedlar	222	82%

*The glass samples were 3/32-inch laboratory glass plates.

**The Tedlar samples were 4-mil sheets.

***The accuracy of these data is not known. They are presented primarily to show the comparative transmittances of glass and Tedlar.

Percentage of Solar Constant
Falling Below Wavelength λ

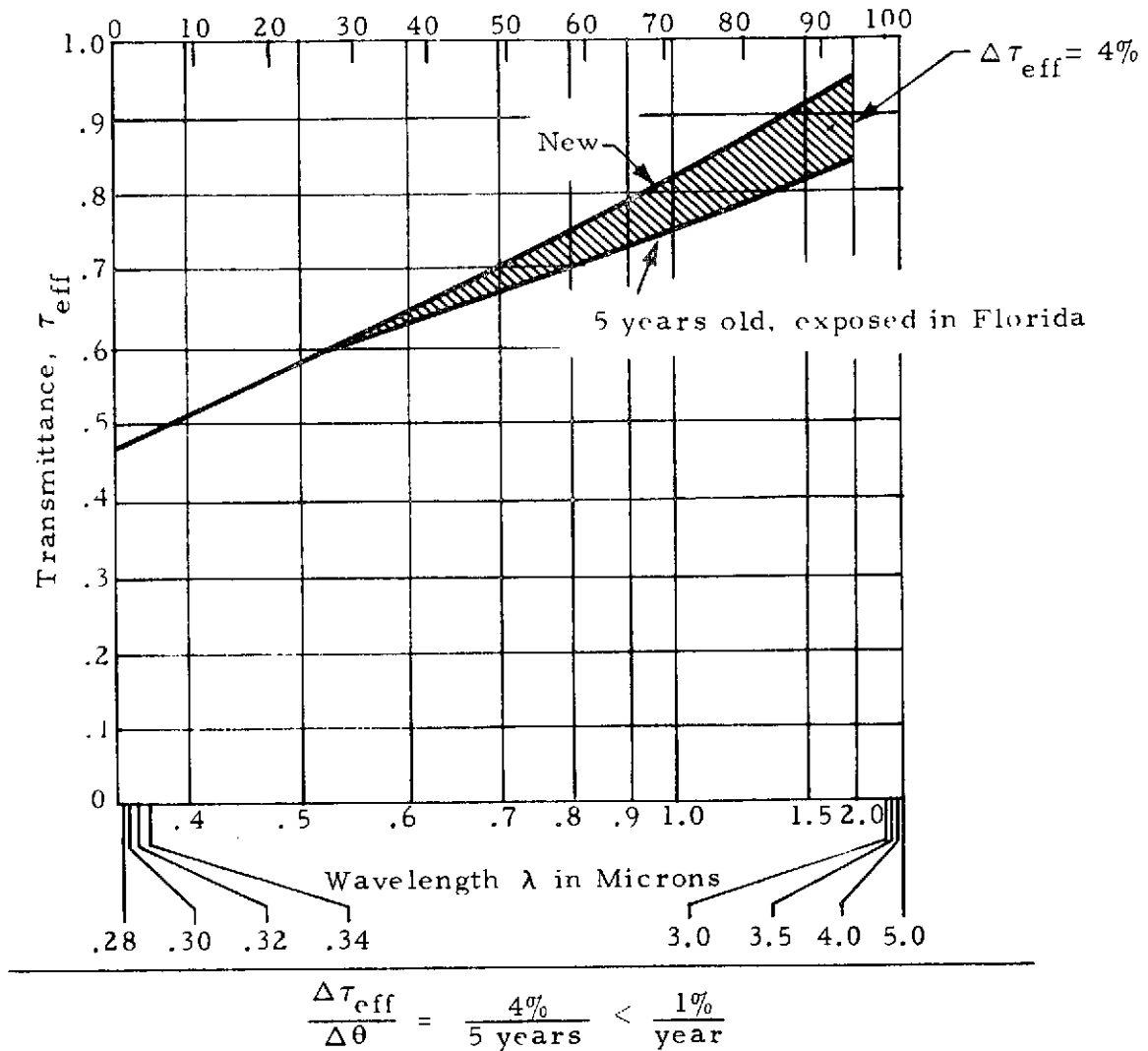


Figure 14. Effect of age and exposure on transmittance of 4-mil thick tedlar.

Figures 15 and 16, although more than 20 tests have been conducted. Also presented in the figures are predictions of collector performance for the measured meteorological conditions (solid curves). The experimental points are below the solid, prediction curve for all three tests. To investigate these relatively small discrepancies between theory and test, a simplified thermal analysis of the edge losses was conducted. When the calculated edge losses

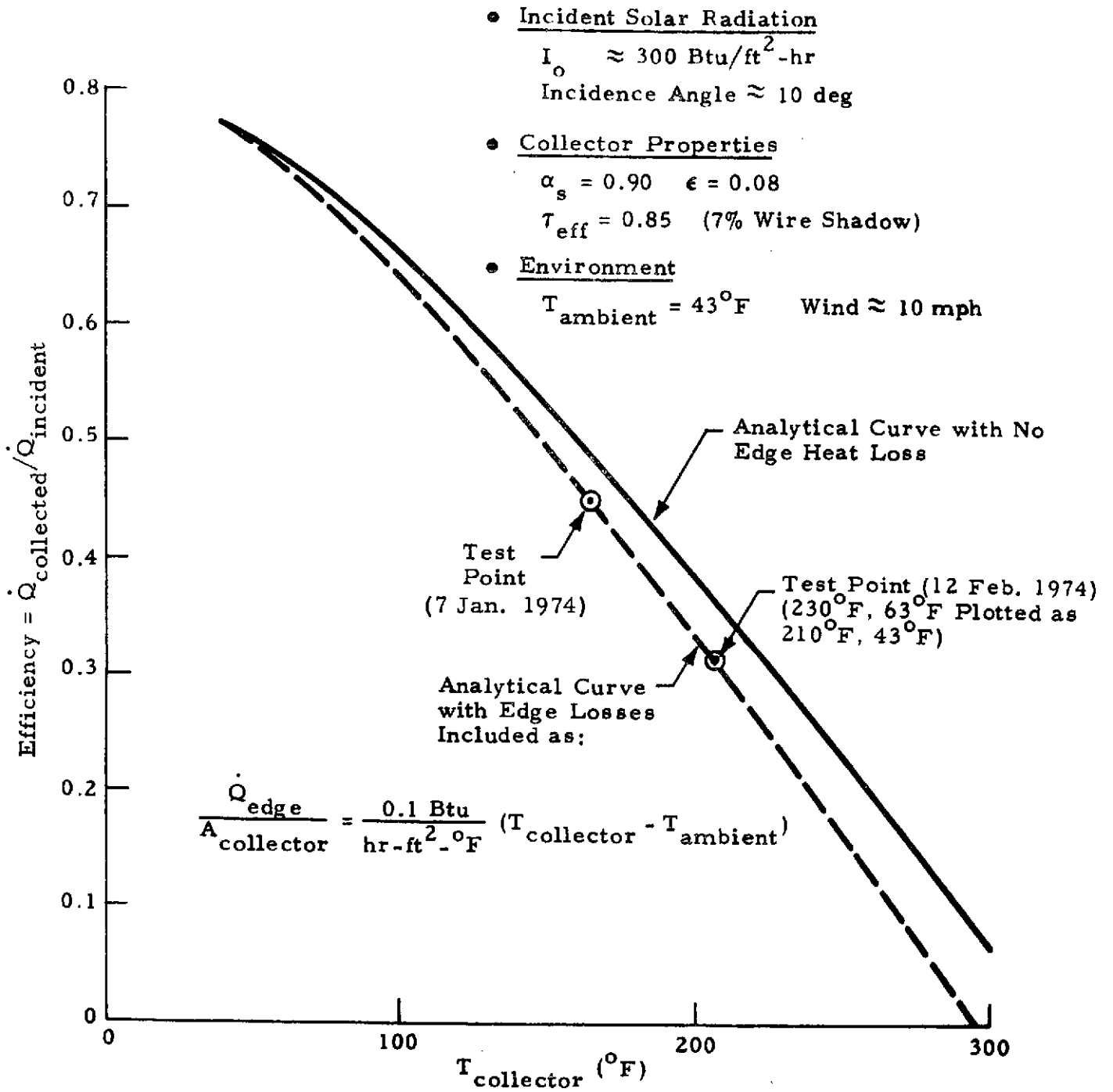


Figure 15. Analytical experimental comparison for solar collector test.

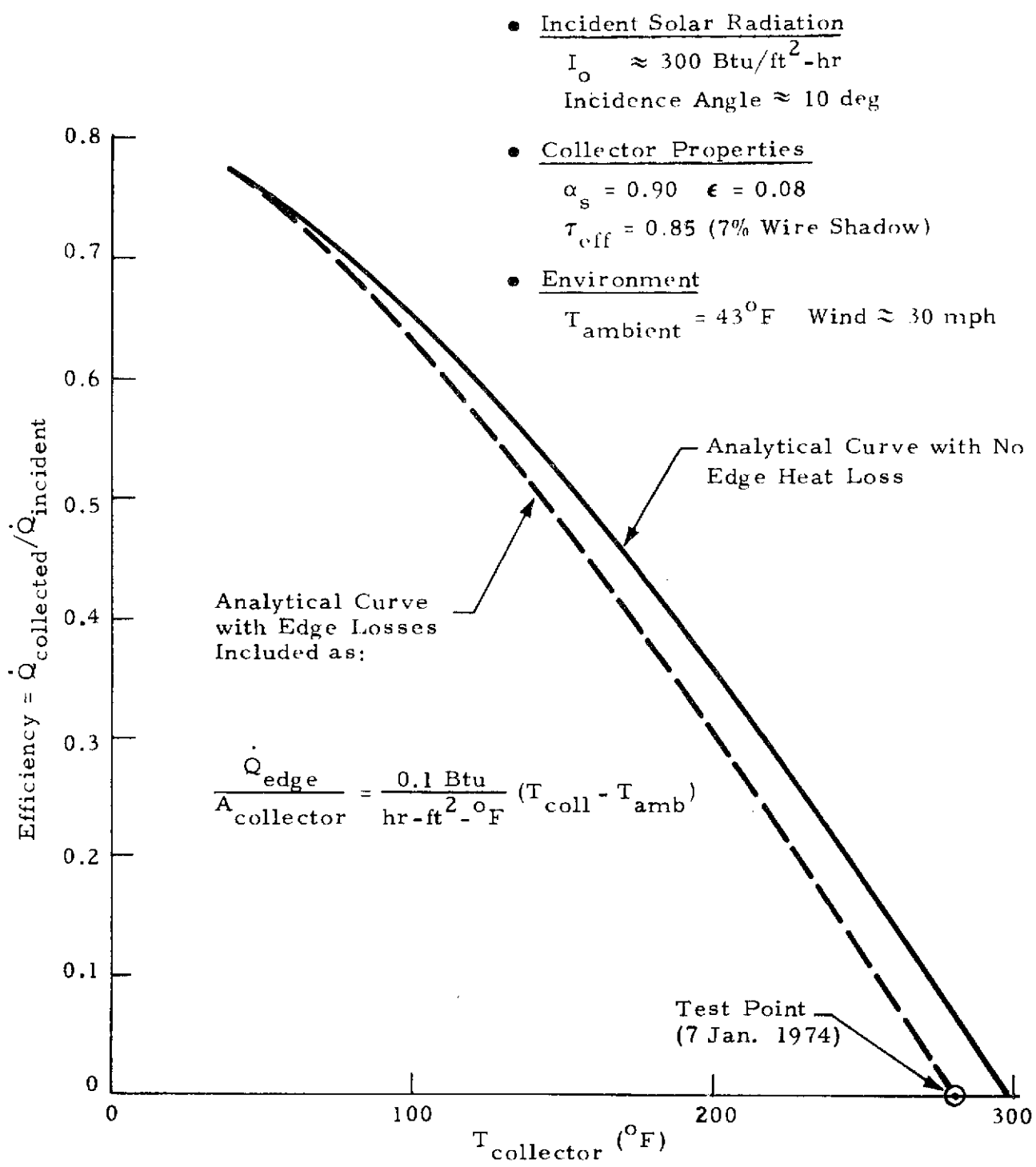


Figure 16. Analytical experimental comparison for 280°F solar collector test.

are included in the collector analysis, the dashed-line efficiency curves of Figures 15 and 16 are obtained. Clearly, the comparison between the dashed-line curves and test points shows excellent correlation, within about 1 percent in each case.

Based upon these data, the design for the full-scale, 1300 ft² collector has been modified to reduce or eliminate the edge losses. Figures 17 and 18 present schematics of all of the energy flows about the collector for two of the test points. These indicate the relative magnitudes of the different energy exchange mechanisms involved.

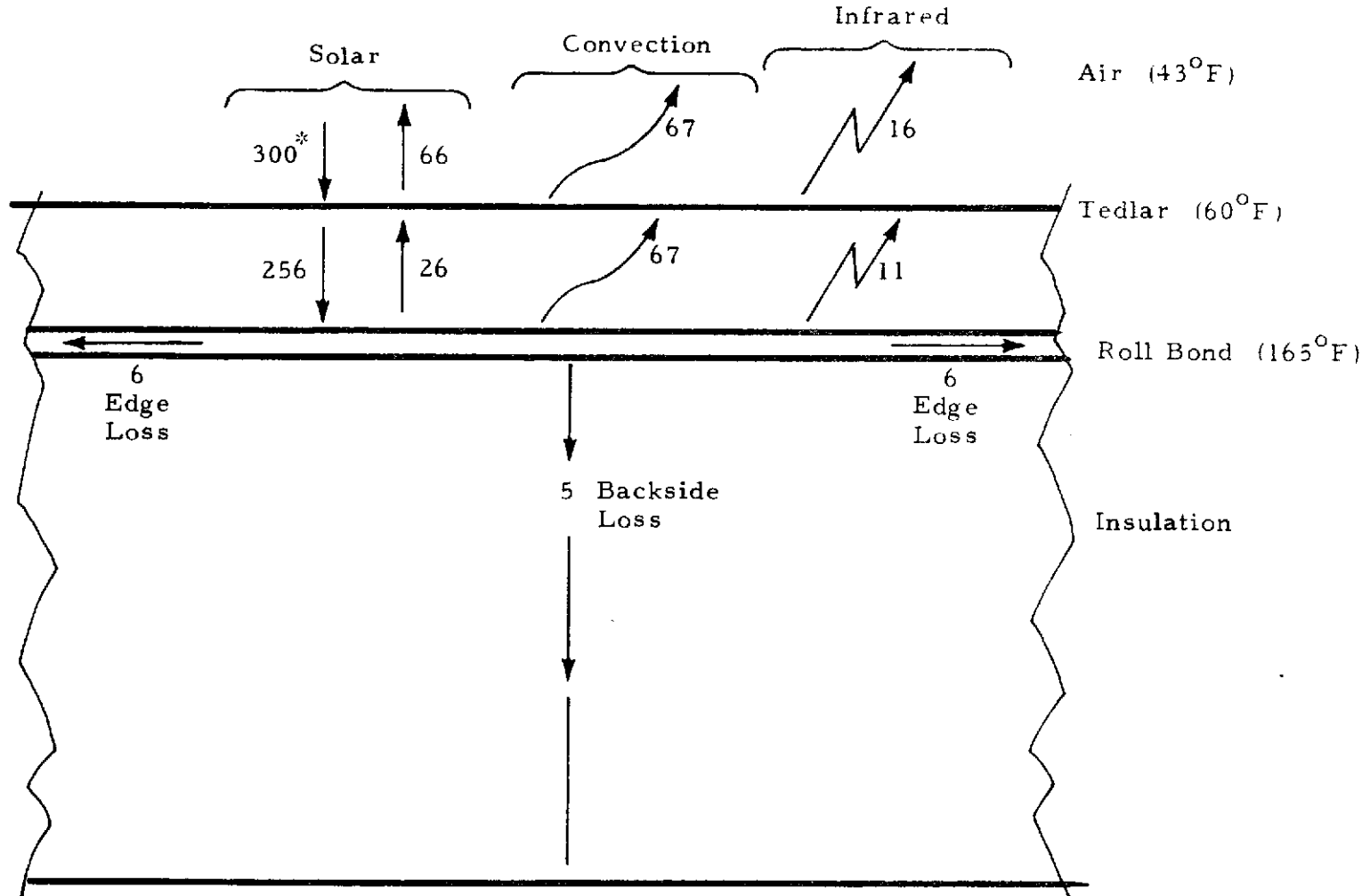
3.9 SOLAR FLUX AND INCIDENCE ANGLE EFFECTS

To extrapolate the findings discussed above to summer operation of the collector, analytical studies were conducted assuming typical summer conditions. Figure 19 presents the results of a study of the effect of solar flux on collector efficiency. The three curves show the performance of three collector designs as labeled. The effect of edge loss is seen to be greater at lower fluxes than at higher fluxes. Also, the performance of a two-cover collector is seen to be far superior to a one-cover collector at lower solar flux levels.

Figure 20 presents the results of a study of the effects of incidence angle on collector performance. The incidence angle is measured between the sun's rays and a vector normal to the collector. Again, both the performance degradation due to edge loss and the performance improvement offered by two covers are seen to be of greatest importance at large incidence angles. Interestingly, the daily average incidence angle during the cooling season, when defined as

$$\theta_{\text{average}} = \cos^{-1} \left[\frac{\int_{\text{Sunrise}}^{\text{Sunset}} \cos \theta \, dt}{t_{\text{sunset}} - t_{\text{sunrise}}} \right],$$

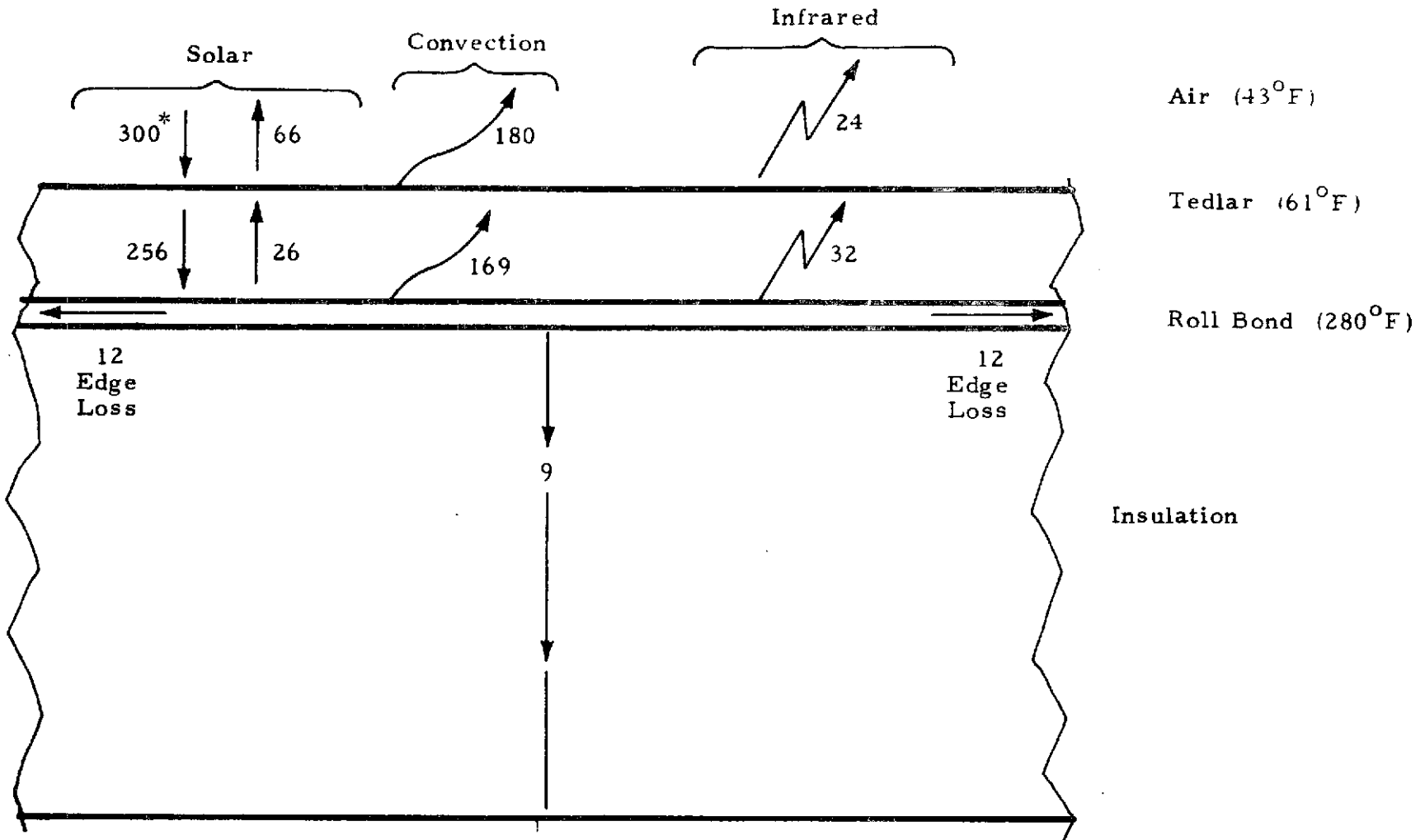
varies from about 55 deg in early summer to about 50 deg in early fall for the MSFC collector with its 45-deg tilt.



*NOTE: All energy flows are Btu per hr per ft² of collector area.

$$\text{Efficiency} = \frac{256 - 26 - 67 - 11 - 5 - 6 - 6}{300} = 45\%$$

Figure 17. Energy flows for 165°F collector test.



* NOTE: All energy flows are Btu per hr per ft² of collector area.

$$\text{Efficiency} = \frac{256 - 26 - 169 - 32 - 9 - 12 - 12}{300} = -1\% \approx 0\%$$

Figure 18. Energy flows for 280°F collector test.

Typical Summer Day

$T_{\text{collector}} = 230^{\circ}\text{F}$

$T_{\text{ambient}} = 80^{\circ}\text{F}$

Wind = 10 mph

Incidence Angle = 0

$\epsilon = .08$

$\alpha_s = .90$

$\tau_{\text{eff}} = .85$

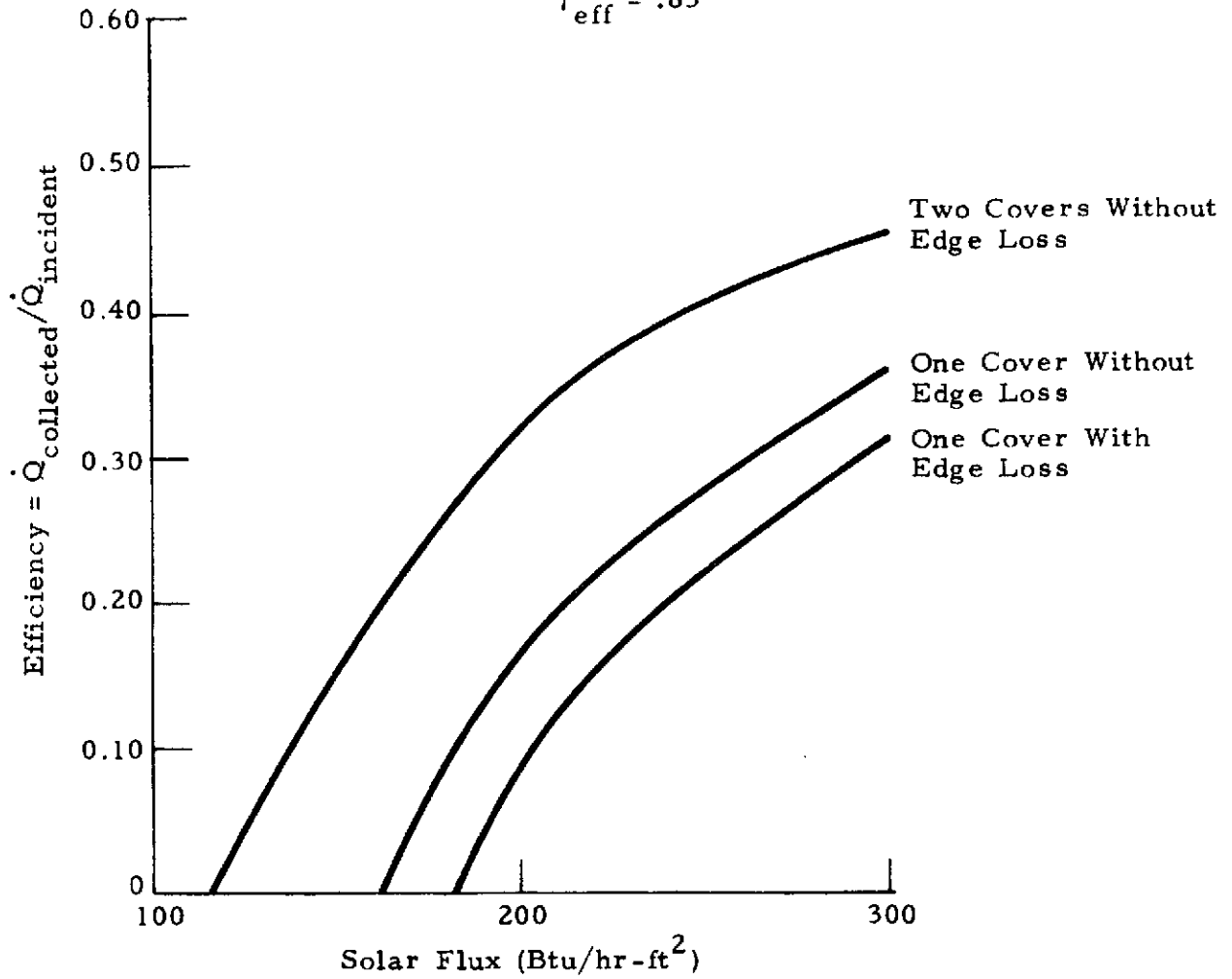


Figure 19. Effect of solar flux on collector performance.

Typical Clear Summer Day

$T_{\text{collector}} = 230^{\circ}\text{F}$

$T_{\text{ambient}} = 80^{\circ}\text{F}$

Wind = 10 mph

Solar Flux = 300 Btu/hr ft^2 (measured perpendicular to sun's rays)

$\epsilon = .08$

$\alpha_s = .90$

$\tau_{\text{eff}} = .85$

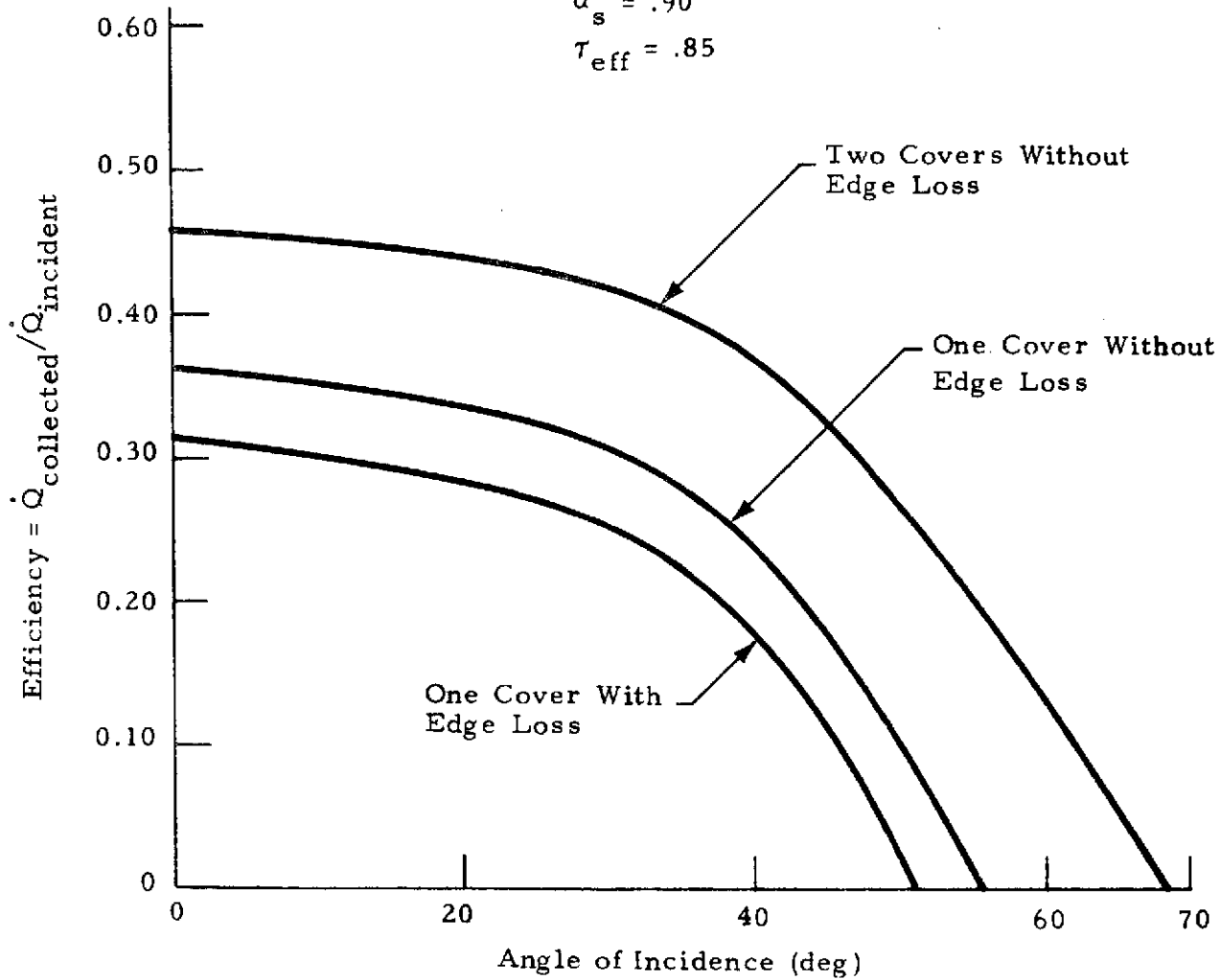


Figure 20. Effect of incidence angle on collector performance.

3.10 FURTHER TILT ANGLE STUDIES

Figure 21 presents an interesting comparison of the total daily insolation on surfaces tilted toward the equator at different tilt angles. These curves

were calculated for Huntsville's latitude. No atmospheric effects were treated — just the geometrical effects of the sun-earth astronomy. Clearly, the 45-deg angle chosen for the MSFC test system is a reasonable choice. It is biased in favor of winter operation, but not so much as to greatly degrade summer operation. Section 5 presents results of some total system performance studies of tilt angle effects which further substantiate the 45-deg tilt angle as being a good year-round choice for Huntsville.

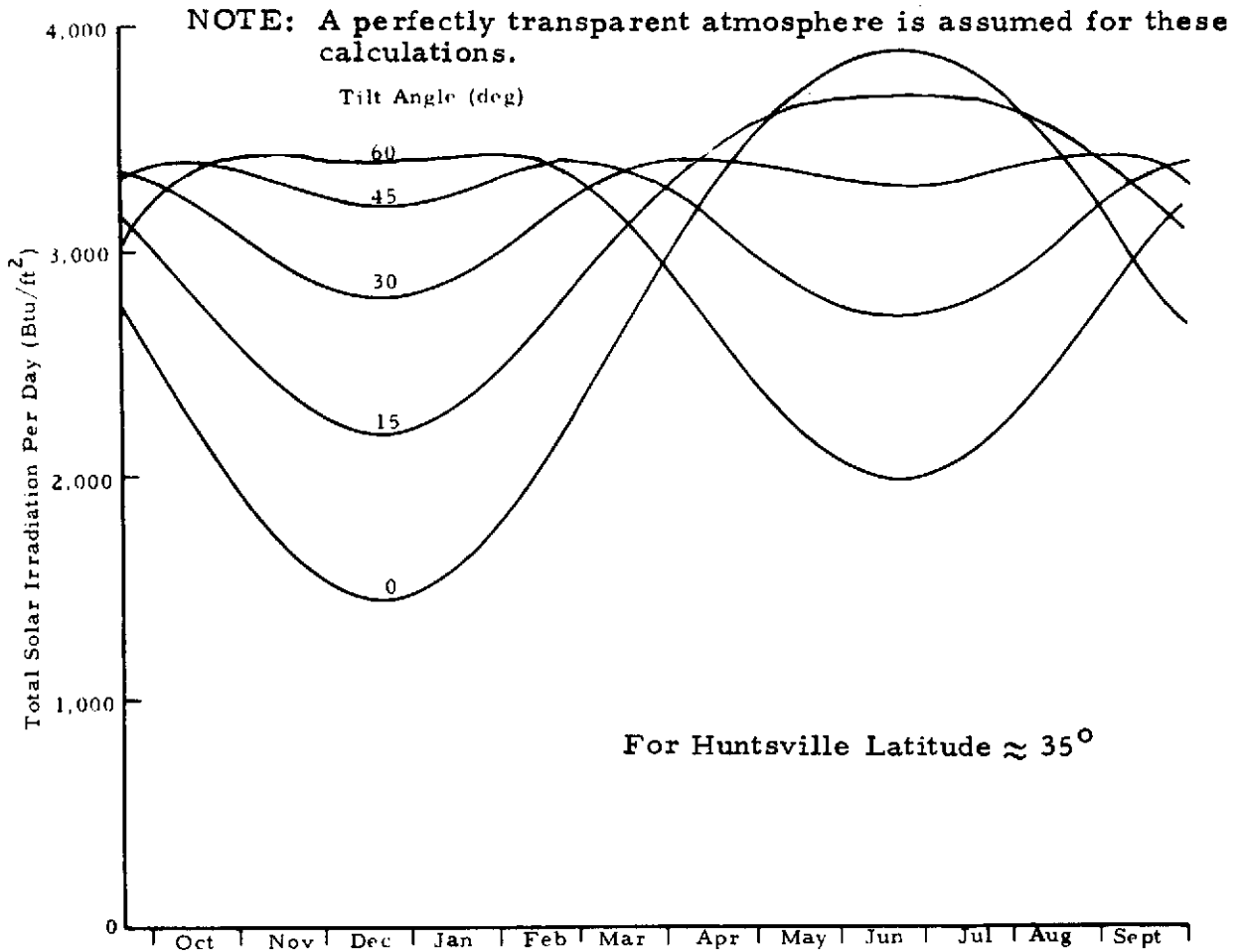


Figure 21. Seasonal variation in ideal solar irradiation for various tilt angles (measured from horizontal).

SECTION 4. ENERGY STORAGE SYSTEM STUDIES

Storage system studies were concentrated in the three areas discussed below.

4.1 TANK SELECTION

Several potential water storage tanks were available at MSFC as surplus material. These tanks varied in size and condition. The tank in best condition was a 4700-gal aluminum tank. This tank would correspond to about 39 000 lbm of energy storage mass if filled with water. Figures 22 through 24 can be used to determine how this tank would work in the total system under consideration.¹ These figures show the effect of varying maximum temperature (which sets the maximum tank pressure), collector area, and storage tank capacity with regard to auxiliary energy requirements. Current plans are to use a collector area of 1300 ft². Accordingly, the figures show that a 34 000 lbm (4200 gal) tank will result in a reasonably small auxiliary energy requirement for any reasonable maximum temperature. Therefore, a 4200-gal water storage system was selected as fully adequate for the demonstration program.

4.2 TANK INSULATION SELECTION

Several materials were considered as insulation candidates, but selection was quickly narrowed to a loose fill fiberglass insulation. The primary criterion used in selecting fiberglass was cost. Table 2 is a properties table that was compiled for the selected material. As the table shows, this material is reasonably cheap. It takes about \$450 to fill the box illustrated in Figure 25, even at a density of 3 lb/ft³. No conductivity data could be obtained at a mean temperature of 150° F, but it should be around 0.025 Btu/hr-ft-° F, based upon extrapolation from reported values.

4.3 THERMAL ANALYSIS OF TANK

Thermal analyses were performed on the water storage tank to be used in the solar home prototype heating and cooling system. These studies were

1. The data presented in these figures were generated early in the study and do not include the effects of building thermal inertia, a finite allowable temperature band within the building, and other beneficial features included in the later total system performance analyses discussed in Section 5. Also, it was decided after choosing the tank to utilize a single-glazed collector rather than the double-glazed collector used to generate these figures. Therefore, please refer to Section 5 for more accurate total system performance predictions.

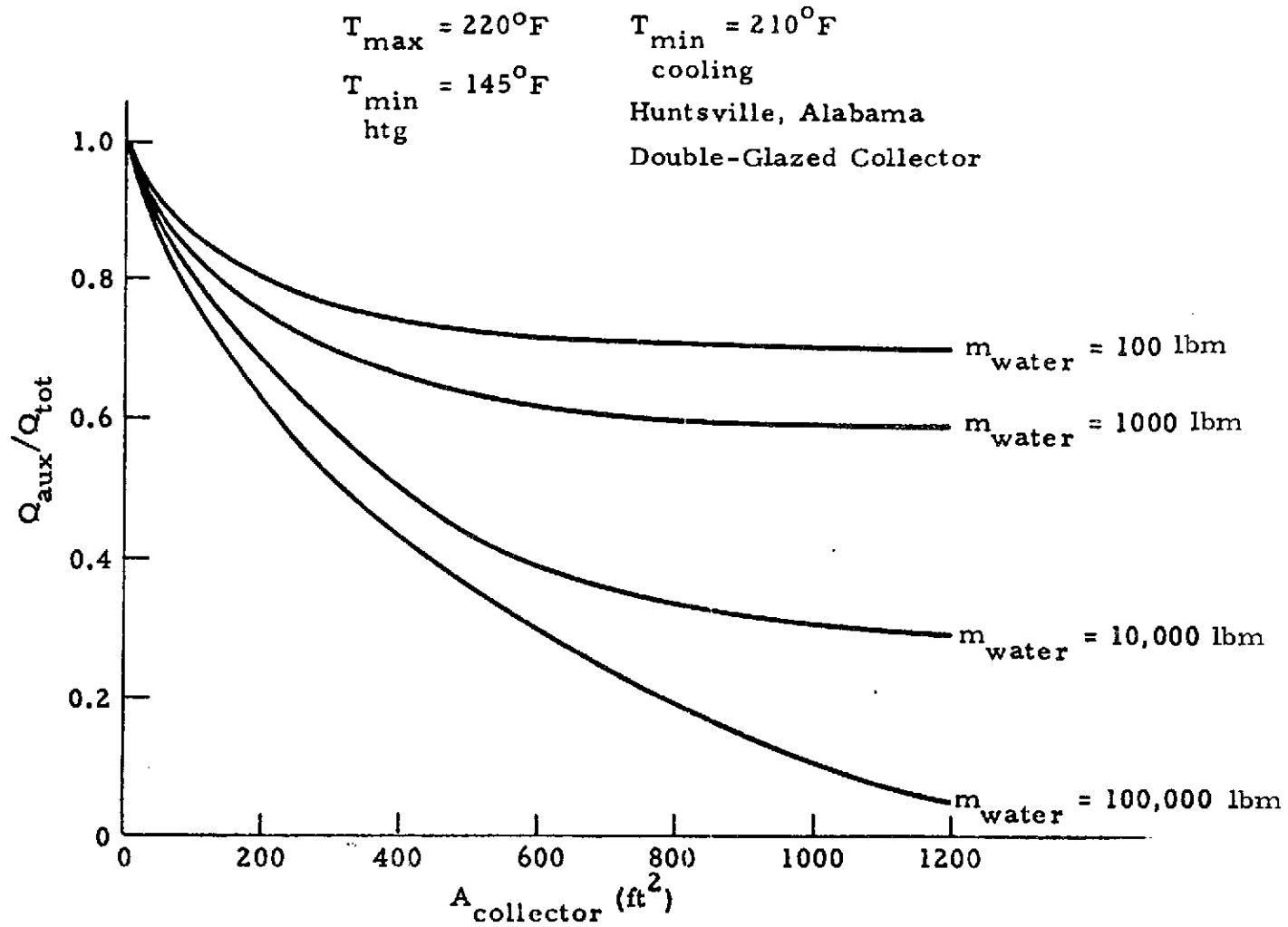


Figure 22. Auxiliary heat required for different collector areas and energy storage system capacities ($T_{\max} = 220^{\circ}\text{F}$).

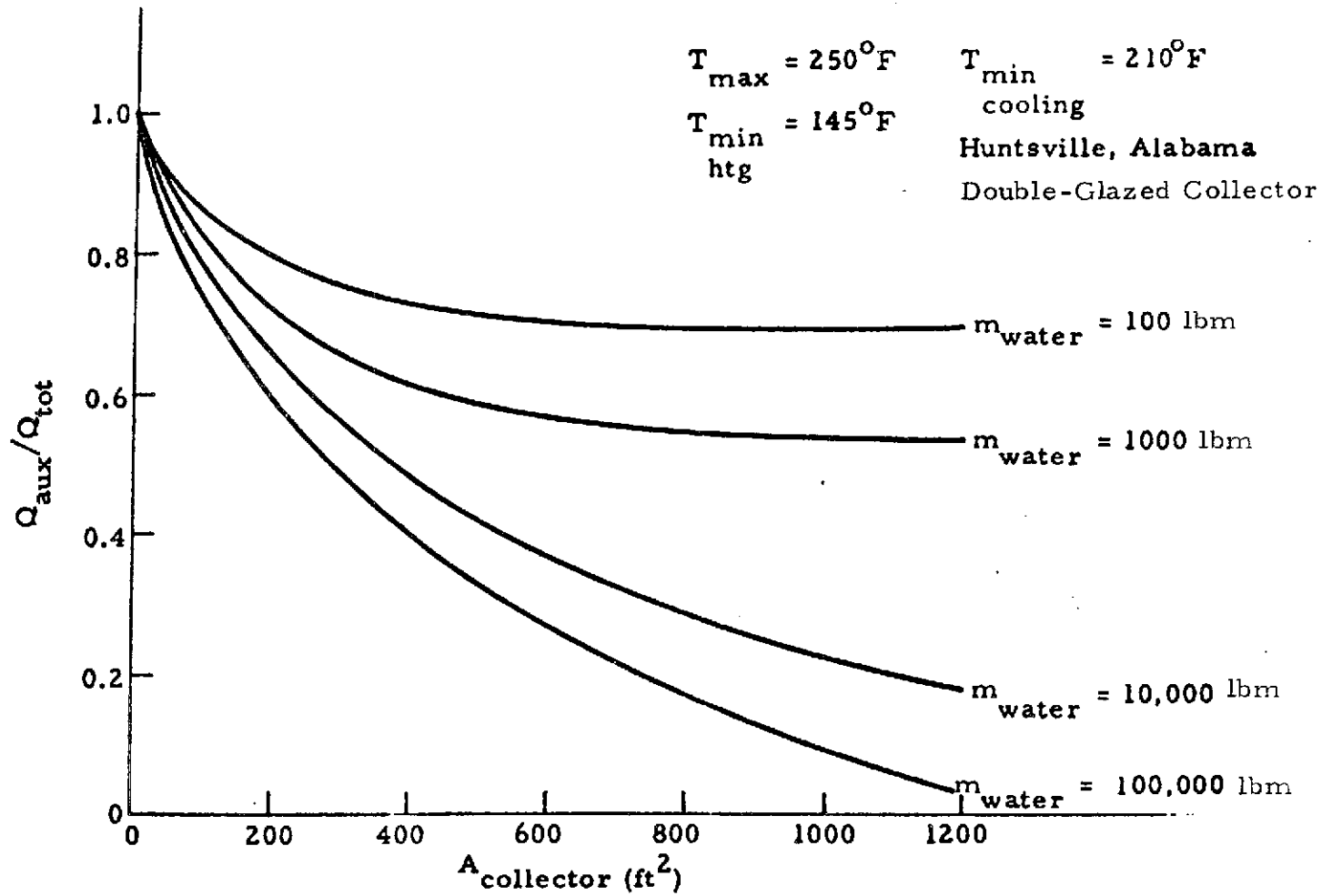


Figure 23. Auxiliary heat required for different collector areas and energy storage system capacities ($T_{\max} = 250^{\circ}\text{F}$).

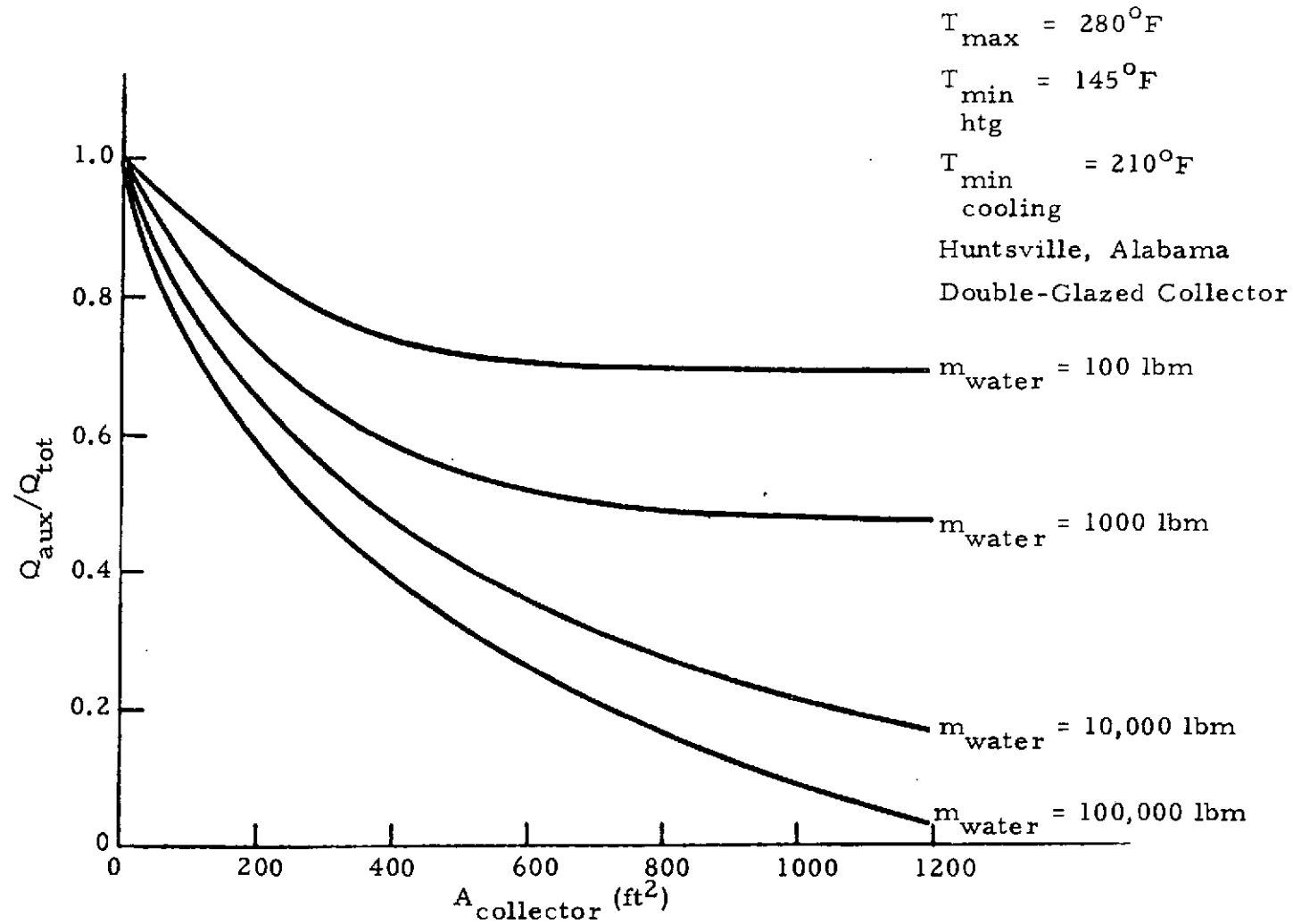


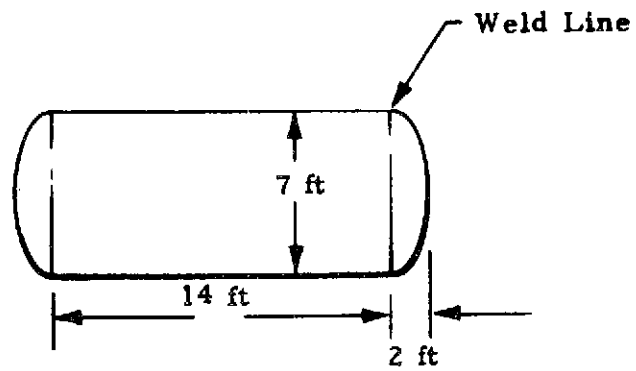
Figure 24. Auxiliary heat required for different collector areas and energy storage system capacities ($T_{\max} = 280^{\circ}\text{F}$).

used to determine the heat loss from the storage tank as a function of insulation thickness (as shown in Figure 25). The heat loss as a function of insulation thickness is shown in Figure 26. Figure 27 is the heat loss through the support structures and water supply lines. This heat loss is independent of the insulation thickness.

TABLE 2. TANK INSULATION

Type: Loose Fill Fiberglass		
Manufacturer: Johns-Manville and Others		
Maximum Service Temperature: > 300° F		
Conductivity: At 75° F	$\rho \approx .8 \text{ lb/ft}^3$	$K \approx .030 \text{ Btu/hr-ft-}^\circ \text{ F}$
	$\rho \approx 3 \text{ lb/ft}^3$	$K \approx .018 \text{ Btu/hr-ft-}^\circ \text{ F}$
Cost: \approx \$.14/lb		
	Box Minimum Wall Clearance	Cost*
	1 ft	450.
	2	700.
	3	1000.
Recommended: $\rho \approx 3 \text{ lb/ft}^3$		
K (estimated) $\approx 0.025 \text{ Btu/hr-ft-}^\circ \text{ F}$		

*At $\rho = 3 \text{ lb/ft}^3$



a. Tank Dimensions

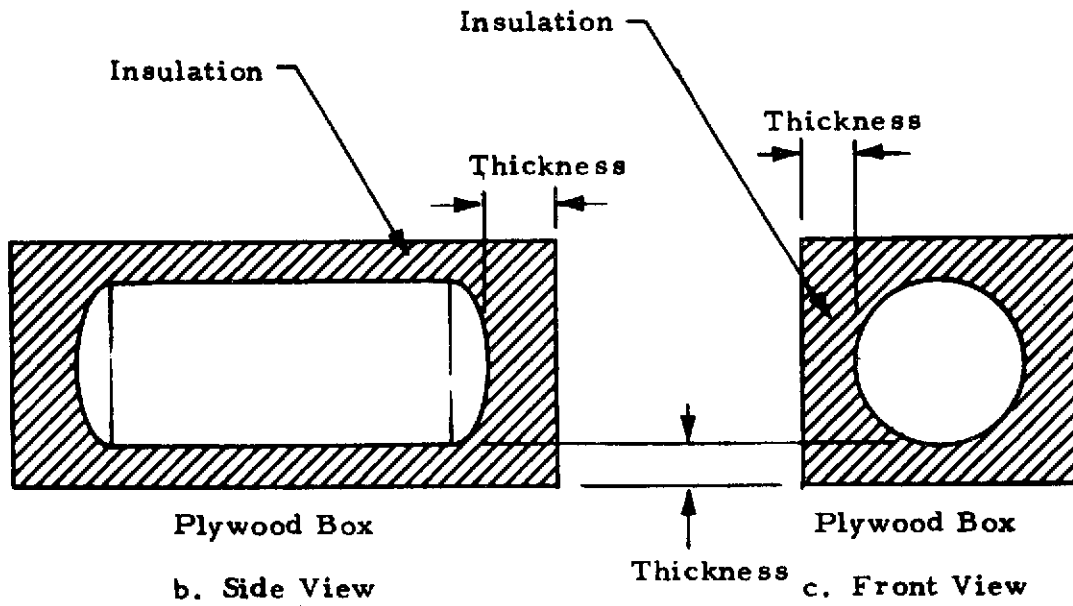


Figure 25. Energy storage tank.

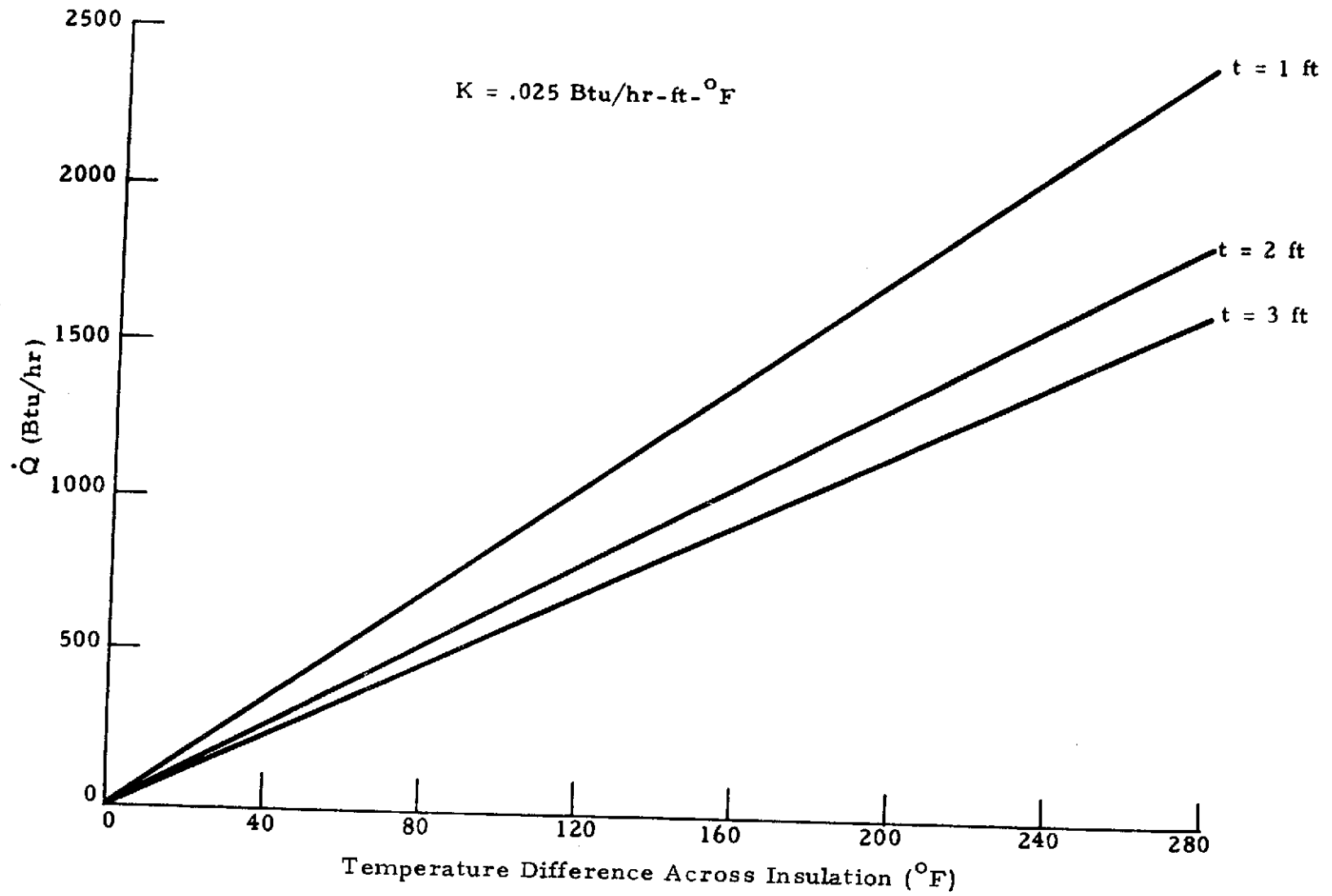


Figure 26. Heat loss through tank insulation.

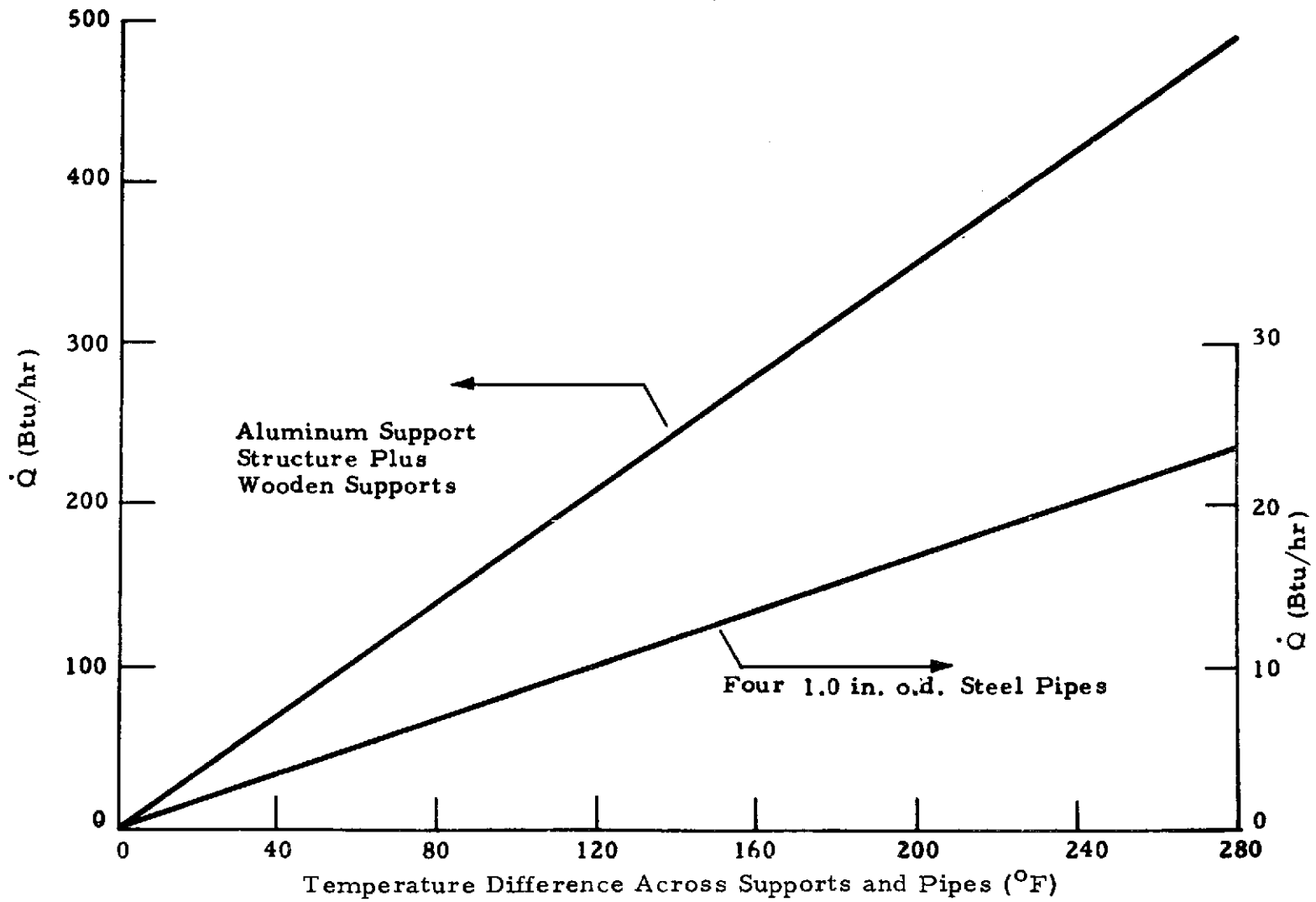


Figure 27. Heat loss through tank support structure and supply lines.

SECTION 5. PARAMETRIC TOTAL SYSTEM PERFORMANCE STUDIES

To evaluate the effect of different design options upon the performance of the total solar-powered system, a computer program has been developed and refined over the last 2.5 years to simulate the transient behavior of the system over an entire year. A brief description of modeling techniques and results of simulations are presented in the following paragraphs.

5.1 MODELING TECHNIQUES

Figure 28 shows the basic components which make up the simulation program. The six subsystems which comprise the total system are each separately modeled. Environmental data in the form of time-varying ambient temperature, wind speed, and direct and diffuse solar fluxes are required inputs. These environmental data are required for an entire year to allow transient analysis over the entire year. When time-varying solar data are not available, as is usually the case, techniques for calculating these data from available, whole-day, total insolation values have been developed. The method which is currently used to recorrelate the whole-day flux totals into time-varying fluxes is to simply determine the average atmospheric attenuation of the solar constant for each day and apply this attenuation factor to the solar constant throughout the day while conducting the system analysis. Thus the solar flux intensity is held constant through the day, while the relative position of the sun to the collector (the incidence angle) is calculated instantaneously throughout the day, based upon input values of latitude and collector tilt angle.

A control system logic routine allows for choices in such parameters as thermostat settings, energy exchanges between components, flow rates, switches, etc.

The six subsystem models used in the computer program to simulate the MSFC solar-powered facility are described below. These models pertain only to the residential solar-powered system being developed at MSFC. Other systems for other buildings in other regions would require different models, although the same simulation approach should prove valuable for analyzing these other systems.

The six subsystem models are very simple, with the exception of the solar collector model, which is a sophisticated mathematical model that allows accurate determination of the transient thermal performance of the collector. Each of the six models is discussed below.

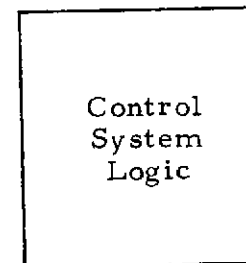
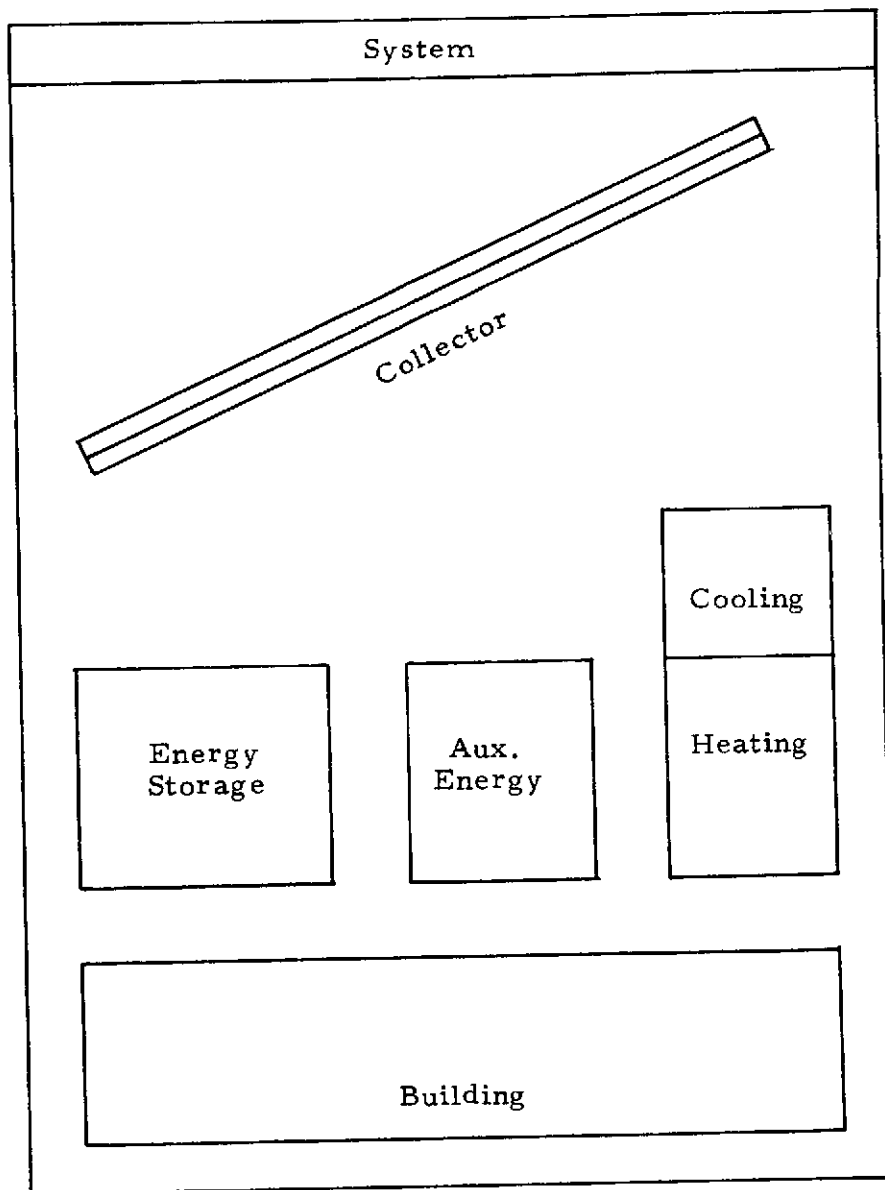
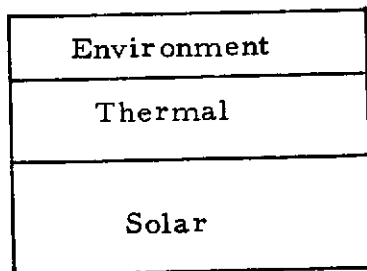


Figure 28. Basic components of the simulation program.

- Building Model

The building is treated as a fixed thermal capacitance connected to the outside environment through a variable thermal resistance. The capacitance is assumed to be 10 000 Btu/°F. This capacitance value represents the effective thermal inertia (mass times specific heat) of the building and its contents, which serve to dampen the effect of external temperature variations on the inside air temperature. The resistance value is different for hot weather than for cold weather. When the ambient temperature is above 70°F, the resistance value is set at 0.0007°F-hr/Btu, which corresponds to a 3-ton (36 000 Btu/hr) cooling load at 95°F ambient temperature. When the ambient temperature is below 70°F, the resistance value is set at 0.00117°F-hr/Btu, which corresponds to a 60 000 Btu/hr heating load at 0°F ambient temperature. The reduced resistance value for cooling is used to include latent loads which are important during the cooling season. These resistance values were based upon MSFC load calculations, and represent the overall heat transfer path between the inside air and the outside air.

- Energy Storage Model

The energy storage system is treated as a fixed thermal capacitance for the MSFC simulations. The capacitance value is an input quantity which represents the mass times specific heat product of the water in the energy storage tank. The storage system heat losses are treated as a fixed thermal resistance, and heat flows through this resistance to the outside environment. A maximum temperature is also a required input.

- Auxiliary Energy Model

The auxiliary energy system is a zero capacitance thermal energy source. Several options are available concerning the control of the auxiliary energy system, including whether the heat is added to storage or used directly to power the heating, cooling, and water heating components. The output heating rate of the auxiliary heater is 60 000 Btu/hr for heating and 55 000 Btu/hr for cooling.

- Heating Model

The space heating model is a zero capacitance input/output unit which utilizes heat from either the collector, energy storage, or the auxiliary energy system, depending on control logic selection and instantaneous conditions. The efficiency of the unit is an input variable, being defined as heat

output divided by heat input. The heating rate output as a function of water temperature and air temperature as these fluids enter the heat exchanger is also input to simulate the actual heat exchanger performance.

- Cooling Model

The space cooling model is a zero capacitance heat-driven air conditioner, with its performance defined by an input coefficient of performance (0.65). This input/output unit may be driven with heat from either the collector, storage or auxiliary, depending on prevailing conditions and control logic selection. The cooling rate is considered constant at 36 000 Btu/hr.

- Solar Collector Model

The solar collector model is a flexible energy transfer model that allows considerable variation in collector design. Input design variables include collector area, tilt angle, number of transparent covers, characteristic dimensions and spacings, and thermophysical properties of absorber plate, transparent covers, and backside insulation. Water is assumed as the energy transport fluid and its flow rate is an input parameter. The thermal capacitances of the plate, covers, insulation, and water are all used in the transient numerical treatment of the collector. The accuracy of the collector model is well verified by test data, as previously discussed in Section 3.

5.2 SIMULATION RESULTS

The computer program takes the inputs and models described above and conducts a transient energy transfer analysis through the year, obtaining all pertinent energy flows including energy used for heating and cooling, energy collected, auxiliary energy used, and energy wasted for lack of storage capacity. Daily totals and cumulative totals throughout the year are determined for all of these energy flows.

This simulation computer program has been widely used to compare different system designs. The major parameter of comparison has been taken as the dimensionless ratio, Q_{aux}/Q_{tot} , which represents the fraction of the total energy requirements for heating and cooling which must be met with conventional, auxiliary energy. Obviously, the smaller this value is, the better the system performance is.

One comparison is presented in Figure 29. This comparison is between two collector designs and two tank sizes, all as a function of collector area. The benefits of using two tedlar covers and large storage are apparent.

The effect of tilting the collector was investigated to some extent as shown in Figure 30. The roof was assumed to be tilted 60 deg from the horizontal during the winter and 30 deg during the remainder of the year. This results in a significant savings in collector area but adds to the initial cost due to having a pivot mechanism. Another point made by this figure is that the fixed-tilt-angle collector at 45 deg with respect to the horizontal performs almost as well as the more complicated double-tilt-angle system, again verifying this selected tilt angle as a good choice for whole-year operation (as previously discussed in Section 3).

The radiation properties of the selective coating and the transparent covers are extremely important to the overall performance of the solar-powered system. The transmittance of the tedlar film currently being manufactured and its possible degradation with age have not been clearly defined. Also, the changes in solar absorptance and infrared emittance of the selective coating with age are currently unknown. Therefore, a sensitivity study was conducted to determine the effect of property degradation on overall performance. The results are presented in Figure 31 for undegraded (good) and degraded properties. The degraded property values were set at levels which might be reached if degradation were to occur.

Figure 32 presents the results of a study to determine the effect of the number of transparent covers on early summer operation. The curves show the auxiliary energy requirements for the 2-month period as a function of collector area for one and two tedlar covers. Clearly, the performance of the two-cover system is superior to the performance of the one-cover system. For example, the auxiliary energy required for the one-cover system with an area of 1500 ft² is identical to that required for the two-cover system with an area of 950 ft².

Figure 33 presents the results of a study to determine the effect of maximum tank operating pressure on early summer operation. The maximum pressure corresponds to the water vapor pressure plus 15 psi to allow for the 30-ft rise in elevation from the tank to the collector, plus another ΔP to allow 20°F temperature rise through the collector without boiling. The maximum temperatures corresponding to the pressures are shown below the pressure axis. The curve shows the auxiliary energy required for June and July

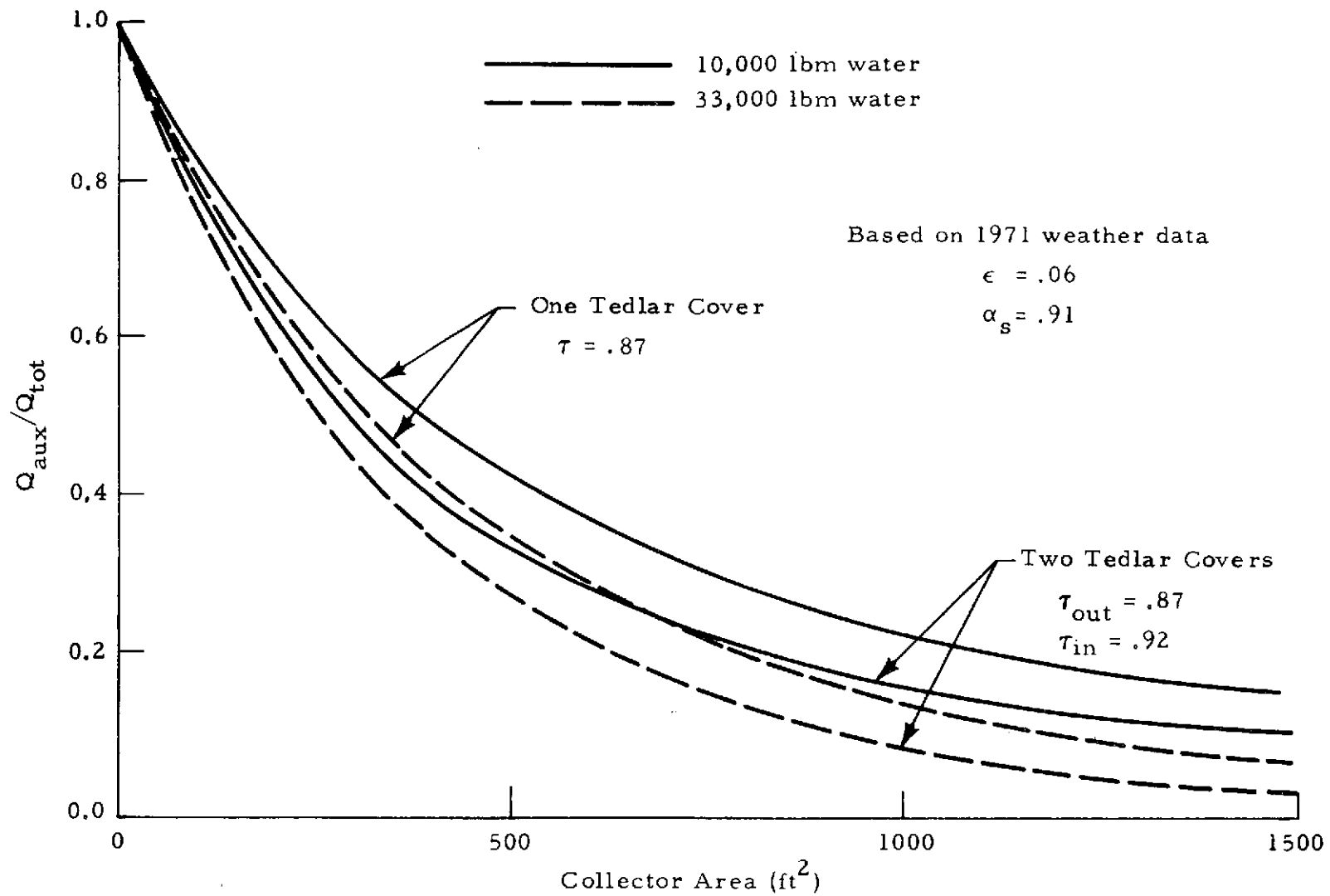


Figure 29. Effect of cover design on system performance.

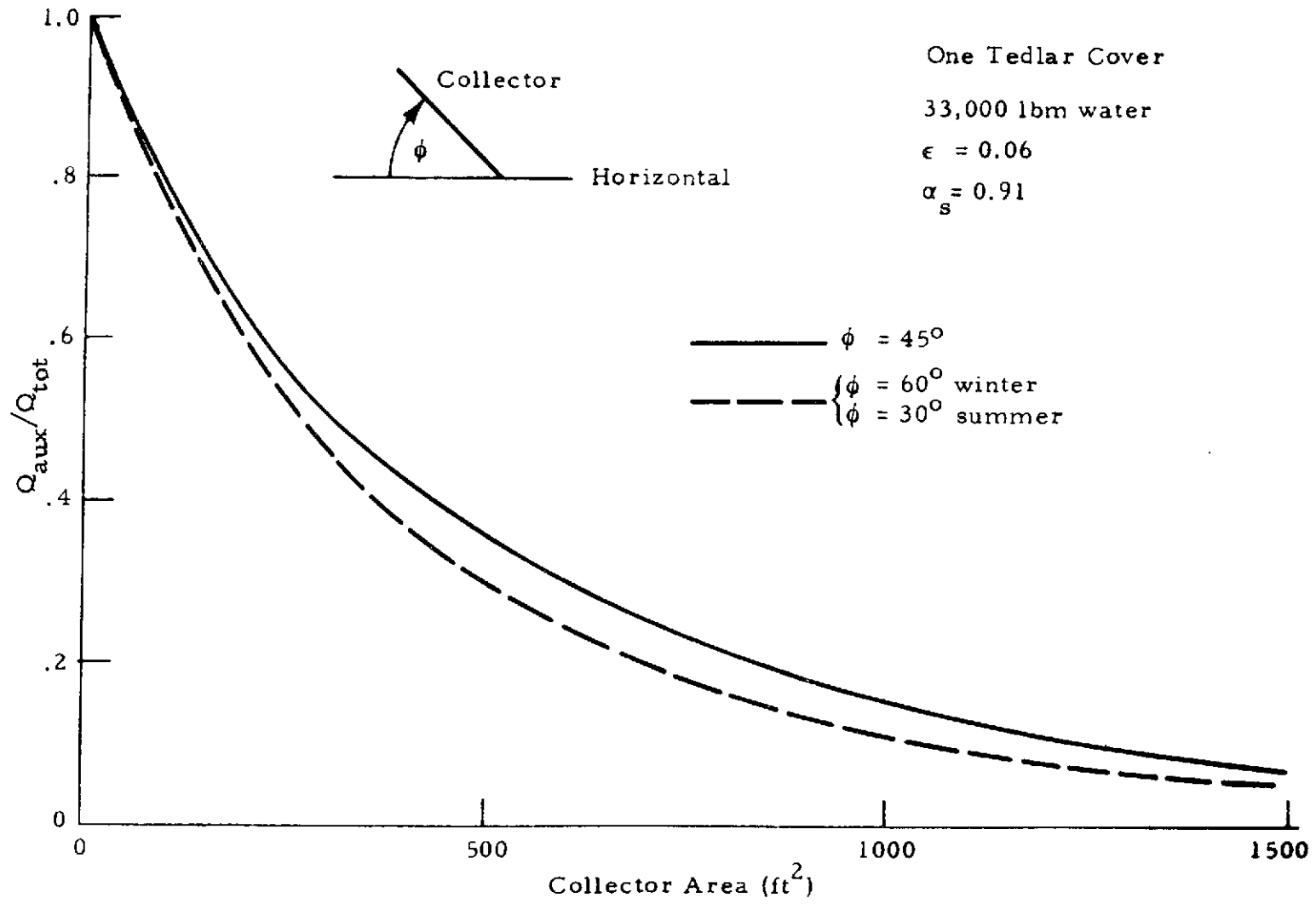


Figure 30. Effect of tilting collector twice a year on heating/cooling performance.

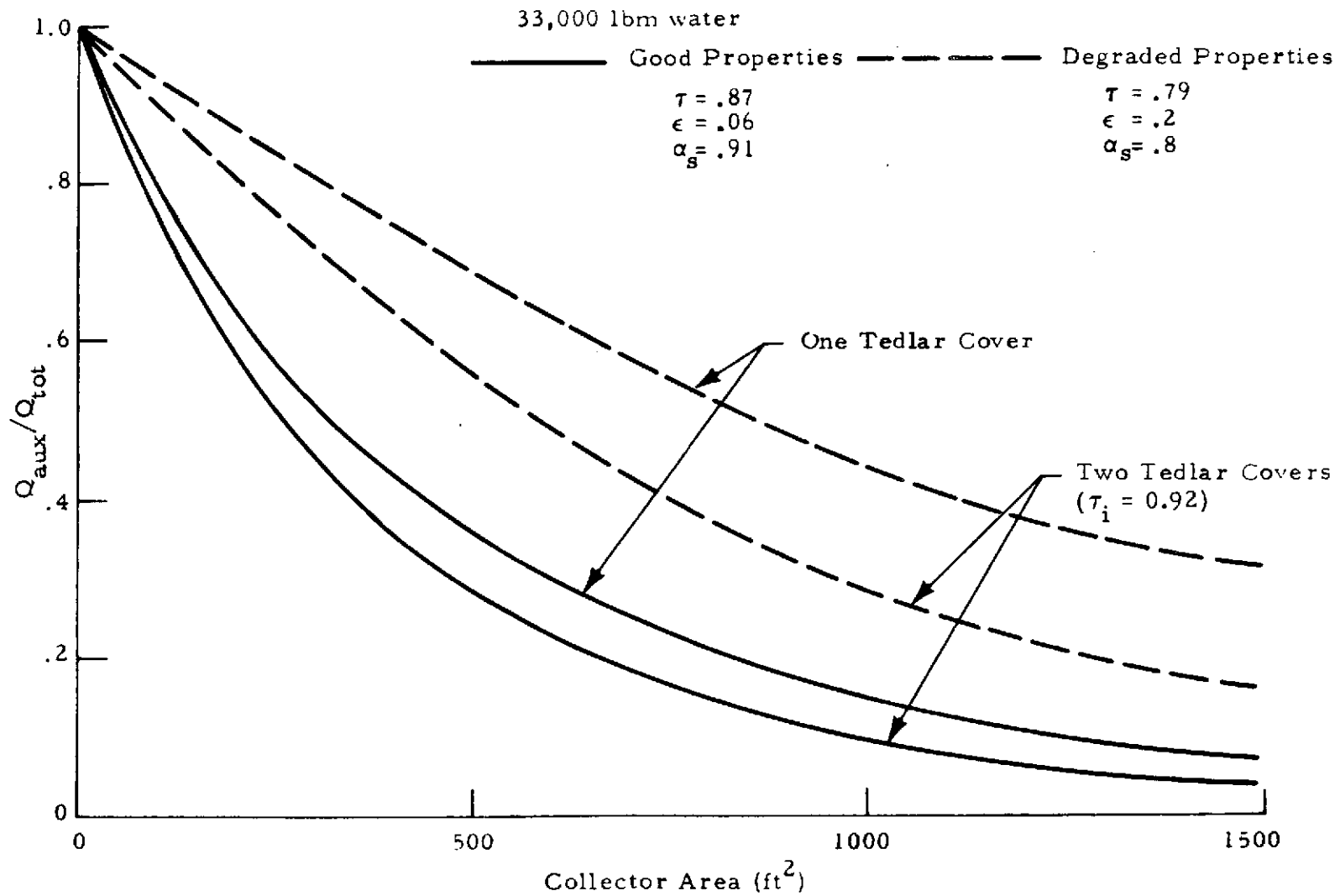


Figure 31. Effect of degraded properties on system performance.

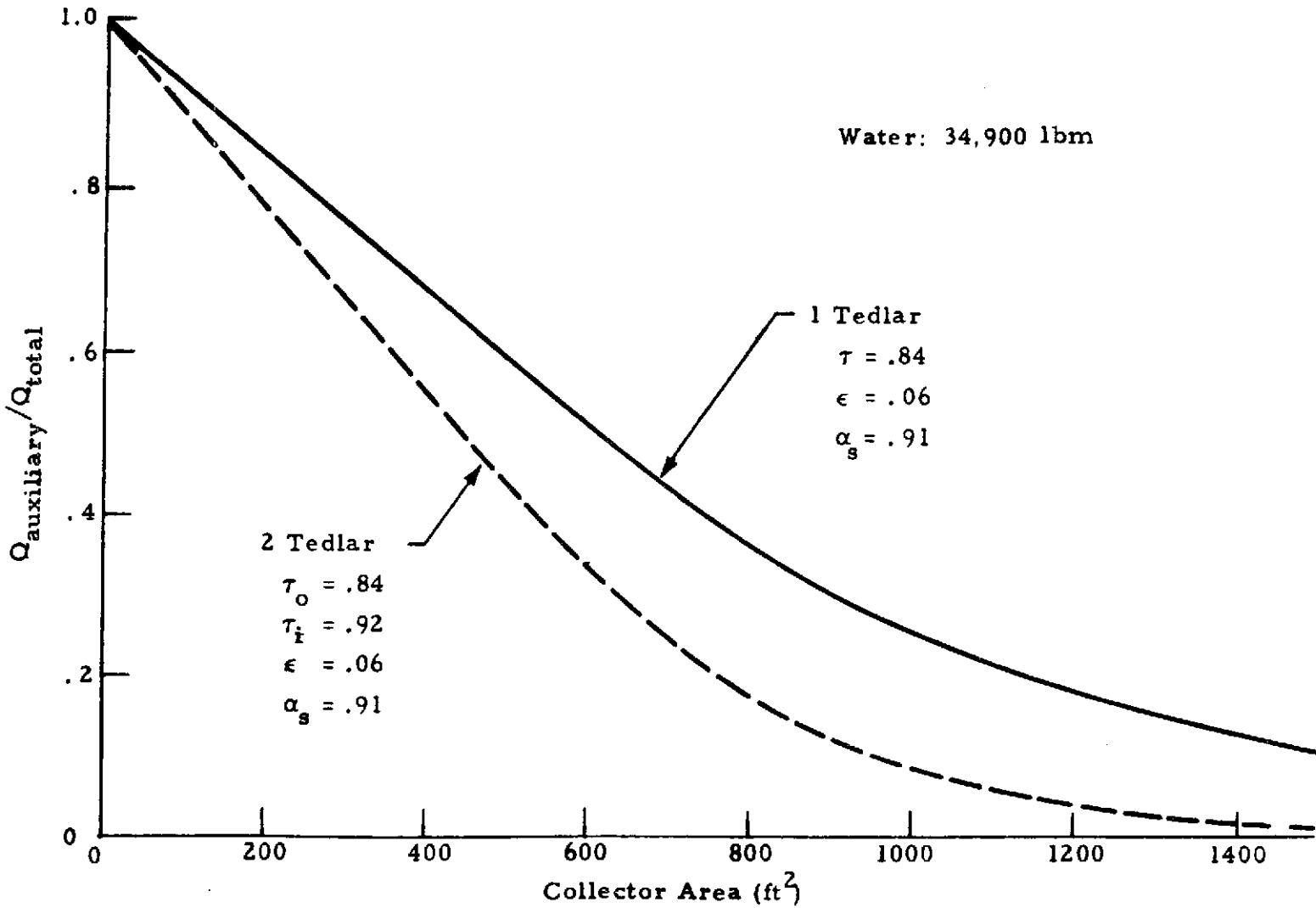


Figure 32. Effect of collector covers on system performance for June and July operation only.

operation. For the large tank under consideration, the improvement in performance with increasing pressure reaches the point of diminishing returns at about 45 psia. For a smaller tank, the curve would probably flatten out at a somewhat higher pressure.

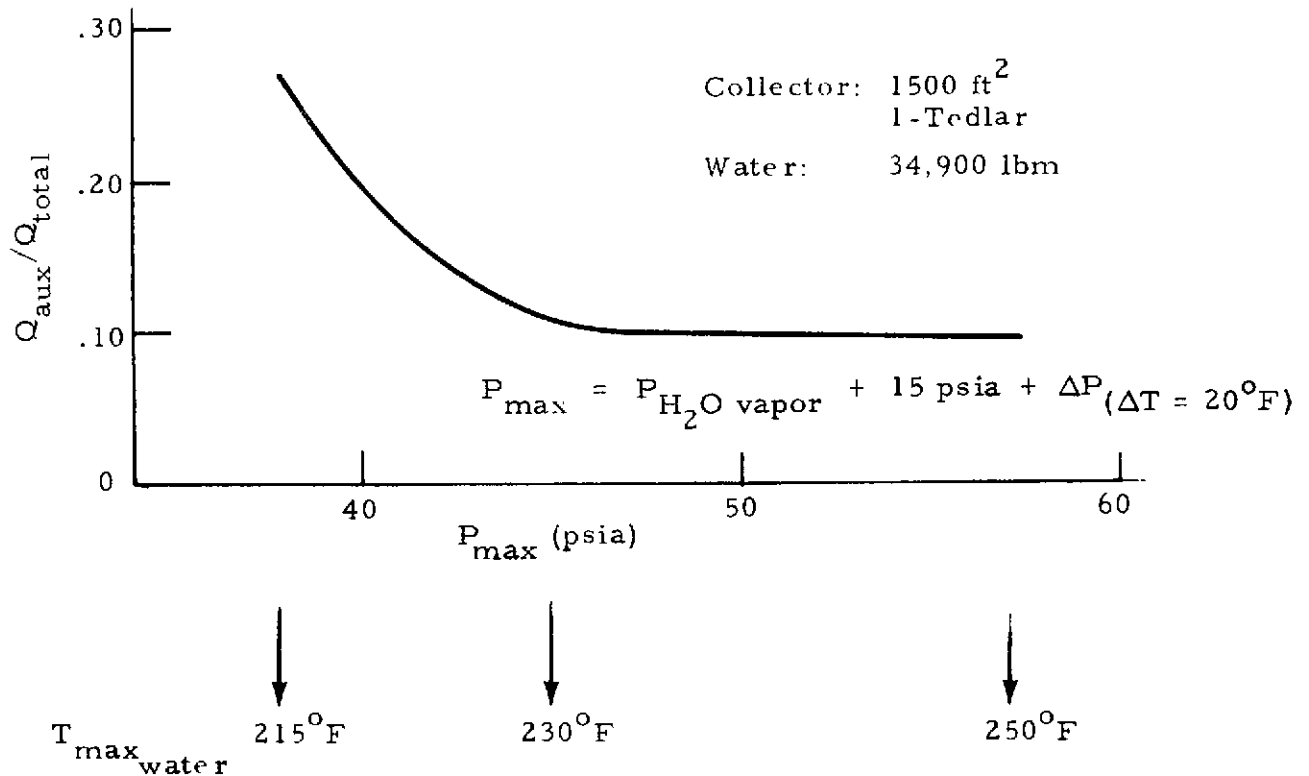


Figure 33. Effect of maximum tank operating pressure on system performance for June and July operation only.

The results of a study to determine the effect of effective transmittance of the tedlar covers on system performance are presented in Figures 34 and 35. The curves show the degradation of performance with decreasing transmittance for both good selective coating properties (solid curves) and for degraded selective coating properties (dashed curves). Although, the superiority of the two-cover system is clearly demonstrated, a single-cover collector was selected for the MSFC demonstration task because of scheduling and cost constraints.

For rapid calculations without having to run the computer program, a differential approximation of system performance sensitivity to small changes in radiation properties and area of the solar collector was developed. The basic sensitivity correlation was developed as shown below.

- $m_{\text{water}} = 33,000 \text{ lb}_m$
- $A_{\text{collector}} = 1500 \text{ ft}^2$
- 1 Tedlar Cover

- — $\epsilon = 0.06, \alpha_s = 0.91$
- - - - $\epsilon = 0.10, \alpha_s = 0.75$

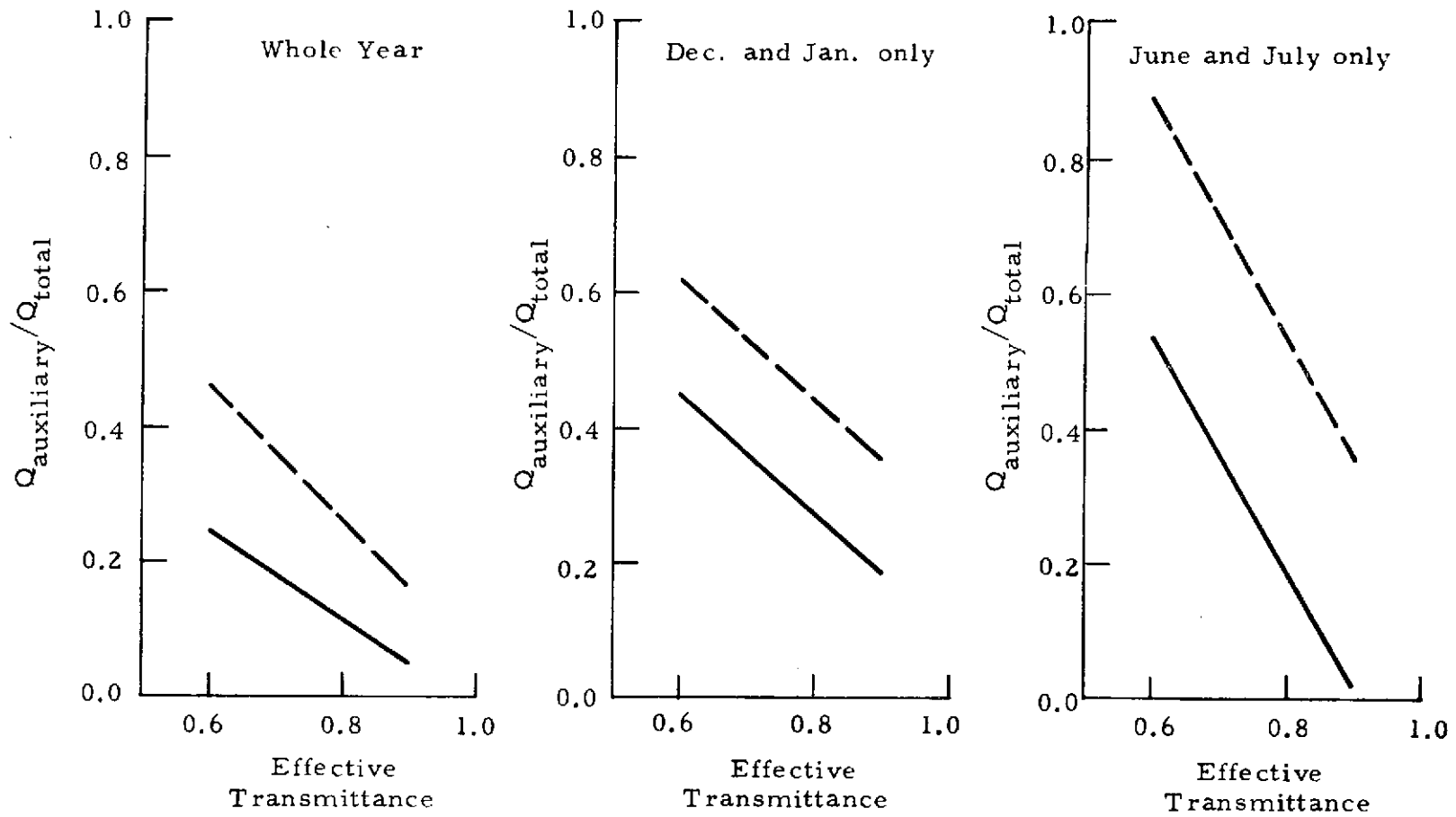


Figure 34. Effect of tedlar transmittance on system performance for one-tedlar cover collector.

- $m_{\text{water}} = 33,000 \text{ lb}_m$
 - $A_{\text{collector}} = 1500 \text{ ft}^2$
 - 2 Tedlar Covers ($\tau_{\text{inner}} = 0.92$)
- ————— $\epsilon = 0.06, \alpha_s = 0.91$
 - - - - - - $\epsilon = 0.10, \alpha_s = 0.75$

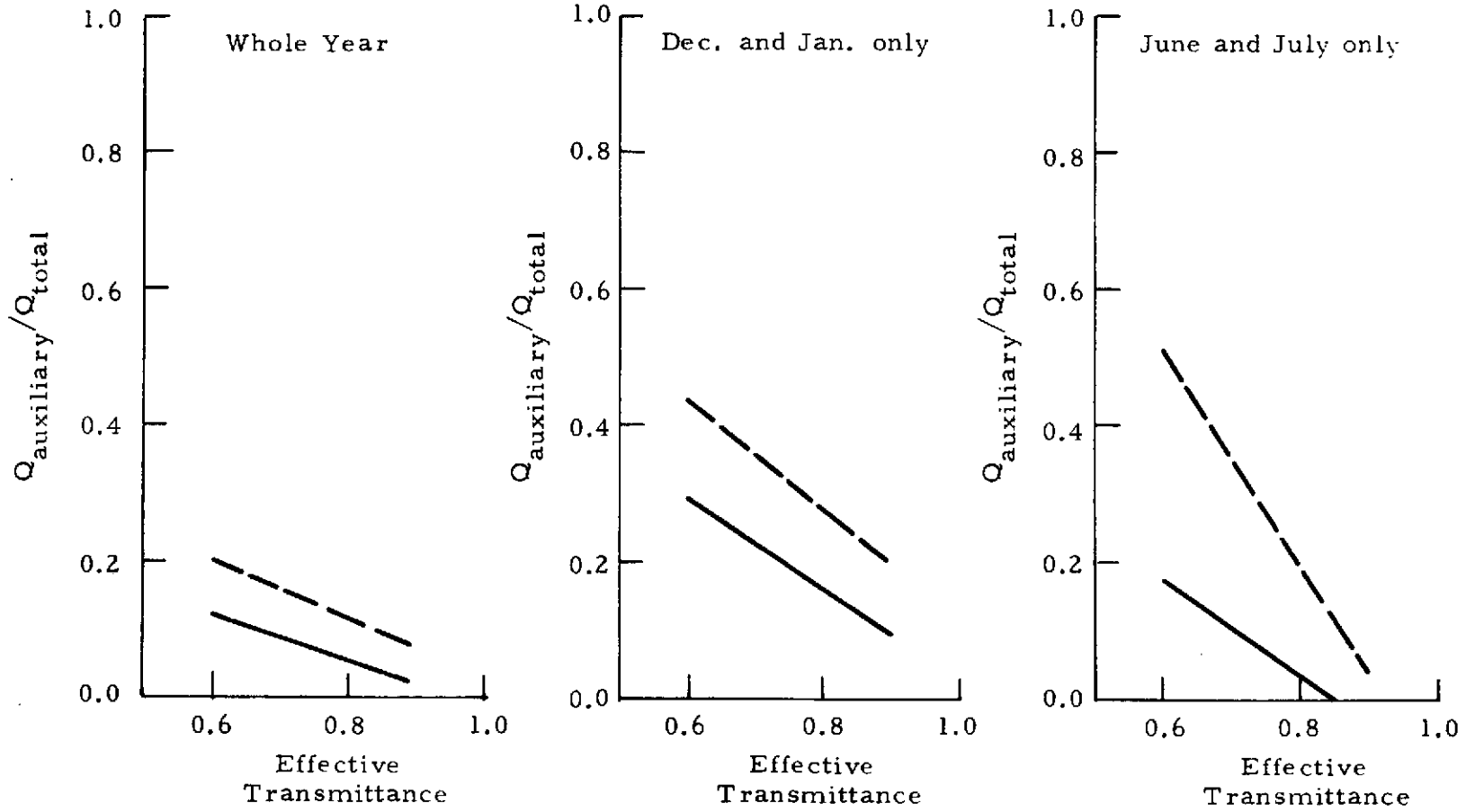


Figure 35. Effect of tedlar transmittance on system performance for two-tedlar cover collector.

Let

$$\sigma = \left(\frac{Q_{\text{auxiliary}}}{Q_{\text{total}}} \right) \text{ June + July } ;$$

then

$$d\sigma = \left(\frac{\partial \sigma}{\partial \alpha_s} \right) d\alpha_s + \left(\frac{\partial \sigma}{\partial \epsilon} \right) d\epsilon + \left(\frac{\partial \sigma}{\partial \tau} \right) d\tau + \left(\frac{\partial \sigma}{\partial A} \right) dA ,$$

where

α_s = solar absorptance of plate

ϵ = infrared emittance of plate

τ = effective transmittance of tedlar

A = collector area (ft²).

Then,

$$\sigma = \sigma_{\text{nominal}} + d\sigma .$$

The nominal values of the variables were:

$$\alpha_s = 0.91$$

$$\epsilon = 0.06$$

$$\tau = 0.84$$

$$A = 1500 \text{ ft}^2 .$$

The computer simulation program was used to evaluate the partial derivatives at the nominal point for both one-tedlar and two-tedlar collector designs. The resulting correlations are given below:

$$\sigma_{1 \text{ cover}} = 0.0954 - 1.81 d\alpha_s + 1.92 d\epsilon - 1.74 d\tau - \frac{0.00031}{ft^2} dA$$

$$\sigma_{2 \text{ cover}} = 0.00392 - 0.786 d\alpha_s + 0.431 d\epsilon - 0.724 d\tau - \frac{0.000147}{ft^2} dA.$$

Care must be taken with the signs of the small changes in α_s , ϵ , τ , and A. Positive changes indicate increases above nominal values and negative signs indicate decreases below nominal values. Spot checks indicate that the correlations are surprisingly accurate for small changes in the variables.

SECTION 6. AUTOMATIC CONTROL SYSTEM DESCRIPTION

6.1 AIR CONDITIONING MODE

When the thermostat inside the dwelling is set on the summer cycle and air temperatures within the dwelling increase to the upper thermostat set point, the system is activated as follows (Fig. 36): the cooling tower pump and fan and the air conditioner fan are energized, the air conditioner loop pump is energized and supplies 11 gpm of water to the system (flow is preset by hand valves HV11 and HV12), and hot water then passes through a 20- μ m particulate filter into a heater (HTR) (whose operation will be explained in the discussion of operating conditions on bypass flow) and then into motor valve MV3 which, on summer thermostat setting, directs 100 percent of the hot water flow to the air conditioner. To maintain generator temperatures within the air conditioner at 190 to 200°F, a stepped bypass flow arrangement is installed to limit maximum heat input to the generator, and it operates as follows: if the control temperature at T4C is between 210°F and 220°F, all flow passes through the air conditioner generator; if the inlet water temperature at T4C increases to 220°F, SV1 opens and 3.7 gpm (flow is initially set by regulating hand valve HV14) is bypassed around the unit; if the temperature at T4C rises to 230°F, SV2 opens and allows an additional 1.8 gpm (flow is initially set by regulating hand valve HV15) to bypass the air conditioner for a total bypass flow of 5.5 gpm. The temperature at T4C will not exceed 240°F. Flow through the ARKLA unit generator is measured by flowmeter F2 and total flow is measured by flowmeter F3, the difference of which gives bypass flow. The hot fluid then passes through HV1 into the thermal storage tank. If the temperature at T4C falls to 225°F, SV2 closes and reduces the bypass flow to 3.7 gpm. When the temperature at T4C drops to 215°F, SV1 closes and allows full flow to again be directed through the air conditioner generator and then through MV1 back to the thermal storage tank.

6.2 BYPASS MODE FLOW

Bypass flow is triggered when the return temperature from the air conditioner measured at T5C is greater than the temperature within the thermal storage tank as measured at T1C; MV3 directs 100 percent of air conditioner pump flow to the thermal storage tank bypass. Check valve CV1 prevents the flow of water from the storage tank. In this mode of operation, all heat required to operate the air conditioner is supplied by electrical energy in heater HTR. Control of electrical heater HTR is independent of the operational mode; i. e., it may be in operation either in the bypass or storage tank flow mode depending upon storage tank water temperature and outside wet bulb

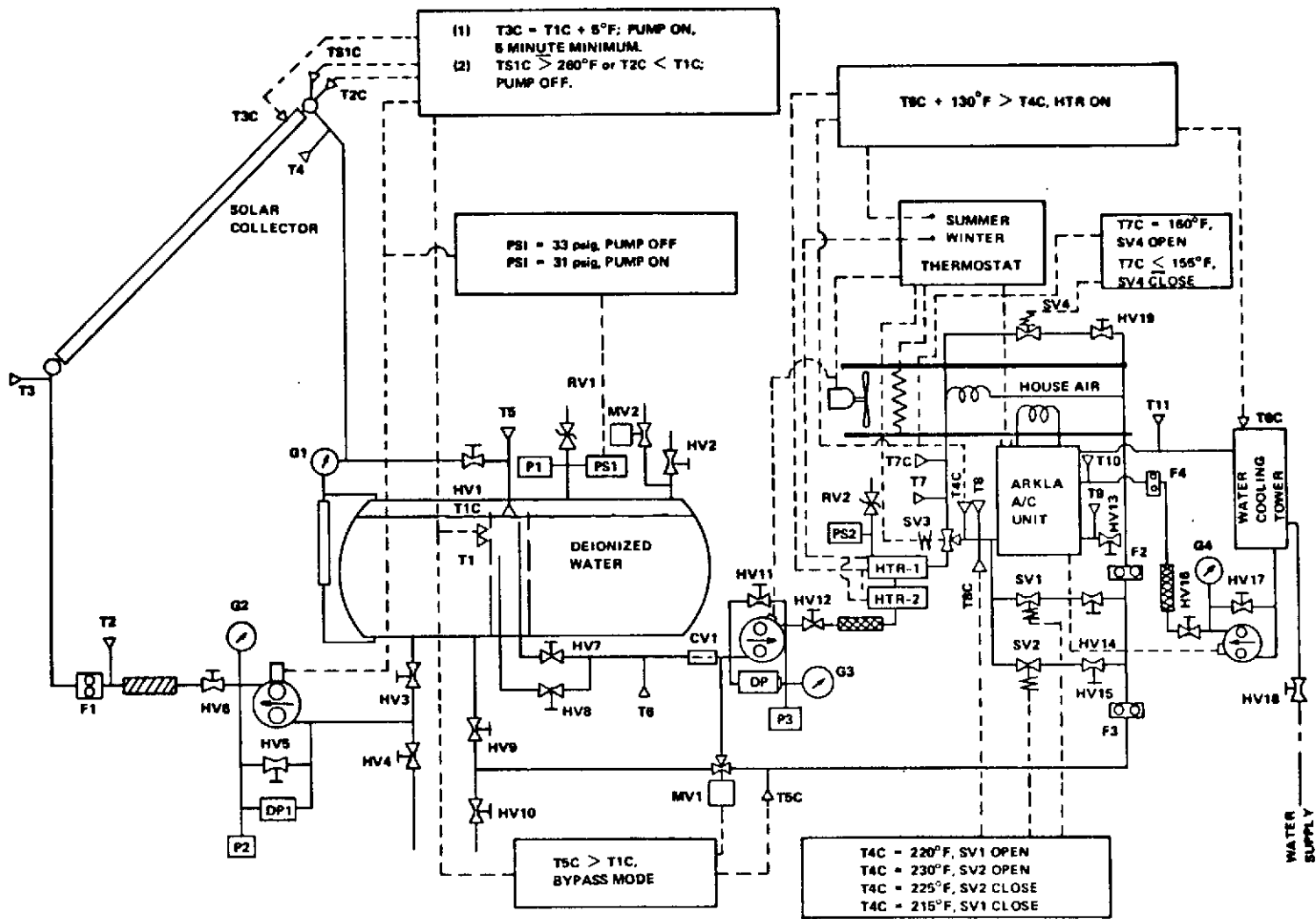


Figure 36. Setup for demonstration test of solar-powered residential heating and cooling system.

temperature. If the sum of cooling tower wet bulb temperature as measured by T6C + 130°F is greater than the temperature at T4C, heater HTR will be energized to supply heat. If the sum T6C + 130°F is less than the pump outlet temperature as measured at T4C, heater HTR will be de-energized. In the bypass mode, the cycling situation described above will continue until the temperature within the storage tank at T1C reaches a value greater than T5C, at which time MV1 will position to provide 100-percent flow to the storage tank. When the air temperature in the dwelling decreases to the lower thermostat set point, the power to the air circulation fan is removed, the air conditioner water pump is stopped, the cooling tower water circulation pump is stopped, and the cooling tower fan is stopped.

6.3 AIR CONDITIONING LOOP – WINTER OPERATION

When heat is required within the dwelling, a switch on the thermostat is turned to the "winter" position (marked as such on the thermostat). In the winter position, heaters 1 and 2 are de-energized, the ARKLA unit except for the circulation fan is de-energized, and the cooling tower pump and fan are de-energized. At the same time, solenoid valve SV3 repositions to send 100 percent of the storage tank water flow to the hot water coils located in the ducting downstream of the ARKLA unit. An additional winter thermostat within the trailers controls electrical resistance strip heaters located in the air ducting downstream of the hot water coils, and it is set 2°F below the aforementioned thermostat. This thermostat comes on when there is not sufficient heat available in the storage tank to supply the needs of the trailer complex. Henceforth in this description, the thermostat that controls the hot water pump and the fan will be designated TH1, and the thermostat controlling the duct strip heaters will be designated TH2.

When the temperature within the dwelling falls to the lower set point of TH1, the thermostat activates the water circulation pump and the air circulation fan located within the ARKLA unit. If the water temperature within the storage tank is sufficient to meet heating requirements, the air temperature within the dwelling will increase to the upper thermostat set point and at that point the fan and pump will be shut off. If the stored water temperatures rises (on the winter cycle only) to 180°F, valve SV4 opens and allows 3.5 gpm of the water flow to be bypassed to avoid elevating the air temperature to a level too high to be practical.

If the temperature of the storage tank water is not sufficient to maintain a comfortable temperature within the dwelling, the temperature will fall to the setting on TH2 and the duct heaters will be energized to supply the additional heat required to elevate the temperature back to the setting on TH1.

Turning the selector switch back to the "summer" position de-energizes the duct strip heaters, positions solenoid valve SV3 to supply 100-percent water flow to the ARKLA unit generator, energizes the air conditioner control circuits, cooling tower fan and pump, and de-energizes the "winter" cycle control circuitry.

SECTION 7. SOLAR COLLECTOR SEGMENT TEST RESULTS

As part of the solar-powered home heating and cooling program, a 2 ft by 21 ft solar collector test unit was set up for preliminary verification of the analytical predictions of collector performance. The collector was made up of seven 3 ft by 2 ft panels in series for a 42 ft² total area. The solar house will use 31 of the 21-ft long collectors as its source of solar energy. Coolant flow through the collectors will provide energy transport to the air conditioner and heating unit. The collectors on the house as well as on the single collector test were inclined at 45 deg to the horizontal.

The test setup and instrumentation locations are shown in Figure 37. Not all of the instrumentation was recorded, but the instruments were available to investigate anomalies as required. A number of tests were run for facility checkout and preliminary evaluation. Initial evaluation appeared favorable; therefore, long duration (all day) tests were run in January and February of 1974 under sunny conditions for performance verification. It had been found earlier that the 2 ft by 21 ft test setup was difficult to evaluate in regard to efficiency under transient conditions; i.e., intermittent cloud cover. The predicted efficiencies for various heat fluxes, ambient temperatures and collector average $(T_{\text{inlet}} - T_{\text{outlet}}/2)$ temperatures, and measured efficiencies are shown in Figure 38 through Figure 41. As can be seen, the predictions are fairly good for the higher solar heat fluxes; however, at the lower heat fluxes it appears that the performance predictions are too low. Since the lower flux data points were obtained as the sun was going down in mid-afternoon, the data are of a transient nature and thermal lag of the collectors, piping, etc., may account for the high efficiencies late in the day. Additional testing is required to verify the predictions at the solar fluxes below 300 Btu/ft²-hr.

Experimental efficiencies were calculated from the relationship

$$\eta = \frac{\dot{m}C_p \Delta T}{Q_{\text{SOLAR}}A}$$

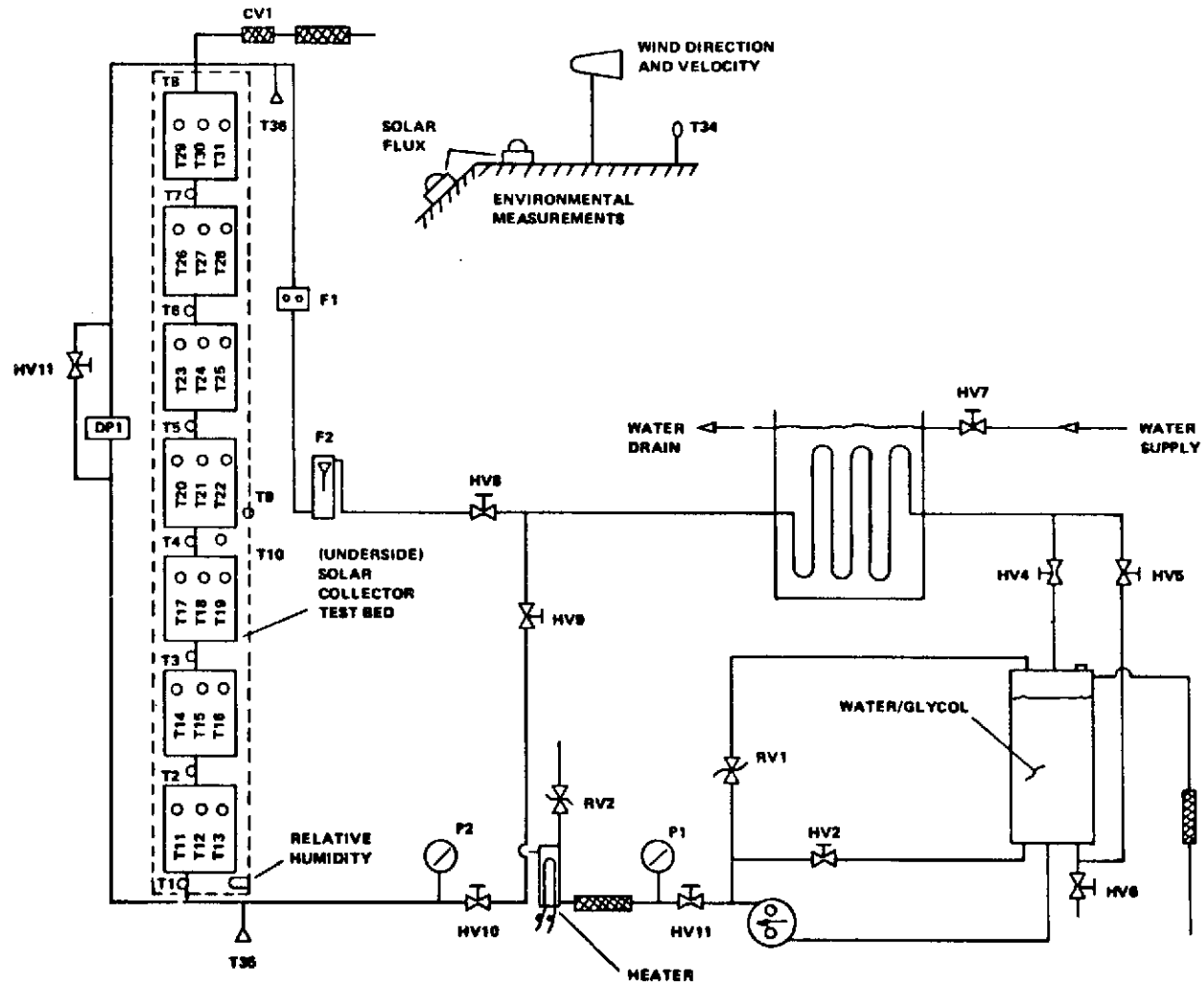


Figure 37. Setup for evaluation of solar collector test bed.

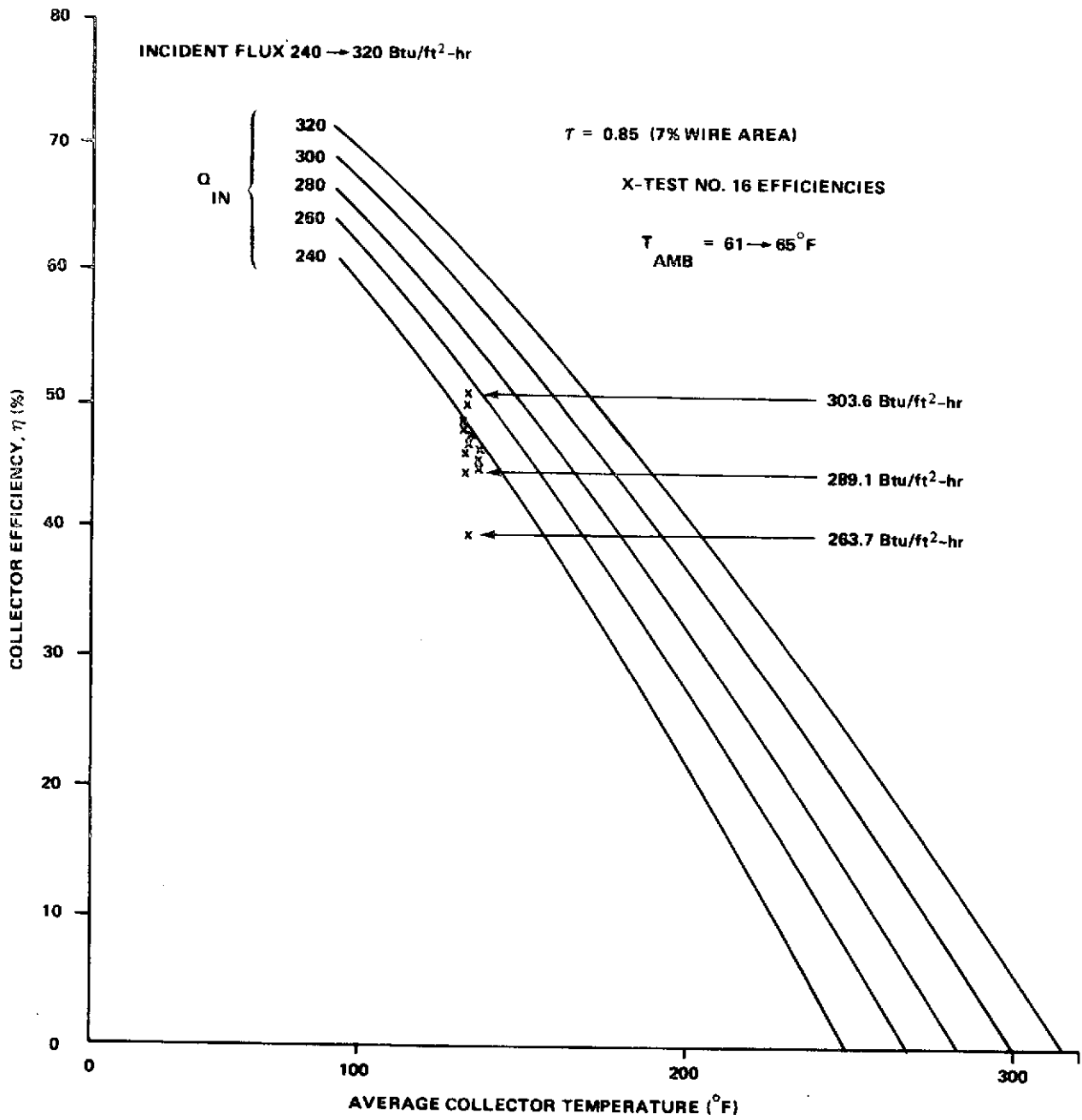


Figure 38. Collector efficiency versus average collector temperatures.

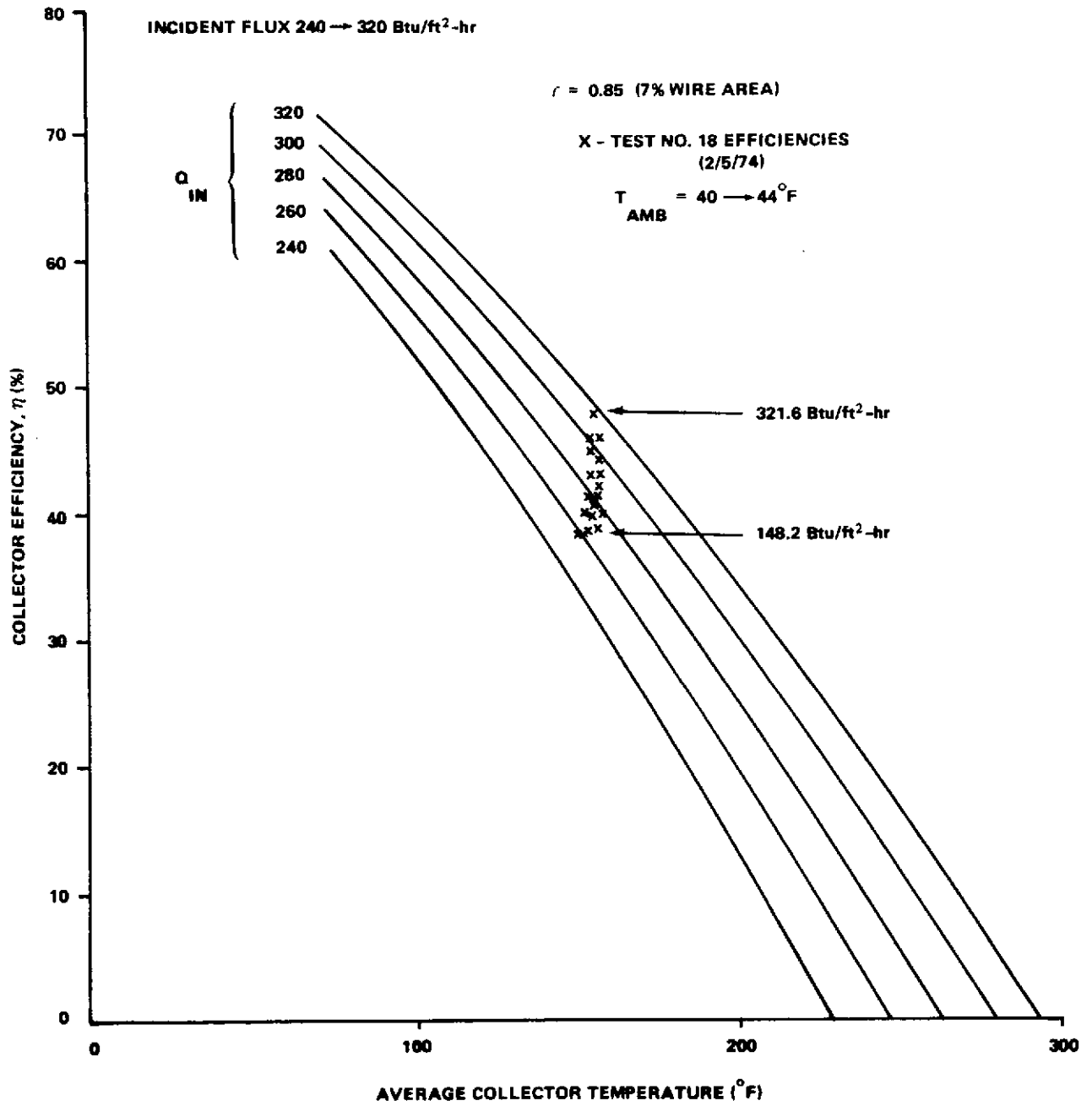


Figure 39. Collector efficiency versus average collector temperatures.

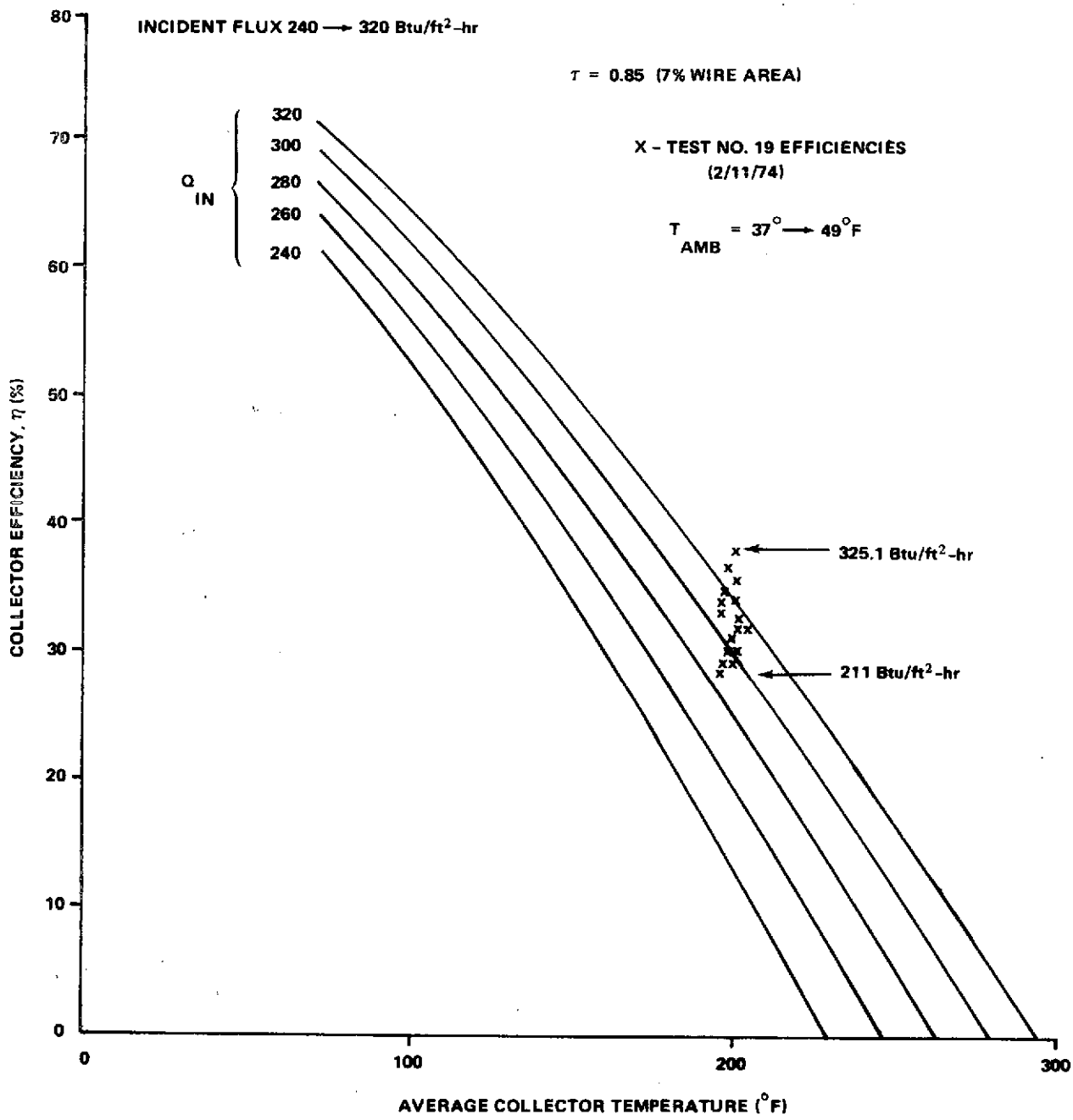


Figure 40. Collector efficiency versus average collector temperatures.

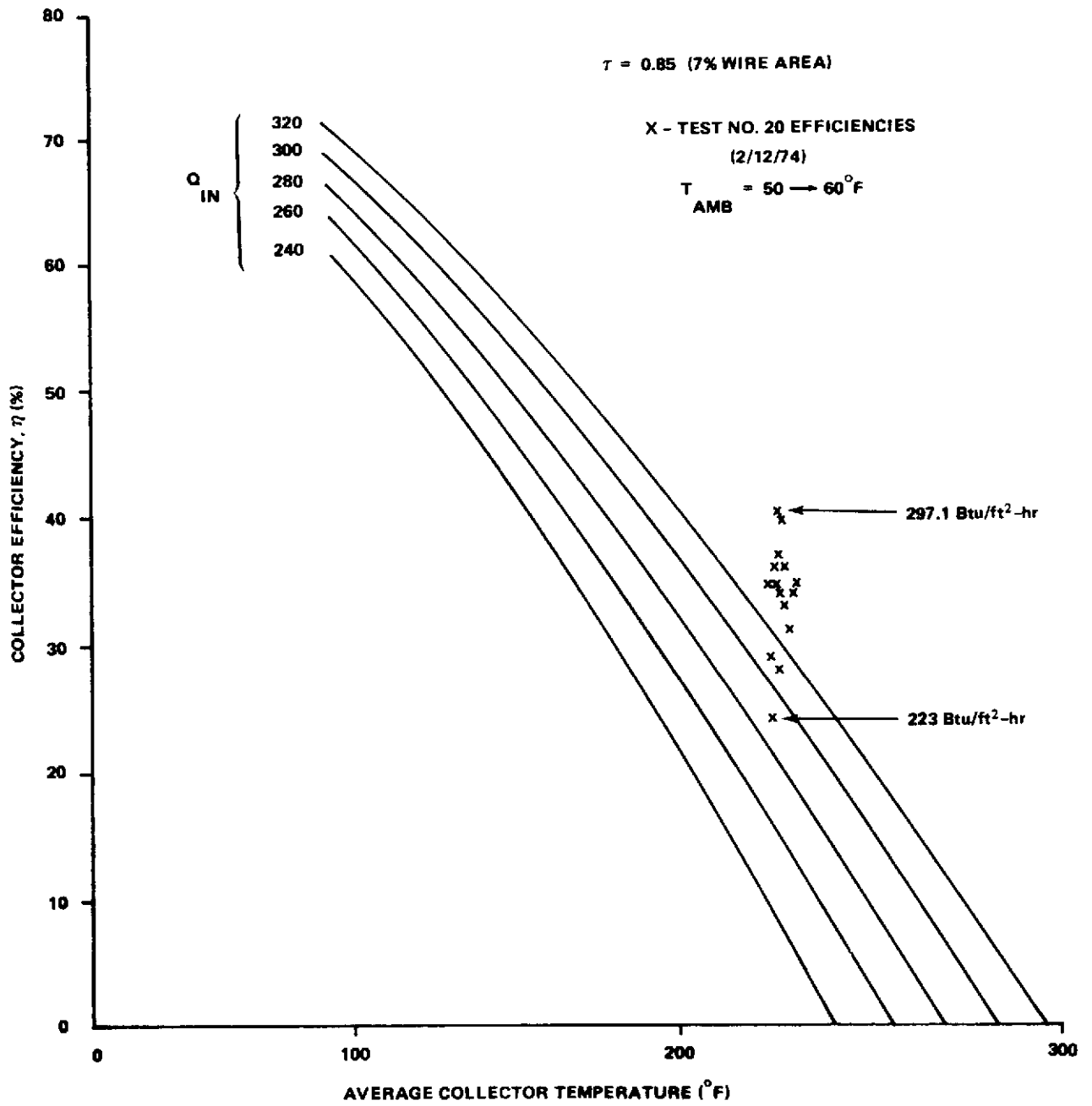


Figure 41. Collector efficiency versus average collector temperatures.

where

\dot{m}	=	coolant flow through the collector, lb/hr
C_p	=	specific heat of the coolant, Btu/lb°F
ΔT	=	temperature difference between coolant inlet and outlet of collector, °F
Q_{SOLAR}	=	solar heat flux measured in the same plane as the collector, Btu/ft ² -hr
A	=	area of the collector, ft ² .

The ΔT is normally obtained from metal skin temperatures of the panels; however, as a check, fluid temperatures at the inlet and outlet were installed early in the program. These checked well with the metal temperatures except at fluid outlet temperatures near 200°F and above. There was poor correlation between metal temperatures and fluid temperatures for tests 19 and 20 which were run at 200 and 230°F respectively to verify that the collector could operate at temperatures required to operate the air conditioner. The comparison of results for metal temperatures and fluid temperatures is shown in Figures 42 and 43. In an effort to resolve the discrepancy, a section of clear tubing was installed at the outlet of the collector to observe boiling or other disturbances that might be occurring at the outlet. Test 20 was repeated and bubble formation was observed at the collector outlet. In view of the uncertainty of the fluid measurements in the presence of vapor, the metal temperatures (T_1 and T_8) have been used for efficiency calculations in lieu of the fluid temperatures above about 180°F.

The following conclusions have been drawn from the test data on the 2 ft by 21 ft test collector:

1. The collector efficiency is predicted well by analysis, and the efficiency is high enough to collect the required energy to operate during both winter and summer.
2. The collector can operate at 200°F inlet and at 230°F outlet at 1-gpm coolant flow (air conditioner temperature requirements).
3. Performance was not degraded measurably in the 2 months that the collector was exposed to winter weather conditions.

$$\eta = \frac{\dot{m} c_p \Delta T}{Q_{\text{SOLAR}} A}$$

- o BASED ON COLLECTOR SKIN TEMPERATURES
- x BASED ON FLUID INLET/OUTLET TEMPERATURES

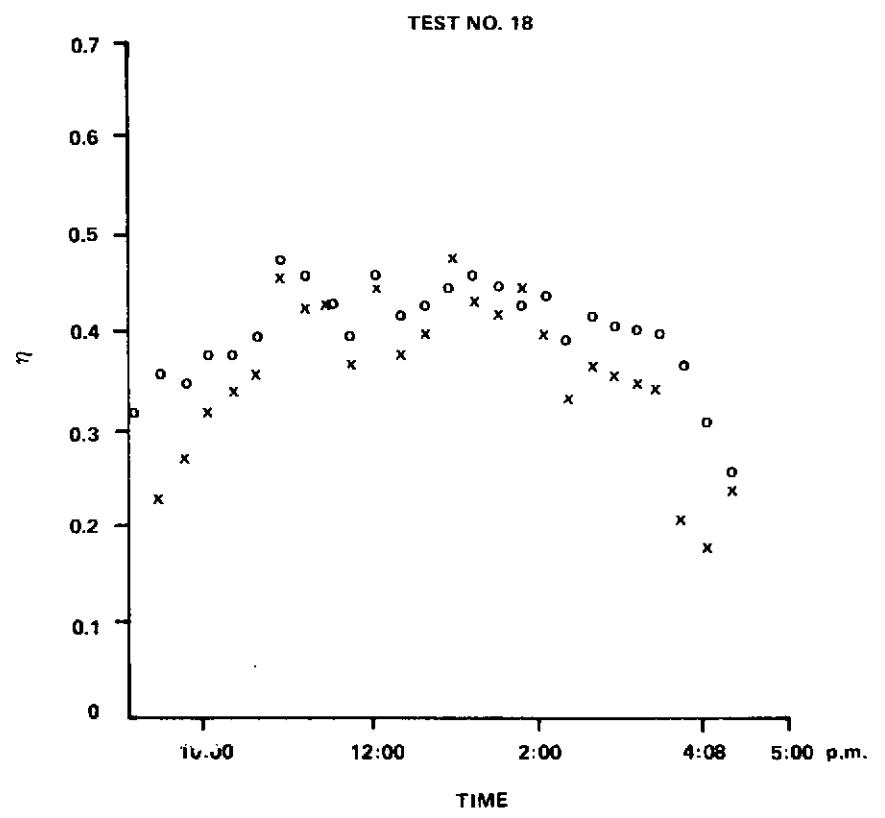
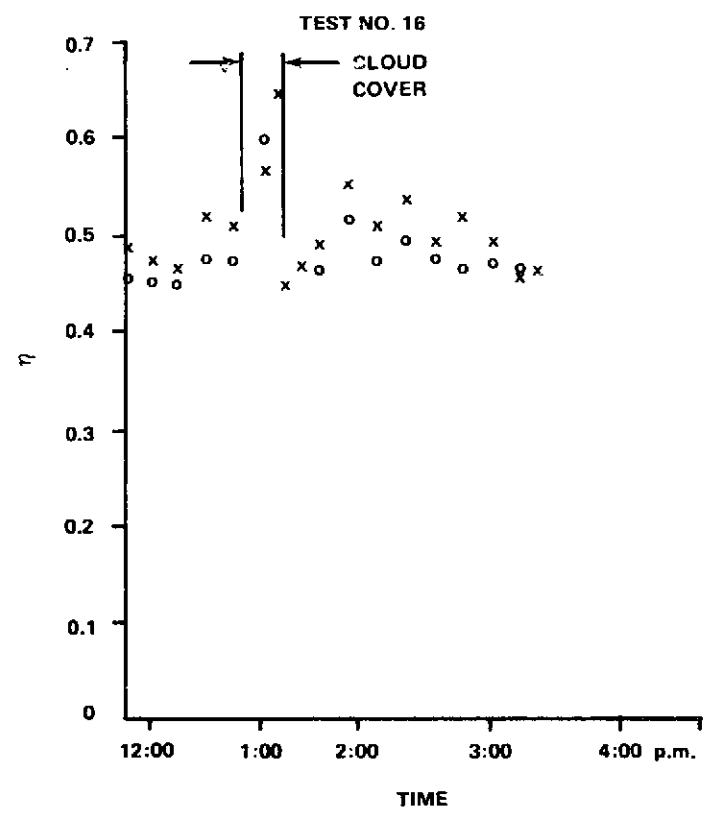


Figure 42. Measured efficiency η for 2 ft by 21 ft solar collector.

$$\eta = \frac{\dot{m} C_p \Delta T}{Q_{\text{SOLAR}} A}$$

- o BASED ON COLLECTOR SKIN TEMPERATURES
- x BASED ON FLUID INLET/OUTLET TEMPERATURES

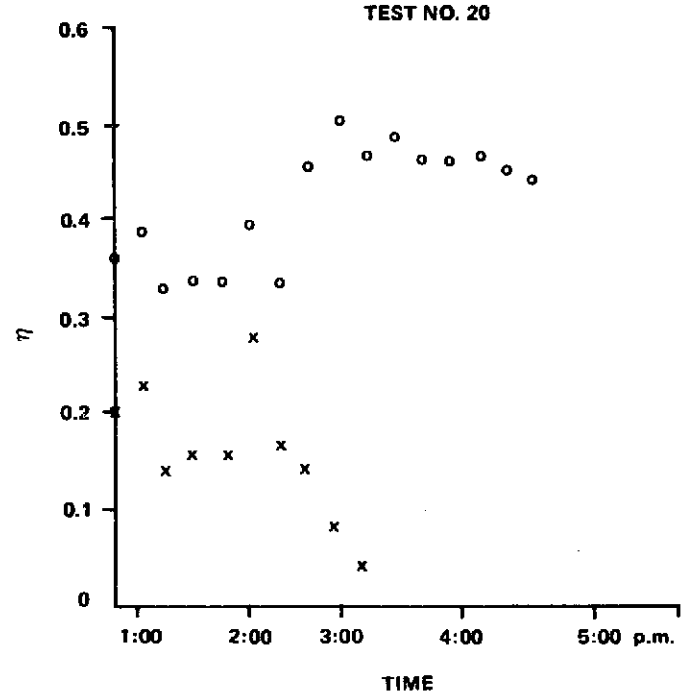
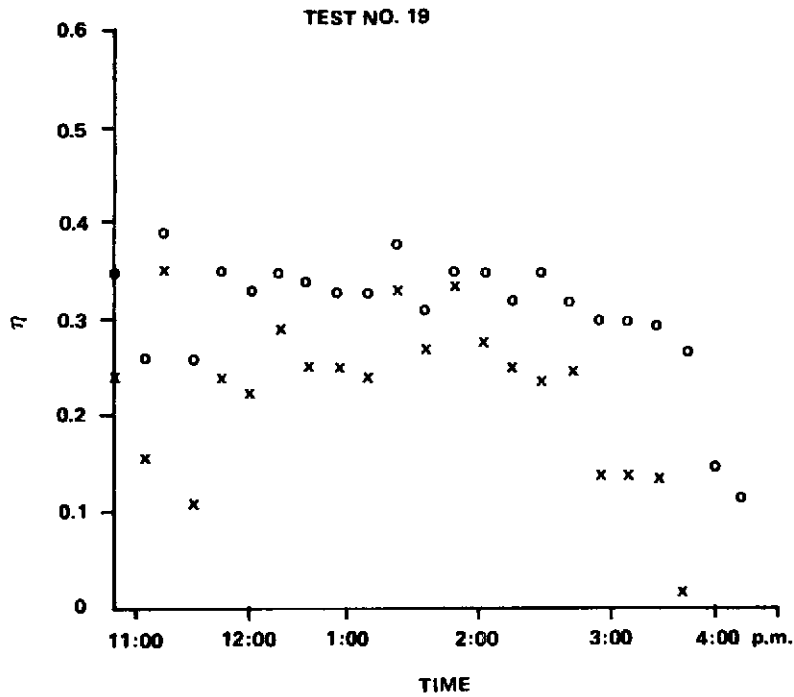


Figure 43. Measured efficiency η for 2 ft by 21 ft solar collector.

4. Based on temperature data, coolant flow through the flow passage of the collector panels is uniform and edge heat leak is not excessive. Note that the temperature increases are not uniform between all panels. This is considered to be a result of measurement inaccuracies. In addition, because of recorder limitations, all of the measurements are not recorded at the same exact time. Typical temperature distributions for two time slices are shown in Figure 44.

It is anticipated that further testing of short duration (1 to 2 hr) and with minimal instrumentation will be accomplished parallel with the home systems demonstration test to verify performance for longer weather exposure times, lower solar fluxes, and for potential design improvements such as double tedlar covering.

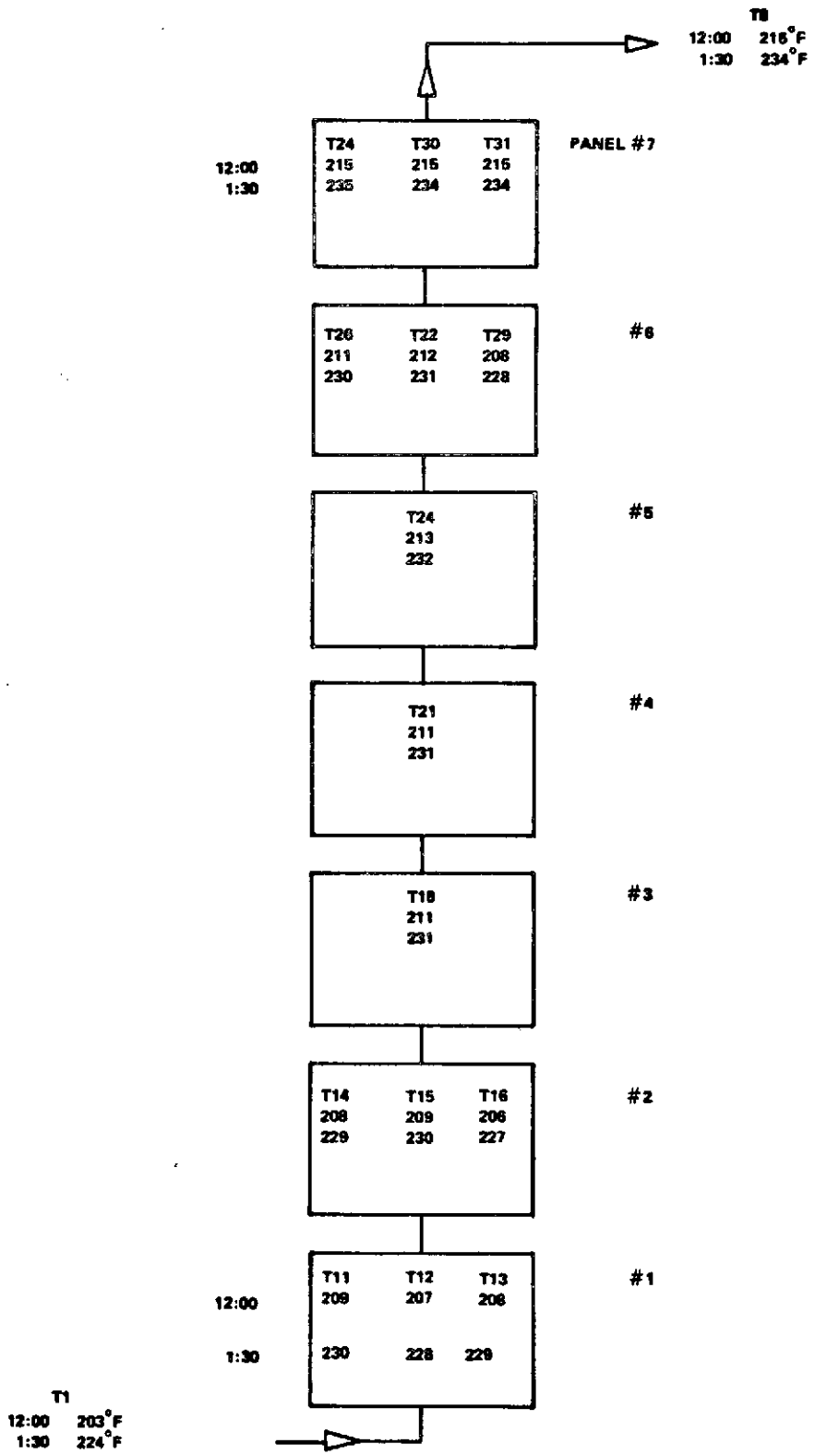


Figure 44. Temperature distribution over 2 ft by 21 ft solar collector for test No. 20 (2/12/74) at approximately 12:00 noon and 1:30 p. m.

SECTION 8. CONCLUSIONS

The following conclusions are drawn, based upon the results of previous studies and tests.

- The utilization of solar energy for space heating and air conditioning is technically feasible with properly applied current technology.
- At the present time, the best solar heating and cooling system design should include:
 1. A solar energy collector with an integral tube-in-sheet absorber plate coated with a selective surface having high α_s and low ϵ_{ir} .
 2. A sensible heat storage system with water as the storage medium (the same water should be used as the energy transport fluid to and from the collector and output units).
 3. An absorption cycle cooling system.
 4. An auxiliary heat source that utilizes storable fuel (fuel oil, propane, etc.) rather than natural gas or electricity. This will prevent peak, simultaneous drains on the conventional utilities by solar-powered installations, whenever several days of cloudy weather occur.
- The use of computerized simulations of solar system performance is essential to compare different system designs, to properly size collector and storage, and to generate near-optimum designs.
- With increases in solar energy useage and technology, system design from handbooks should be possible.